



IMPLEMENTATION REPORT 5-6652-01-1

TxDOT PROJECT NUMBER 5-6652-01

Shear Behavior of Spliced Post-Tensioned Girders with UngROUTED Tendons: Final Report

Sangyoung Han
Jarrod Zaborac
Zachary D. Webb
Jongkwon Choi
Anca C. Ferche
Oguzhan Bayrak

May 2022

Published September 2022

<https://library.ctr.utexas.edu/ctr-publications/5-6652-01-1.pdf>



Technical Report Documentation Page

1. Report No. FHWA/TX-22/5-6652-01-1	2. Government Accession No.	3. Recipient's Catalog No.	
4. Title and Subtitle Shear Behavior of Spliced Post-Tensioned Girders with UngROUTED Tendons: Final Report		5. Report Date Submitted: May 2022 Published: September 2022	
		6. Performing Organization Code	
7. Author(s) Sangyoung Han, Jarrod Zaborac, Zachary D. Webb, Jongkwon Choi, Anca C. Ferche, and Oguzhan Bayrak		8. Performing Organization Report No. 5-6652-01-1	
9. Performing Organization Name and Address Center for Transportation Research The University of Texas at Austin 3925 W. Braker Lane, 4 th Floor Austin, TX 78759		10. Work Unit No. (TRAIS)	
		11. Contract or Grant No. 5-6652-01	
12. Sponsoring Agency Name and Address Texas Department of Transportation Research and Technology Implementation Division 125 E. 11th Street Austin, TX 78701		13. Type of Report and Period Covered Technical Report May 2019–May 2022	
		14. Sponsoring Agency Code	
15. Supplementary Notes Project performed in cooperation with the Texas Department of Transportation and the Federal Highway Administration.			
16. Abstract <p>This experimental study was developed to evaluate the shear performance of spliced post-tensioned girders with grouted and ungrouted ducts. Demand for expedited construction processes and increased girder spans make spliced girder systems attractive options for medium- to long-span bridges. Since the spliced girder elements are subjected to significant shear forces, it is required to check the shear capacity of post-tensioned girders containing grouted and ungrouted ducts. The current shear design provisions in the American Association of State Highway and Transportation Officials Load and Resistance Factor Design (AASHTO LRFD) Bridge Design Specifications include shear strength reduction factors to account for the presence of the duct in the web and its condition (i.e., grouted or ungrouted). These factors are applied to the shear resistance provided by the concrete component, as well as to the shear resistance provided by the shear reinforcement. The reduction factors in AASHTO LRFD were developed from a limited database that did not include ungrouted post-tensioning systems, resulting in incomplete code specifications. This lack of knowledge served as the motivation for this study. The experimental program involved the design and test of six large-scale specimens incorporating the following main variables: (i) three different duct layouts (straight, parabolic, and hybrid) and (ii) the utilization of grouted and ungrouted ducts. Two tests were performed on each specimen, resulting in a total of twelve tests. All tests resulted in similar failure modes, such as localized web crushing at the duct area in the critical section, regardless of duct filler and tendons profile. Additionally, the normalized shear stress values were similar for the grouted and ungrouted specimens. These tests serve as validation studies for the updated shear strength reduction factors proposed for implementation in AASHTO LRFD.</p>			
17. Key Words AASHTO LRFD, Grouted Duct, MCFT, Nominal Shear Resistance, Post-Tensioned Member, Post-Tensioning, Shear, Spliced Precast Girder, UngROUTED Duct		18. Distribution Statement No restrictions. This document is available to the public through the National Technical Information Service, Alexandria, Virginia 22312; www.ntis.gov.	
19. Security Classif. (of report) Unclassified	20. Security Classif. (of this page) Unclassified	21. No. of pages 181	22. Price



**THE UNIVERSITY OF TEXAS AT AUSTIN
CENTER FOR TRANSPORTATION RESEARCH**

Shear Behavior of Spliced Post-Tensioned Girders with UngROUTED Tendons: Final Report

Sangyoung Han
Jarrod Zaborac
Zachary D. Webb
Jongkwon Choi
Anca C. Ferche
Oguzhan Bayrak

CTR Technical Report:	5-6652-01-1
Report Date:	Submitted: May 2022
Project:	5-6652-01
Project Title:	Shear Behavior of Spliced Post-Tensioned Girders with UngROUTED Tendons
Sponsoring Agency:	Texas Department of Transportation
Performing Agency:	Center for Transportation Research at The University of Texas at Austin

Project performed in cooperation with the Texas Department of Transportation and the Federal Highway Administration.

Center for Transportation Research
The University of Texas at Austin
3925 W. Braker Lane, 4th floor
Austin, TX 78759

<http://ctr.utexas.edu/>

Disclaimers

Author's Disclaimer: The contents of this report reflect the views of the authors, who are responsible for the facts and the accuracy of the data presented herein. The contents do not necessarily reflect the official view or policies of the Federal Highway Administration or the Texas Department of Transportation (TxDOT). This report does not constitute a standard, specification, or regulation.

Patent Disclaimer: There was no invention or discovery conceived or first actually reduced to practice in the course of or under this contract, including any art, method, process, machine manufacture, design or composition of matter, or any new useful improvement thereof, or any variety of plant, which is or may be patentable under the patent laws of the United States of America or any foreign country.

Engineering Disclaimer

NOT INTENDED FOR CONSTRUCTION, BIDDING, OR PERMIT PURPOSES.

Project Engineer: Oguzhan Bayrak

Professional Engineer License State and Number: Texas No. 106598

P.E. Designation: Research Supervisor

Acknowledgments

The authors are grateful to the Texas Department of Transportation (TxDOT) for providing funds to conduct this research study. The contributions of the Project Monitoring Committee—Joanne Steele (Project Manager), Christina Gutierrez, Greg Turco, Jason Tucker, Joe Roche, Leon Flournoy, and Michael Hyzak—are deeply appreciated. Many thanks are due to Valley Prestress Products, Inc. in Eagle Lake, Texas, for fabricating the girders that were used for the experimental program. Special thanks are also offered to the numerous students and staff members at Ferguson Structural Engineering Laboratory for ensuring the successful completion of the research project.

Table of Contents

Chapter 1. Introduction	1
1.1. Overview	1
1.2. Project Objective and Scopes.....	3
1.3. Organization.....	4
Chapter 2. Literature Review	5
2.1. AASHTO LRFD General Procedure	5
2.1.1. Nominal Shear Resistance in AASHTO LRFD.....	5
2.1.2. Effective Web Width Factor, b_v	6
2.1.3. Shear Strength Reduction Factor, λ_{duct}	7
2.2. Shear Resistance of the Post-Tensioned Beam	9
Chapter 3. Fabrication of Test Specimens	10
3.1. Design of Test Specimens.....	10
3.1.1. Overview	10
3.1.2. Post-Tensioning Layout	11
3.1.3. End-Block	12
3.1.4. Pretensioning Strands.....	14
3.1.5. Post-Tensioning Anchorage.....	14
3.1.6. Capacity Estimation	15
3.2. Test Specimen Fabrication.....	18
3.2.1. Overview	18
3.2.2. Concrete Mixture and Materials Sampling	19
3.2.3. Test Specimen Fabrication.....	21
3.2.4. Post-Tensioning Procedure	26
3.2.5. CIP Deck Concrete	32
3.3. Instrumentation during Fabrication.....	33
3.3.1. Overview	33
3.3.2. Installation of DAQ System.....	33
3.3.3. Configuration of DAQ System	35
3.3.4. Monitoring Test Specimens at VPP	36
3.4. Summary of Fabrication	37
Chapter 4. Experimental Program.....	38
4.1. Structural Test Configuration and Protocol	38
4.2. Instrumentation during Structural Test	44

4.2.1. Agilent DAQ System	45
4.2.2. Campbell DAQ System.....	46
4.2.3. Motion Capture System	47
4.3. Experimental Results and Observations	48
4.3.1. Input Properties for AASHTO Shear Design.....	48
4.3.2. Failure Mechanism.....	51
4.3.3. Web Behavior	57
4.3.4. Behavior of Specimen with UngROUTED Ducts	63
4.3.5. Summary of Test Results	65
4.3.6. Experimental Shear Capacity versus AASHTO LRFD	75
4.4. Summary of Experimental Program	76
Chapter 5. Development of Design Recommendations	77
5.1. Overview	77
5.2. Proposed Modification for the Calculation of $V_{n1}=V_c+V_s+V_p$	78
5.2.1. Effective Web Width Factor, b_v	78
5.2.2. Duct Diameter Correction Factor, δ	80
5.3. Proposed Modification for the Calculation of $V_{n2}=0.25f'_c b_v d_v$	81
5.4. Evaluation of Proposed Modifications.....	89
5.5. Summary of Design Recommendations.....	91
Chapter 6. Summary and Conclusion	92
6.1. Summary	92
6.2. Proposed Changes to the AASHTO LRFD	92
6.3. Concluding Remarks.....	94
References.....	95
Appendix A. Test Specimen Drawings.....	98
Appendix B. Rendering of End-Block Reinforcement	109
Appendix C. Post-Tensioning: Assemblies	112
Appendix D. Daily Reports for Fabrication.....	114
Appendix E. Embedded Location of VWGs.....	153
Appendix F. Prestress Loss Calculation	155
Appendix G. Internal Cracking Survey	159
Appendix H. Strength Capacity Calculation.....	160
Appendix I. Proposed Modification of AASHTO LRFD	164

List of Tables

Table 3.1 Moment capacity of each specimen at critical section and loading point	17
Table 3.2 Shear capacity calculation based on AASHTO LRFD	17
Table 3.3 Concrete mixture design used in test specimens	19
Table 3.4 Results of slump flow test.....	20
Table 3.5 Samples of reinforcing bars and strands collected.....	20
Table 4.1 Web expansion at the critical section determined by VWGs	59
Table 4.2 Service level cracking for grouted and ungrouted specimens	68
Table 4.3 Test result Summary with a ratio of test result to nominal shear resistance.....	76
Table 5.1 Proposed modification for shear design of girders containing post-tensioned ducts.....	89
Table E.1 Proposed number of VWGs for each test specimen.....	153
Table F.1 Comparison of prestress loss between AASHTO LRFD estimation and actual prestress loss using the monitored strain data in test specimens with grouted tendon.....	158
Table F.2 Comparison of prestress loss between AASHTO LRFD estimation and actual prestress loss using the monitored strain data in test specimens with ungrouted tendon	158
Table H.1 Moment capacity of each specimen at critical section and loading point	160

List of Figures

Figure 1.1 Construction Process of Continuous Spliced Girder (Reproduced from Dolan and Hamilton 2019).....	3
Figure 2.1 Accounting for the Reduction in Shear Strength as a result of a Post-Tensioning Duct by Reducing the Transverse Reinforcement Contribution (Adopted from Moore et al., 2015).....	7
Figure 2.2 Shear Force Resisting Mechanisms in a Cracked, Post-Tensioned Beam	9
Figure 3.1 Cross Sections of Test Specimens of Tx62-PSG and Tx62-PSU: (a) End-Block; (b) Critical Section; and (c) Mid-Span	10
Figure 3.2 Duct Layout with the Location of Couplers	11
Figure 3.3 Strut-and-Tie Models for Vertical and Horizontal Bursting Forces....	13
Figure 3.4 Stress-Strain Curve for Prestressed Reinforcing Bars	16
Figure 3.5 Precast Plant with the Location of Prestressing Beds and Batch Plants	18
Figure 3.6 As-Built Construction Schedule and Procedures at Precast Plant.....	19
Figure 3.7 Completion of Production for Prestressed Girders at the Precast Plant	21
Figure 3.8 Production of Prestressed Girders: (a) Strands and End Forms Placement; (b) Single Strand Prestressing; (c) Post-Tensioning Anchorage Assembly; (d) Rebar Placement; (e) Side Form Close; and (f) Concrete Casting	24
Figure 3.9 Preparation for Post-Tensioning Procedure: (a) Delivery of Prestressed Girder; (b) Inspection of Each Duct before Strands Placement; (c) Inserted Strands; and (d) Instrumentation during Post-Tensioning	27
Figure 3.10 Post-Tensioning Procedure: (a) Cutting Strands before Inserting Anchor Head; (b) Inserted Anchor Head; (c) Installation of Wedges; (d) Installation of Center-Hole Ram; (e) Post-Tensioning Strands; and (f) Completion of Post-Tensioning	30
Figure 3.11 Installation of (a) Supports and (b) CIP Deck Concrete.....	32
Figure 3.12 The Model 4200 of vibrating wire gauge (Geokon 2017).....	33
Figure 3.13 Locations of Embedded VWGs: (a) Longitudinal Direction of VWGs (i.e., Tx62-PSG & PSU); (b) Out-of-Plane Direction of VWGs (i.e., Tx62-PSG & PSU); and (c) VWGs along the Length of Test Specimen (i.e., Tx62-0SG & 0SU)	34
Figure 3.14 Fully Equipped Enclosures for Field Monitoring: (a) Enclosure with a Data Logger (Model: CR 3000) and Two Analyzers (Model: AVW 200) and (b) Enclosure with a Multiplexer (Model: AM 16/32B)	35
Figure 3.15 Configuration of the DAQ System for Field Monitoring	35

Figure 3.16 Logistics Plan for Production and Storage Areas of Fabricated Test Specimens: (a) Overhead View of Key Logistics Areas; (b) Fabricated Test Specimens in Storage Area; and (c) Protected DAQ System with Solar Panels ..	36
Figure 4.1 The Design of Shear Structural Test Schematic.....	38
Figure 4.2 As-Built Structural Schematic: (a) Overall Structural Setup with the Test Specimen and (b) Designed Monitoring and Controlling Area during the Test	38
Figure 4.3 Rendering of Structural Test (Elevated Slab in FSEL)	39
Figure 4.4 The Location of Loading Plate and Bottom Supports Cause Two Shear Failures and Corresponding Cracks in One Test Specimen.....	40
Figure 4.5 The Governed Failure Cracks of Moore et al.'s Specimens in Red (Moore et al., 2015)	42
Figure 4.6 The Corresponding Shear Diagram from Applied Load, Loading Frame, and Self-Weight	43
Figure 4.7 The Overall Plan View of Structural Testing Schematic and Locations of Instrumentation	44
Figure 4.8 Instrumentation Used during Structural Testing: (a) Load Cell for Total Load and L-Pot for Deflection; (b) Surface Strain Gauge and Inverted U-Frame for Web Responses; and (c) Electrical Resistance–Based Strain Gauge Applied to Strands.....	45
Figure 4.9 Fully Equipped Enclosures for Field Monitoring: (a) Enclosure with a CR 3000 Datalogger and Two AVW 200 Analyzers; (b) Enclosure with CR 6 Datalogger; and (c) Enclosure with AM 16/32B Multiplexer Model.....	46
Figure 4.10 Cross-Sectional View of the Locations of Embedded VWGs: (a) Location of Longitudinal Direction of VWGs (Tx62-PSU & PSG) and (b) Location of Out-of-Plane Direction of VWGs (Tx62-PSU & PSG)	47
Figure 4.11 Motion Capture System Used for Monitoring during the Structural Test: (a) a Camera with Motion Capture System Markers Applied on the Web Surface and (b) Sample Data after Post-Processing	47
Figure 4.12 The Results of Material Tests: (a) the Compressive Test Results of Concrete at 28 Days and Test Day; (b) the Yield Strength of Reinforcing Bars and 0.6-In. Seven-Wire Strands for Pretensioning and Post-Tensioning; and (c) Stress-Strain Response of Reinforcing Bars and Strand.....	49
Figure 4.13 Prestress Loss of Test Specimen: (a) Garber Model to Determine the Prestress Loss based on Embedded VWGs and (b) the Final Gauge-Measured Prestress Loss Compared to the AASHTO LRFD Estimation	50
Figure 4.14 Structural Setup and Three Distinct Cracking Modes Related to Loading and Deflection.....	51
Figure 4.15 Shear Load-Deflection Plots of All Test Specimens with Surface Cracks	52

Figure 4.16 Surface Cracking Survey along the Girder Length after Two Combined Tests	55
Figure 4.17 Internal Cracking Survey at Critical Section.....	56
Figure 4.18 Internal Compressive Stress Flow in Thin Web of Post-Tensioned Girder and Concrete Panel Analogy of the Specimens without Duct, Grouted Duct, and Empty Duct (Adopted from Moore et al., 2017).....	57
Figure 4.19 Splitting and Crushing Failure Mechanisms of Panel-Based Specimens (Wald et al., 2017)	58
Figure 4.20 Cross-Sectional Area with the State of Compressive and Tension in terms of the Increased Thickness (Moore et al., 2015).....	58
Figure 4.21 Vertical Strain Development at the Critical Section during the Structural Test.....	60
Figure 4.22 Vertical Strain Development at the Critical Section during the Structural Test.....	61
Figure 4.23 Determined Principal Strain of ε_1 (Left Column) and ε_2 (Right Column)	62
Figure 4.24 Behavior of Post-Tensioning Strands and Corresponding Loads during the Test: (a) Post-Tensioning of Tx62-P0U and (b) Post-Tensioning of Tx62-0SU.....	63
Figure 4.25 CIP Overlay Repair Concrete Placement: (a) Anchored Rebar Cage and (b) Completion of Repair Concrete Placement on Each Damaged Side.....	64
Figure 4.26 The Analysis of Service Level Loading: (a) Initial Cracking at the Critical Section; (b) Attached Surface Gauges; and (c) Vertical Strain Development	67
Figure 4.27 Summary of Failure Loads from the 12 Tests: (a) Failure Load from Each of the 12 Tests and (b) Average of Two Tests' Failure Load for Each of the Six Tested Specimens	69
Figure 4.28 Stiffness Analysis to Define Nonlinear Behavior (Left Column) and Shear Force Behavior (Right Column) with Respect to Deflection	70
Figure 4.29 Normalized Ultimate Shear Stress: (a) Using the Effective Web Width (b_v) and (b) Using the Gross Web Width (b_w)	74
Figure 5.1 Cracking Propagation and Average Cracking Spacing at the Ultimate Load Level	78
Figure 5.2 The State of Residual Tensile Stress Using Vision System: (a) Vision System Monitoring the Shear Span and (b) State of Tensile Stress at the Ultimate Load Level	79
Figure 5.3 Duct Diameter Correction Factor (δ) for: (a) the Current Edition of AASHTO LRFD for Grouted Duct and (b) the Proposed Modification for Ungrouted Duct.....	80

Figure 5.4 The Ultimate Failure Mode of Localized Web Crushing in Specimens with Grouted (Tx62-0SG) or UngROUTed (Tx62-0SU) Ducts	81
Figure 5.5 The Conceptual Theory of Internal Stress Flow for Grouted and UngROUTed Ducts: (a) Currently Adopted Mechanism Considering Elasticity (Muttoni et al., 2006; Moore et al., 2015) and (b) Proposed Approach Considering Plasticity at the Ultimate Load Level.....	82
Figure 5.6 The State of Stress Condition: (a) Concrete and (b) Transverse Reinforcement Component	84
Figure 5.7 Theory Related to Web Crushing: (a) the Simplified MCFT (Reproduced by Bentz et al., 2006) and (b) the Concept of Effective Web Width Factor	85
Figure 5.8 The Normalized Shear Stress Level Using the Structural Test with Respect to the Effective Web Width Correction Factor, k	87
Figure 5.9 The Calculation of Nominal Shear Resistance using: (a) Current AASHTO LRFD Equations and (b) Proposed Modifications	90
Figure B.1 Rendering of End-Block Reinforcement (Isometric View).....	109
Figure B.2 A Bars	110
Figure B.3 C Bars	110
Figure B.4 D Bars	110
Figure B.5 DS Bars	110
Figure B.6 H Bars	110
Figure B.7 HS Bars	110
Figure B.8 R Bars	111
Figure B.9 RE Bars	111
Figure B.10 Spiral	111
Figure B.11 T Bars.....	111
Figure B.12 U Bars	111
Figure E.1 Proposed Location of VWGs for the Test Specimens Containing the Grouted Tendon	153
Figure E.2 Proposed Location of VWGs for the Test Specimens Containing the UngROUTed Tendon	154
Figure G.1 Internal Cracking Survey at Critical Section from all 12 tests	159
Figure H.1 Shear Parameters for Shear Capacity Estimations	161

Chapter 1. Introduction

1.1. Overview

Spliced post-tensioned girder technology has emerged as a powerful construction application in the U.S. bridge network since the late 1900s (Castrodale & White, 2004). The configuration of the spliced post-tensioned girder implementation incorporates various post-tensioning systems in continuous prestressed precast members. The key to a successful construction process is to fabricate the prestressed concrete girders off-site, and thereafter unify the transferred precast girders by using post-tensioning tendons at the construction site, as shown in Figure 1.1 (Dolan & Hamilton, 2019). This construction process enables several attractive features such as expediting construction and increasing the bridge length to approximately 300 feet (Hamilton & Brenkus, 2013). Due to the aforementioned benefits, the spliced post-tensioned precast girder system has been widely adopted. Design guidelines for this system have been implemented in the American Association of State Highway and Transportation Officials Load and Resistance Factor Design (AASHTO LRFD) Bridge Design Specification, establishing shear strength reduction factors based on the diameter of the duct and its condition (i.e., grouted or ungrouted ducts; AASHTO, 2020). The shear capacity of a post-tensioned concrete girder can be determined by using these factors with the established AASHTO LRFD shear equation, which is based on the Modified Compression Field Theory (MCFT; Vecchio & Collins, 1986).

When spliced girders with multistrand post-tensioning systems are utilized, post-tensioning ducts are injected with a cement-based mix, as the primary choice for corrosion protection, referred to as grouted duct hereafter (Collins & Mitchell, 1991). The grout mix plays a pivotal role in providing an alkaline environment for the post-tensioning duct, thereby maintaining a high level of pH—chemical protection from corrosion deterioration.

However, once the post-tensioning ducts are grouted, it is difficult to inspect the status of tendons and the quality of grout. As a non-destructive inspection method for the inside condition of the post-tensioning duct is not available, the determination of tendon's status solely relies on a destructive inspection. Although recent grout quality has been significantly improved, inspection and long-term quality assurance of tendons embedded in the grout are still challenging, and corrosion issues have been reported (FDOT, 2002). More importantly, the perfect bond condition makes it significantly difficult to replace the damaged tendons without costly demolition of precast girders. This led to the interest in post-

tensioned concrete girder that uses commercially available flexible fillers in lieu of cementitious grout to fill the post-tensioning ducts, referred to as ungrouted duct hereafter. Based on the anticipated benefits of ungrouted duct system, Hamilton et al. (2017) evaluated the constructability using non-cementitious flexible filler materials, such as petroleum wax, grease, and gel, and successfully proved viable options for the replacement of grout mix. The use of flexible fillers can overcome the innate problem of grout quality and ease prospective tendon replacement procedures. To this end, an alternative non-cementitious material to fill the post-tensioning duct has been adopted by the Florida Department of Transportation (FDOT 2022).

The University of Texas at Austin's series of research investigations on the implications of spliced girder technology (Moore et al., 2015; Wald et al., 2017; Williams et al., 2015) indicated that the large-scale experimental program's results are in disagreement with the assumptions of the small-scale panel tests by Muttoni et al. (2006) and Wald et al. (2017). The findings from Moore et al. (2015) resulted in updating the AASHTO General Procedure for shear design (hereafter AASHTO LRFD), which was originally evaluated based on the results of small-scale panel tests of precast girders with post-tensioning ducts. However, Moore et al. (2015) evaluated large-scale post-tensioned members with grouted ducts only. Thus, the AASHTO LRFD general shear design provisions were therefore based on an incomplete database of specimens and could result in potentially poorly designed post-tensioned girders with ungrouted ducts. Thus, large-scale testing was necessary to investigate the response of ungrouted post-tensioning systems.

This research need led to the development of the work presented herein, conducted to evaluate the shear performance of ungrouted ducts in the post-tensioned girders. This objective could be accomplished with a well-designed experimental program comparing the same post-tensioning profiles under grouted and ungrouted conditions. In addition, various post-tensioning profiles that adopt the post-tensioning design variations were also considered in this study. Thus, the experimental program included the following main variables: (i) three different duct layouts (i.e., straight, parabolic, hybrid) and (ii) grouted and ungrouted ducts for each layout. Note that since the contribution of flexible filler to shear behavior is presumably negligible, it was assumed that the shear performance of post-tensioning girders with flexible fillers would be the same as for those with empty ducts (i.e., ungrouted duct).

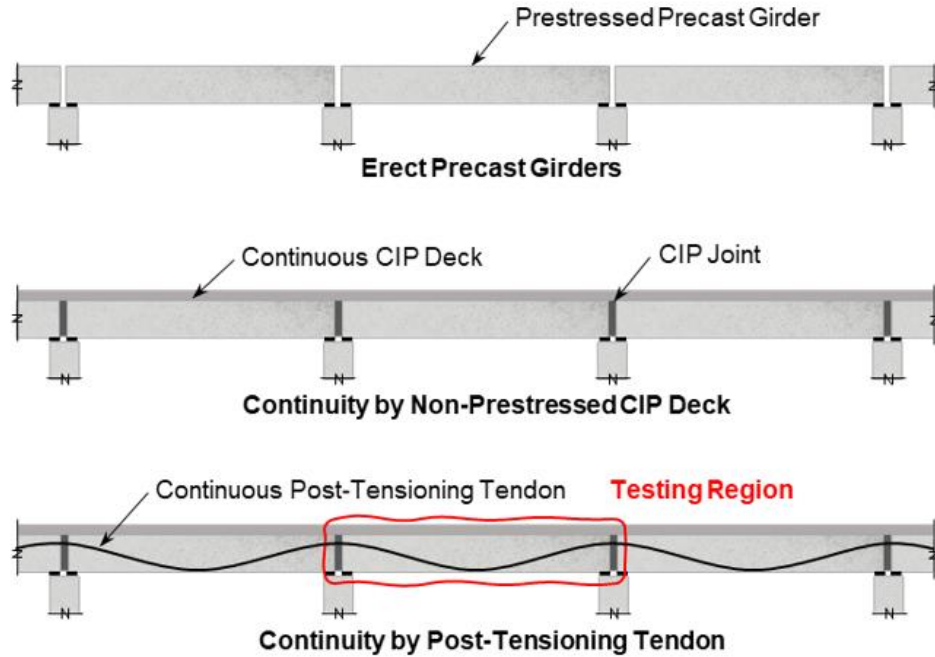


Figure 1.1 Construction Process of Continuous Spliced Girder (Reproduced from Dolan and Hamilton 2019)

1.2. Project Objective and Scopes

The primary objective of this research project was to develop recommendations for the shear design of post-tensioned I-girders with ungrouted ducts or for cases in which ducts are injected with flexible fillers. Grouting condition (i.e., grouted vs. ungrouted) and duct layout (i.e., straight, parabolic, hybrid) were selected as the primary test variables. To achieve the research objective, this study (i) prepared six test specimens fabricated in a precast plant, to ensure the fabrication practices were consistent with those used for precast bridge elements; (ii) conducted twelve full-scale laboratory tests on the girders to study the shear behavior; and (iii) evaluated the structural responses from full-scale tests and compared the test results to the estimation of shear strength according to AASHTO LRFD. The findings from large-scale, realistic tests could offer not only realistic shear strength reduction factors to be incorporated into AASHTO LRFD but also a better understanding of the failure mechanism in post-tensioned concrete members.

1.3. Organization

This research report summarizes the proposed modifications to the guidelines for the shear design of post-tensioned concrete members in AASHTO LRFD. The proposed changes were derived from an in-depth analysis of the results from the experimental program undertaken in this implementation project (5-6652-01), as well as the relevant test data from TxDOT project 0-6652-1 (Moore et al., 2015). This research report is organized as follows: Chapter 2 reviews the rational theories for shear strength calculation and sectional shear design using AASHTO LRFD for the post-tensioned concrete member. Chapter 3 details the fabrication of the test specimens along with their structural design and instrumentation plan. Chapter 4 describes how the experimental program was conducted and the research team's observations. Chapter 5 analyzes the results of the structural test alongside the relevant test data from 0-6652-1 (Moore et al., 2015) and recommends modifications to the shear design specification in AASHTO LRFD. Finally, Chapter 6 summarizes the project's findings and conclusions. Additionally, Appendices A through I provide supplemental information such as test specimen drawings, renderings of end-block reinforcement, brochures for post-tensioning assemblies, daily fabrication reports, details of the embedded locations of vibrating wire gauges, prestress loss calculations, internal cracking survey, strength capacity calculation, and proposed in-line revisions to the current AASHTO LRFD provisions.

Chapter 2. Literature Review

2.1. AASHTO LRFD General Procedure

The AASHTO LRFD General Procedure for sectional shear design is based on the MCFT (Vecchio & Collins, 1986), which is a behavioral model for the response of cracked reinforced concrete members subjected to in-plane loading. A series of simplifying assumptions were made to recast MCFT into design equations, such as the following: the longitudinal strain is distributed linearly over the depth of the member; the orientation of the compressive stress field is unchanged over the depth; and the stirrups yield before concrete crushing.

2.1.1. Nominal Shear Resistance in AASHTO LRFD

The nominal shear resistance in AASHTO LRFD (2020) is calculated as the lesser of the following two equations:

$$V_{n1} = V_c + V_s + V_p \quad \text{Equation 1}$$

$$V_{n2} = 0.25 f'_c b_v d_v + V_p \quad \text{Equation 2}$$

Equation 1 represents the shear resistance provided by the concrete component, V_c , the transverse reinforcement, V_s , and the component of prestressing force in the direction of the shear force, V_p , taken as positive if it is resisting the applied shear. Equation 2 is an upper limit on the nominal shear resistance intended to ensure that the concrete in the web will not crush prior to the yield of the transverse reinforcement.

The shear resistance contribution of the concrete, V_c , represents the ability of cracked concrete to carry shear stresses through aggregate interlock action, and it is evaluated as:

$$V_c = 0.0316 \beta \sqrt{f'_c} b_v d_v \quad \text{Equation 3}$$

where b_v represents the effective web width (to be discussed in detail in Section 2.1.2), d_v indicates the effective shear depth, f'_c is the compressive strength of concrete for use in design, and β indicates the ability of diagonally cracked concrete to transmit tension and shear.

The shear resistance provided by the transverse reinforcement, V_s , was derived from a truss model, initially developed by Ritter (1899), and is calculated as:

$$V_s = \frac{A_v f_y d_v (\cot \theta + \cot \alpha) \sin \alpha}{s} \lambda_{duct} \quad \text{Equation 4}$$

where A_v is determined by the area of a transverse reinforcement within distance s , d_v indicates the effective shear depth, f_y is the specified minimum yield strength of reinforcement, s is the spacing of transverse reinforcement, α is the angle of inclination of transverse reinforcement to the longitudinal axis, θ is the angle of inclination of diagonal compressive stresses, and λ_{duct} accounts for the reduction in shear strength due to the presence of a post-tensioning duct in the thin web, to be discussed in detail in Section 2.1.3.

One of the assumptions of the shear design provisions in AASHTO LRFD is that the stirrups shall yield before the concrete fails in compression through web crushing. A study by Bentz et al. (2006) derived an ultimate shear stress limit of $0.25f'_c$ and validated the normalized shear stress to prevent concrete crushing prior to stirrup yielding. This led to the development of Equation 2 as an upper limit imposed on the nominal shear resistance.

2.1.2. Effective Web Width Factor, b_v

The reduction in shear resistance due to the presence of ungrouted ducts is taken into account by reducing the web width, as per Article 5.7.2.8 in AASHTO LRFD. The effective web width, b_v , is calculated as:

$$b_v = b_w - k \cdot \phi_{duct} \quad \text{Equation 5}$$

where b_w is the gross web width, k is the effective web width correction factor, and ϕ_{duct} is the duct diameter. For post-tensioned members with ungrouted ducts, the web width is reduced by the diameter of the duct; therefore, k has a value equal to 1.0. No web width reduction is applied for grouted ducts; as such, k has a value equal to 0.0 for post-tensioned systems with grouted ducts.

Historically, the coefficient of k has been evaluated based on results obtained from small-scale panel tests, designed to be representative of the diagonal compressive strut formed by shear loading within a beam (Muttoni et al., 2006; Wald et al., 2017). The coefficient k was assigned values based on the duct material (corrugated metal or plastic), as well as the duct conditions (grouted or ungrouted). The current values for k in AASHTO LRFD were derived from large-scale post-tensioned tests on I-girder specimens conducted by Moore et al. (2015) and solely consider the duct conditions.

2.1.3. Shear Strength Reduction Factor, λ_{duct}

AASHTO LRFD accounts for the reduction in shear resistance due to the presence of grouted ducts through the shear strength reduction factor, λ_{duct} , introduced in the calculation of the transverse reinforcement contribution, V_s . The shear strength reduction factor, λ_{duct} , was derived based on the reduction in the strength of the concrete compressive diagonal strut due to the presence of a post-tensioning duct, as shown in Figure 2.1. The reason behind this approach is rooted in the fact that the transverse reinforcement contribution to the nominal shear strength is limited by the ability of the truss mechanism to resist the shear force demand through both the tensile capacity of the transverse reinforcement and the compressive capacity of the concrete in the web (Kuchma, 2013; Moore et al., 2015).

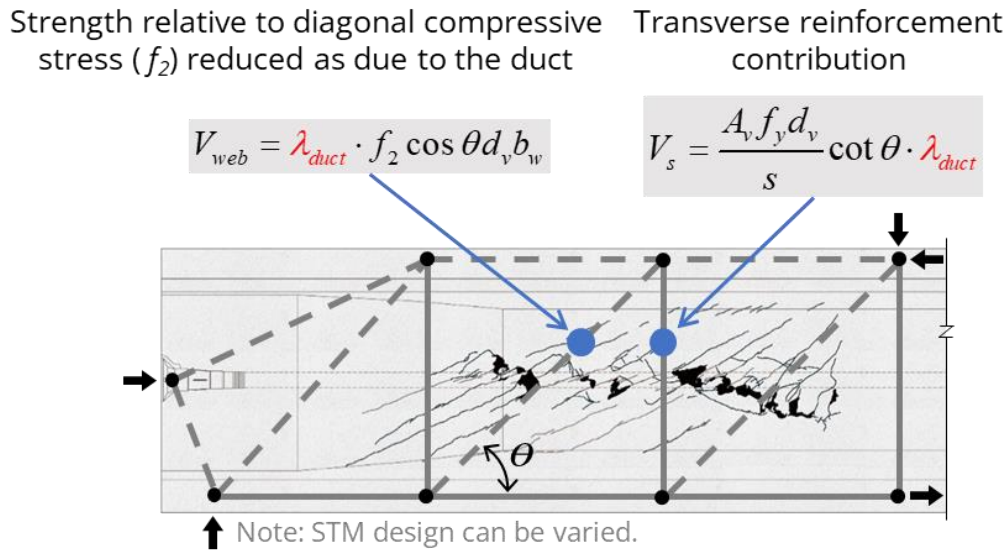


Figure 2.1 Accounting for the Reduction in Shear Strength as a result of a Post-Tensioning Duct by Reducing the Transverse Reinforcement Contribution (Adopted from Moore et al., 2015)

The discontinuity in the concrete compressive stress field, introduced by the presence of the duct, disrupts the internal force transfer in the assumed truss mechanism between the transverse reinforcement and the concrete compression struts. The detrimental effect of the presence of the duct was expressed through the introduction of λ_{duct} in the calculation of the force developed in the concrete compression strut, V_{web} , as per Equation 6:

$$V_{web} = \lambda_{duct} \cdot f_2 \cos \theta d_v b_w \quad \text{Equation 6}$$

From equilibrium, the vertical component of the concrete compressive strut is equal to the force developed in the tie, representing the transverse reinforcement, as shown in Equation 7:

$$(\lambda_{duct} \cdot f_2 \cos \theta d_v b_w) \sin \theta = \frac{A_v f_y d_v \cot \theta}{s} \cdot \lambda_{duct} \quad \text{Equation 7}$$

Thus, the nominal shear resistance, V_{nl} , can be expressed as per Equation 8, which is similar to the AASHTO LRFD (2020) shear strength equation when the direction of transverse reinforcement is vertical ($\alpha = 90^\circ$).

$$V_{nl} = V_c + V_s + V_p = 0.0316 \beta \sqrt{f'_c} b_v d_v + \frac{A_v f_y d_v \cot \theta}{s} \lambda_{duct} + V_p \quad \text{Equation 8}$$

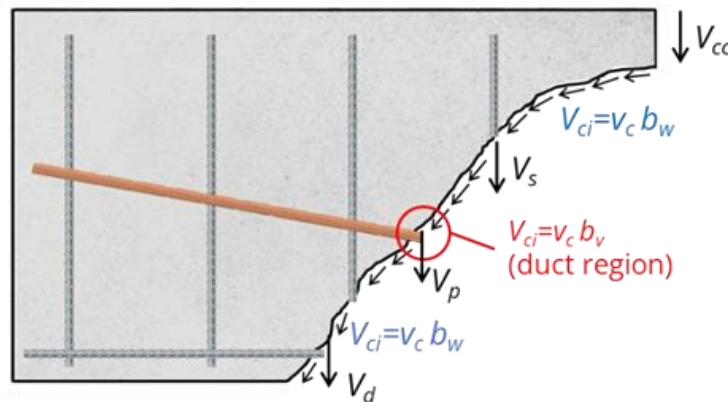
The factor λ_{duct} is calculated as a function of the duct diameter correction factor, δ , duct diameter, ϕ_{duct} , and gross web width, b_w , as shown in Equation 9:

$$\lambda_{duct} = 1 - \delta \cdot \left(\frac{\phi_{duct}}{b_w} \right)^2 \quad \text{Equation 9}$$

The value of δ accounts for whether the post-tensioning duct is grouted or ungrouted. Moore et al. (2015) validated the value of δ equal to 2.0 for grouted ducts based on the results of their large-scale experimental program. For ungrouted ducts, the value of δ was taken as 0.0 to remove the capacity of the shear strength reduction factor (λ_{duct}), as no data were available. This lack of knowledge led to the present study to establish the shear strength reduction factor (λ_{duct}) of ungrouted ducts.

2.2. Shear Resistance of the Post-Tensioned Beam

Figure 2.2 illustrates the shear resistance of the post-tensioned beam after the onset of the inclined shear crack. The shear resisting mechanism incorporates the combined shear contributions from the uncracked concrete region, aggregate interlock across the crack interface, dowel action in the longitudinal reinforcement, transverse reinforcement crossing the diagonal crack, and prestressing force in the direction of shear force. The shear resistance of concrete (V_c) in the AASHTO LRFD accounts for the aggregate interlock force (V_{ci}), which relies on the aggregate interlock stress (v_{ci}) acting along the crack across the gross web width (b_w). More importantly, this conceptual figure shows where the aggregate interlock force is reduced by the embedded duct; however, it indicates the negligible effect of the duct on the overall aggregate interlock force due to the small area of duct size compared to the overall height of the beam.



Notation:

- V_{cc} : Shear in uncracked concrete
- V_{ci} : Aggregate interlock
- V_d : Dowel action from longitudinal reinforcement
- V_s : Transverse reinforcement
- V_p : Vertical component of tensioned strand

Figure 2.2 Shear Force Resisting Mechanisms in a Cracked, Post-Tensioned Beam

Chapter 3. Fabrication of Test Specimens

3.1. Design of Test Specimens

3.1.1. Overview

This section summarizes the key properties of the test specimens designed for the current project. Reference drawings are presented in Appendix A. The test specimens were uniformly 50-foot-long Tx62 girders, identical to those fabricated for project 0-6652-1 (Moore et al., 2015). The web width and the duct diameter were selected as nine inches and four inches, respectively, to best represent the construction practices of Texas Department of Transportation (TxDOT) girders, following input from the Project Monitoring Committee. To accommodate the post-tensioning anchorages, a thickened end-block using Washington State Department of Transportation (WSDOT) details was selected and designed considering the post-tensioning tendons layout proposed for this experimental program. The overall dimensions of these girders are shown in Figure 3.1.

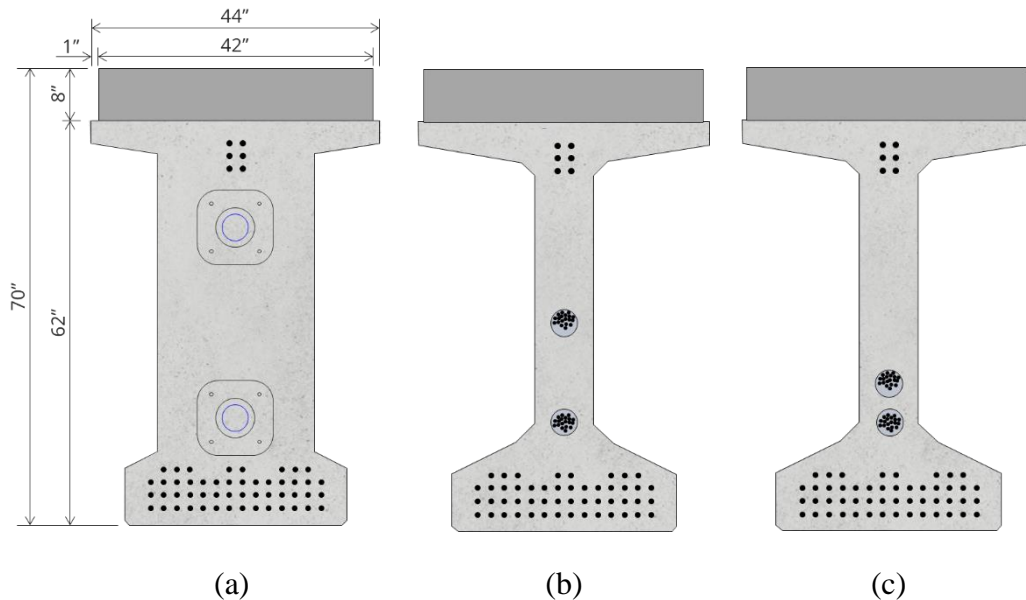


Figure 3.1 Cross Sections of Test Specimens of Tx62-PSG and Tx62-PSU: (a) End-Block; (b) Critical Section; and (c) Mid-Span

3.1.2. Post-Tensioning Layout

The girder specimens were fabricated with three different post-tensioning duct profiles: one straight duct, one parabolic duct, and a combination of one parabolic and one straight duct, as shown in Figure 3.2. More specifically, the first set of specimens, referred to as Tx62-0SG and Tx62-0SU, were fabricated with a straight duct positioned at the mid-height of the composite girder—Tx62 girder, a 62-in. in height with an 8-in. thick deck on top—which is identical to the location used in TxDOT Project 0-6652-1 (Moore et al., 2015). The second set of test specimens, referred to as Tx62-P0G and Tx62-P0U, were fabricated with a parabolic duct to investigate the effect of tendons curvature on sectional stress flow. The last set of fabricated specimens, referred to as Tx62-PSG and Tx62-PSU, had a parabolic duct at the same location as the second set and one additional straight duct at the intersection between the web and bottom flange.

Note the locations of the couplers in Figure 3.2—they were installed at mid-span and in the end regions. These locations were selected to avoid any undesired influence that the larger diameter duct coupler could have on the shear performance within the test region. Figure 3.2 illustrates the three different post-tensioning duct layouts, including the coupler locations.

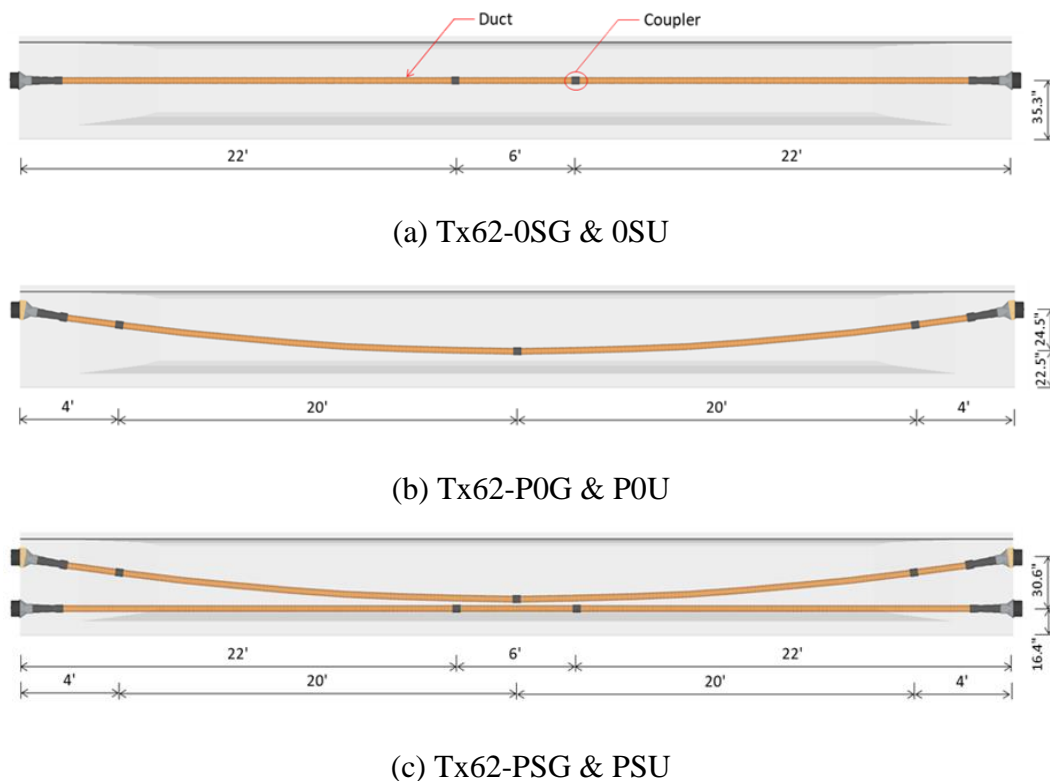


Figure 3.2 Duct Layout with the Location of Couplers

3.1.3. End-Block

To accommodate post-tensioning anchorages at the end regions of Tx62 girders and prevent any undesired end region failures, a typical enlarged WSDOT-type end-block was employed for this experimental program. Since the objective of this research project is to investigate the shear behavior of the beam web, not the behavior of the end-block or support region, the overall end-block design was done in a conservative manner. To this end, the most load-demanding post-tensioning layouts for the end blocks, including two post-tensioning ducts with nineteen strands per duct (Tx62-PSG and Tx62-PSU), were selected to design the bursting and splitting reinforcement. This was used for the end-block reinforcement for all test specimens.

3.1.3.1. Bursting Reinforcement

The bursting force, T_{burst} , and the location of the bursting force, d_{burst} , owing to the post-tensioning forces, may be calculated using Article 5.8.4.5.3 of AASHTO LRFD (2020) or a strut-and-tie method as per Article 5.8.2.7 of AASHTO LRFD (2020). To ensure the end-blocks were designed conservatively, the bursting and splitting forces were calculated using both methods and the most conservative result were selected to design the reinforcing steel. In cases where simplified methods were used based on Article 5.8.4.5.3 of AASHTO LRFD (2020), the bursting forces in the anchorage zone were calculated as follows:

$$T_{burst} = 0.25 \sum P_u \left(1 - \frac{a}{h} \right) + 0.2 \left| \sum (P_u \sin \alpha) \right| \quad \text{Equation 10}$$

The location of the bursting force, d_{burst} , can be taken as:

$$d_{burst} = 0.5(h - 2e) + 5e \sin \alpha \quad \text{Equation 11}$$

where T_{burst} is the tensile force in the anchorage zone acting ahead of the anchorage device and transverse to the tendon axis, P_u is the factored tendon force, d_{burst} is the distance from the anchorage device to the centroid of the bursting force, a is the lateral dimension of the anchorage device or group of devices in the direction considered, e is the eccentricity of the anchorage device or group of devices with respect to the centroid of the cross-section; always taken as positive, h is the lateral dimension of the cross-section in the direction considered, and α is the angle of inclination of a tendon force with respect to the centerline of the member, either positive for concentric tendons or if the anchor force points toward the centroid of the section or negative if the anchor force points away from the centroid of the section.

As shown in Figure 3.3, a strut-and-tie model (STM) was developed in accordance with Article 5.8.2.7 of AASHTO LRFD (2020). To simplify STM design, the inclination of the top post-tensioning anchorage was neglected and assumed as the perpendicular load to the end face of the end-block. The strut inclination of both STMs was assumed as a 1:2 slope; as such, both vertical and through-thickness tie forces were obtained as $P_{PT_u} / 4$.

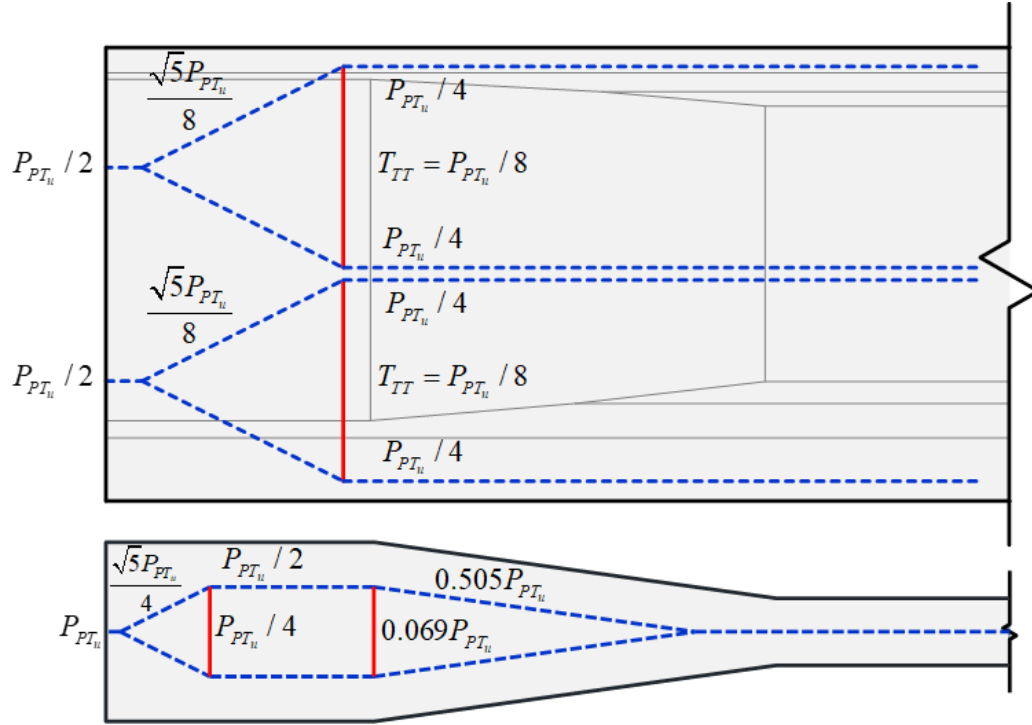


Figure 3.3 Strut-and-Tie Models for Vertical and Horizontal Bursting Forces

All pretensioning strands were assumed to be stressed to 75% of the ultimate tensile strength f_{pu} (i.e., $0.75f_{pu} = 202.5$ ksi). Thus, the total factored tendon force P_{PT_u} was calculated as 2004 kip, with a load factor of 1.2, according to Article 3.4.3.2 of AASHTO LRFD (2020) for the design force for post-tensioning anchorage zones, and the vertical and through-thickness tie forces were 501 kip and 639 kip, respectively. Therefore, the vertical and through-thickness bursting reinforcement areas were obtained as $A_{b,vertical} = 11.1 \text{ in}^2$ and $A_{b,through-thickness} = 11.4 \text{ in}^2$, respectively.

To prevent an undesired failure of the end block, the most conservative bursting load case was selected and used for the design of bursting reinforcement. A total of 36-#5 reinforcing bars were provided in the vertical direction and a total of 56-#4 reinforcing bars were distributed around the post-tensioning anchorages in the through-thickness direction.

3.1.3.2. Splitting Reinforcement (Article 5.9.4.4.1)

To provide splitting resistance at the ends of prestressed girders, the “four-percent” method of Article 5.9.4.4 in AASHTO LRFD (2020) was used to calculate the splitting reinforcement at the end region.

$$P_r = f_s A_s \geq 0.04(\text{pretensioning force}) \quad \text{Equation 12}$$

where f_s is the stress in the steel, not to exceed 20 kip, A_s is the total area of reinforcement located within the distance $h/4$ from the end of the beam, and h is the overall dimension of the precast member in the direction in which splitting resistance is being evaluated.

The splitting force was 98.4 kip, and the required splitting reinforcement was calculated as 4.92 in². Therefore, a total of 16-#5 reinforcing bars were distributed within 15.5 in. from the end of the member. The detailed rebar design of the end-block is summarized in Appendix B.

3.1.4. Pretensioning Strands

For this experimental program, 0.6-in. low-relaxation strands were used for pretensioning. A total of 58 pretensioning strands were provided; therefore, the total area of pretensioning strands was 12.15 in². Note that this is slightly less than the total area of pretensioning strands, 12.24 in², used for TxDOT Project 0-6652-1 (Moore et al., 2015). A total of 50 strands were provided at the tension side and 6 strands were placed at the compression side to relieve the top and bottom of stresses. To further control the concrete stresses at the beam ends, a total of 12 strands (21.4% of total strands in the tension side) were debonded over a total distance of 3 feet from each end of the girders.

3.1.5. Post-Tensioning Anchorage

Each test specimen contained one or two post-tensioning tendons comprised of nineteen 0.6-in. diameter low-relaxation prestressing strands. Anchorage assemblies (Model: ECI 6-19 Stressing Anchorage) and post-tensioning ducts (PT-Plus Duct) provided by VSL International were used as the multi-strand post-tensioning system for this project. The technical details of anchorage devices can be found in Appendix C.

3.1.6. Capacity Estimation

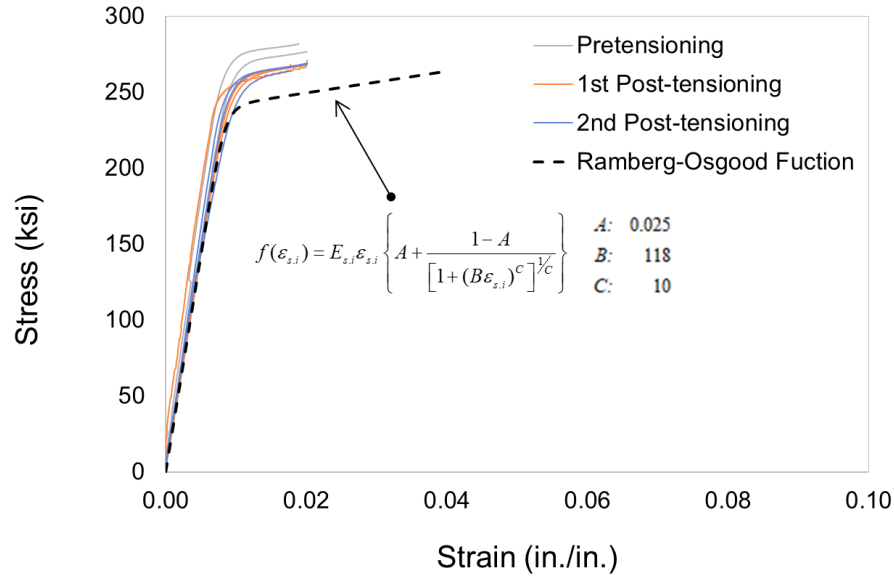
For the purpose of preliminary capacity estimation, the concrete strength at the test day, f'_c , was assumed to be 10 ksi. The ultimate tensile strength of pretensioning strands, f_{pu} , was assumed to be 270 ksi. The yield strength of non-prestressed bars, f_y , was assumed to be 60 ksi. Capacity estimations were used to ensure the shear-dominant failure of the test specimens.

3.1.6.1. Moment Capacity

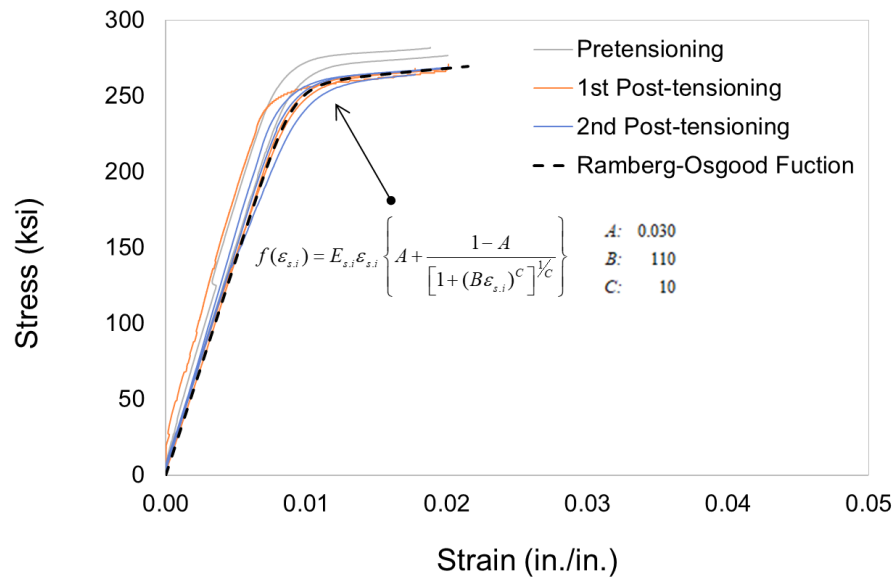
The moment capacities of the test specimens were calculated using the rectangular stress block approach. Concrete strain at failure is assumed as 0.003 in./in. and the rupture strain of strands is assumed as 0.043 in./in. The Ramberg-Osgood function recommended by Mattock (1979) for reinforcing bars was used as the constitutive model, expressed as:

$$f(\varepsilon_{s,i}) = E_{s,i} \varepsilon_{s,i} \left\{ A + \frac{1-A}{[1 + (B\varepsilon_{s,i})^C]^{1/C}} \right\} \quad \text{Equation 13}$$

where $E_{s,i}$ is Young's modulus of elasticity of the reinforcement, $\varepsilon_{s,i}$ is the strain of the reinforcement, A is the coefficient determined from the slope of the post-yielding branch, B is the coefficient determined from the intersection of the post-yielding branch and the stress axis, and C is the coefficient determined by trial-and-error to ensure a smooth transition between the two lines, as shown in Figure 3.4.



(a) Design Phase



(b) After Calibration

Figure 3.4 Stress-Strain Curve for Prestressed Reinforcing Bars

For the case of unbonded post-tensioning strands, the stress in the post-tensioning strands was calculated based on Article 5.6.3.1.2 of the AASHTO LRFD (2020). The moment capacities of each specimen, summarized in Table 3.1, were evaluated at the critical section and at the loading point during the design phase.

Table 3.1 Moment capacity of each specimen at critical section and loading point

Specimen ID	M_n (k-in.)	
	at critical section	at loading point
Tx62-0SG	189,916	189,916
Tx62-0SU	190,435	190,435
Tx62-P0G	190,714	199,360
Tx62-P0U	191,186	199,327
Tx62-PSG	227,007	234,962
Tx62-PSU	227,330	235,470

To ensure a shear-dominant failure of the test specimens, the anticipated ultimate moment at the loading point was increased by 20% and compared to the moment capacity. Based on the criteria proposed above, all of the elevated maximum moments $1.2M_u$ were less than the moment capacity M_n . As such, the controlling failure mechanism for all girders was expected to be the shear failure.

$$1.2M_u < M_n$$

Equation 14

3.1.6.2. Shear Capacity

For the purpose of estimating the shear capacity of test girders, the general shear design procedure in AASHTO LRFD (2020) was used. Since the primary purpose of this procedure is to evaluate the shear capacity of test girders, load and resistance factors were assumed to be 1.0. The key parameters, shear capacity estimations, and relevant moments are summarized in Table 3.2.

Table 3.2 Shear capacity calculation based on AASHTO LRFD

Specimen ID	β	θ	ε_s	V_n (kip)	M_u at critical section (k-in.)	M_u at loading point (k-in.)
Tx62-0SG	5.47	28.43	-0.000163	830.8	67,297	142,076
Tx62-0SU	5.53	28.38	-0.000176	805.6	65,254	137,762
Tx62-P0G	6.05	28.03	-0.000276	951.9	77,104	162,780
Tx62-P0U	6.13	27.99	-0.000290	924.4	74,878	158,081
Tx62-PSG	6.00	28.07	-0.000266	948.8	76,852	162,248
Tx62-PSU	6.08	28.02	-0.000280	948.8	74,642	157,583

3.2. Test Specimen Fabrication

3.2.1. Overview

The specimens were fabricated at a local precast plant, Valley Prestress Products, Inc. (VPP) in Eagle Lake, Texas. The precast plant has the full capacity for building precast bridge elements, housing ten prestressing beds and providing the necessary equipment, batch plants, skilled labor, and storage yard, as shown in Figure 3.5. The research team was on-site daily during production to coordinate with the facility and record pertinent details of the test specimens; install the post-tensioning hardware, instrumentation, and lifting hooks prior to concrete placement; and conduct concrete and reinforcing steel materials sampling. To ensure the test specimens were produced in accordance with the design and bridge standards, TxDOT QA inspectors stationed at VPP assisted the research team with the inspection of the girders.

The construction schedule and procedures are depicted in Figure 3.6. The fabrication of prestressed girders commenced with the placement of bars and post-tensioning hardware on February 25, 2020 (i.e., working day 1). Working with only one set of end-block forms, concrete placement was conducted at the rate of one girder per day. Finally, the research team confirmed the work process of the individual strand prestressing release on March 10, 2020 (i.e., working day 12), after checking that the cylinder compressive strength, f'_{ci} , was greater than the design strength of 7.5 ksi.

The research team's daily reports including attendees, overall work progress, key events, and a summary of schedules are provided in Appendix D.

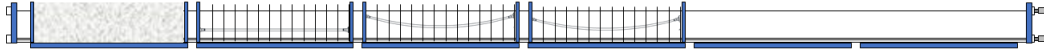


Figure 3.5 Precast Plant with the Location of Prestressing Beds and Batch Plants

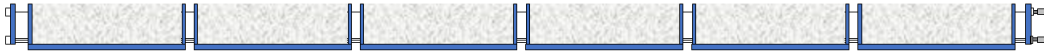
Working Day 1: Start fabrication of reinforcing bars (Feb. 25th)



Working Day 5: Start concrete casting (Mar. 2nd)



Working Day 10: End of concrete casting (Mar. 7th)



Working Day 12: Prestress release (Mar. 10th)



Figure 3.6 As-Built Construction Schedule and Procedures at Precast Plant

3.2.2. Concrete Mixture and Materials Sampling

A self-consolidating concrete (SCC) mix was used for the test specimens, consistent with standard practice for the construction of Tx-Girders. All test specimens were cast with the same concrete mix supplied by the batch plants in the precast plant. No issues, such as consolidation or unacceptable-sized honeycomb, were reported during the casting of any of the test girders. The concrete mix design used is provided in Table 3.3.

Table 3.3 Concrete mixture design used in test specimens

Material	Detail	Amount	Unit
Cementitious Material	Type III Cement	600	lb./yd ³
	Class F Fly Ash	150	
Fine Aggregate	Sand (F.M. = 2.88)	1,266	
Coarse Aggregate	Natural Gravel (3/4" nom. Max)	1,733	
Water	Water	235	
	w/cm Ratio	0.34	
Admixtures	Sika-Viscocrete 2110 (super plasticizer)	7.0	oz. per hundredweight
	Plastiment (retarder)	1.0	
	CNI (corrosion inhibitor)	51.0	
	Stabilizer VMA (viscosity modifier)	3.5	

The research team conducted a thorough sampling of the concrete material to examine the fresh and hardened properties. Two slump flow tests were performed on-site for the first and the last batch of concrete for each girder, in accordance with ASTM C1611/C1611M (2021). Table 3.4 presents the slump flow results for each concrete mix used for the test specimens. All mixtures had the slump flow within 22 to 27 in. the acceptable range (TxDOT, 2014). In addition, 20 standard cylindrical concrete samples for each test specimen (a total number of 120 samples for 6 test specimens) were cast for compression tests at four later occasions: prestressing release, 28 days, post-tensioning, and structural testing. These samples were left in the molds on-site before being transported to the UT Ferguson Structural Engineering Laboratory (FSEL) and placed in a water/lime bath to cure until the compression test was completed.

Table 3.5 presents the summary of samples of reinforcing steel (i.e., rebar and strand) collected during the fabrication of the test specimens. Time-dependent concrete material tests continued, and the samples of reinforcing steels were retained for later tests. The results for all material tests are discussed in Chapter 4 along with other measured properties used to calculate the nominal shear resistance of the test specimen using AASHTO LRFD provisions.

Table 3.4 Results of slump flow test

	Tx62-0SU (in.)	Tx62-0SG (in.)	Tx62-P0U (in.)	Tx62-P0G (in.)	Tx62-PSU (in.)	Tx62-PSG (in.)
Slump flow from 1 st batch	25.5	24.0	23.0	23.5	25.5	26.5
Slump flow from 4 th batch	24.5	24.0	24.0	22.0	25.5	27.0

Table 3.5 Samples of reinforcing bars and strands collected

Type	Stressing History	Nominal Diameter (in.)	Sample Length (in.)	Collected Quantity
#4 reinforcing bar	No	0.500	40	6
#5 reinforcing bar	No	0.625	40	6
0.6-in. seven-wire strand (low relaxation)	No	0.600	48	6
0.6-in. seven-wire strand (low relaxation)	Yes	0.600	48	6

3.2.3. Test Specimen Fabrication

This section describes the four sequential stages of construction performed by VPP: (i) strand placement and pretensioning; (ii) assembly of post-tensioning hardware and rebar placement; (iii) concrete placement and curing; and (iv) prestress release. Figure 3.7 provides an overhead view of specimens in the prestressing bed after the removal of the forms.

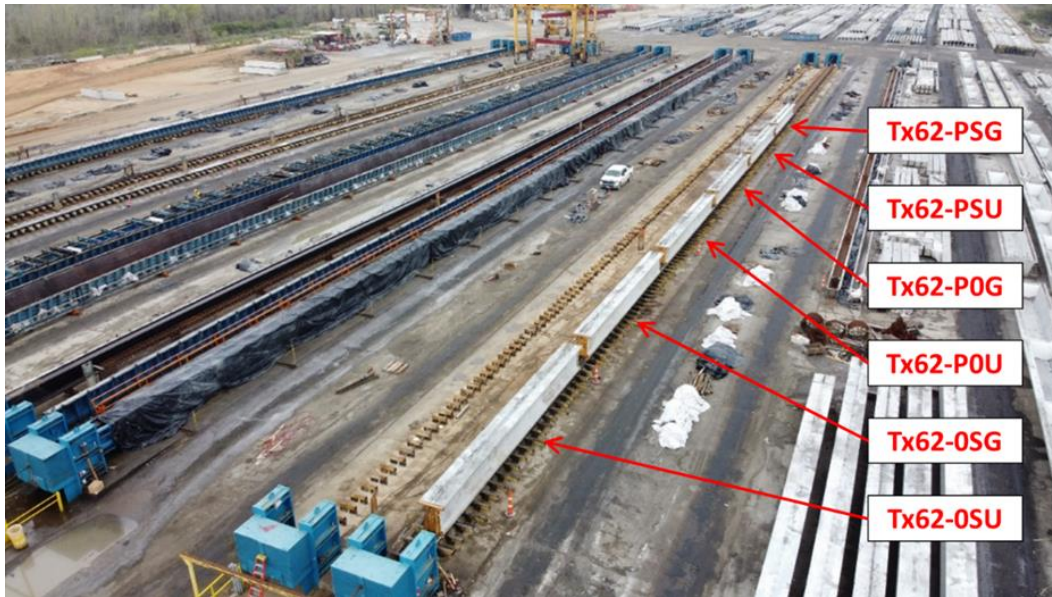


Figure 3.7 Completion of Production for Prestressed Girders at the Precast Plant

Strand Placement and Pretensioning

In accordance with the design, 6 top strands and 50 bottom strands with 12 wooden end forms were placed along the prestressing bed, as shown in Figure 3.8(a). After the installation of strands and end forms, the VPP construction team made use of a single-strand stressing method for tensioning the top and bottom strands, as shown in Figure 3.8(b). First, the VPP construction team cut away the excess strand and performed an initial stressing to remove the slack of the strand. Each strand was tensioned to 5,000 lbs, equivalent to 23 ksi. After the initial stressing, the process of final stressing was conducted up to the designed prestress level of 202 ksi according to the limited stress of $0.75 f_{pu}$. The actual observed prestress was 206 ksi, within the acceptable tolerance of $\pm 5\%$ (TxDOT, 2014).

Assembly of Post-Tensioning Hardware and Rebar Placement

For the post-tensioning of the test specimens, the multistrand system (Model: ECI 6-19 Stressing Anchorage) manufactured by VSL was chosen and shipped directly to VPP in advance of the fabrication. After the top and bottom strands were tensioned, the post-tensioning anchorages were attached to the wooden end forms as shown in Figure 3.8(c). To prevent the cement paste from leaking into the post-tensioning hardware during concrete placement, all joints were sealed with silicon. After the post-tensioning hardware was completely secured at the designed location, the ducts were installed using couplers. Note that the coupler locations were carefully selected in the middle and end-block regions in order to eliminate the unfavorable effects of the couplers on the shear capacity of the specimens. Detailed information about the duct profiles and the location of couplers is provided in Section 3.1.2.

After the assembly of the post-tensioning hardware and duct, the transverse reinforcement was placed, followed by the longitudinal reinforcement. The through-thickness bars located in the end-block region were then tied. Lastly, the reinforcing bars in the region of the top flange were placed. Figure 3.8(d) shows the completed reinforcing bar assembly on one specimen. A detailed rendering of the end-block reinforcement is provided in Appendix B.

Concrete Placement and Curing

Prior to the concrete casting, the steel side forms were closed and external vibrators were installed on the forms to consolidate the concrete, as shown in Figure 3.8(e) and (f). At VPP, two on-site batch plants provided the fresh concrete mix and dispatched it to the location of the specimens. One girder typically required four batches to finish the concrete casting.

The side forms were kept in place for one day for each girder to ensure adequate support while the concrete was cured. Furthermore, proper curing measures, such as curing tarps and plastic sheets, were immediately implemented, as shown in Figure 3.8(g) and (h). In addition, water was periodically sprayed on the specimens, as shown in Figure 3.8(i).

Prestress Release

Before prestressing release, two essential activities were conducted: (i) initiating DAQ system monitoring to record internal strains and (ii) measuring the compressive strength of the companion cylinders to ensure the concrete reached the design release strength of 7.5 ksi. After checking the DAQ system and testing to ensure the compressive strength was fully developed, the single-strand prestressing release was performed by the VPP construction team, as shown in Figure 3.8(k). The test specimens were separated by flame-cutting all strands after release. Finally, all girders were transported to the storage yard in the precast plant, as shown in Figure 3.8(l).



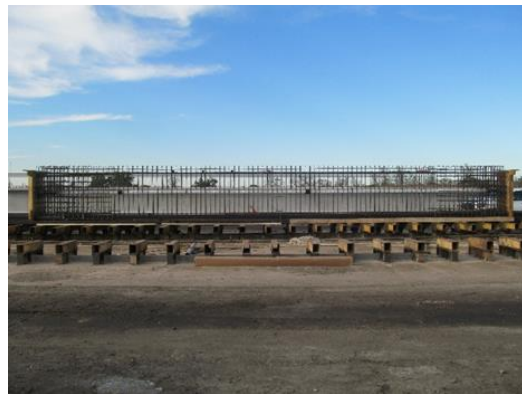
(a)



(b)



(c)



(d)



(e)



(f)

Figure 3.8 Production of Prestressed Girders: (a) Strands and End Forms Placement; (b) Single Strand Prestressing; (c) Post-Tensioning Anchorage Assembly; (d) Rebar Placement; (e) Side Form Close; and (f) Concrete Casting



(g)



(h)



(i)



(j)



(k)



(l)

Figure 3.8 (cont.) Production of Prestressed Girders: (g) Curing Tarp on Top of the Girder; (h) Curing Tarps and Plastic Sheets for Preventing Excessive Drying Shrinkage and Thermal Cracking; (i) Providing Water; (j) Side Form Removal; (k) Individual Strand Prestressing Release; and (l) Transferring Girder

3.2.4. Post-Tensioning Procedure

The prestressed girders were fabricated at a precast plant, VPP in Eagle Lake, Texas, as documented in Section 3.2.3. The remaining activities completed before conducting the structural test were (i) post-tensioning strands and grouting ducts as required; (ii) placing cast-in-place (CIP) deck concrete; and (iii) placing CIP overlay repair concrete in the region damaged during the first test to repair the ungrouted duct specimen prior to the second test.

The research team coordinated with a specialized post-tensioning operating company experienced with VSL hardware systems, Structural Technologies in Dallas, Texas, to perform stressing and grouting for two separate groups of test specimens (one with grouted duct and another with ungrouted duct). This operating plan considered the limited logistic space at FSEL and maintained similar time-dependent post-tensioning losses within the same group of duct's conditions (grouted and ungrouted). Three technicians certified as PTI Level 2 Bonded PT Field Specialists from Structural Technologies first visited to stress and grout three specimens on July 17, 2020; the three remaining ungrouted specimens were stressed on January 28, 2021.

Beforehand, the research team arranged the following activities in order to successfully complete the post-tensioning operation: (i) transferring the prestressed specimens using two crane systems upon arrival at FSEL (three grouted specimens delivered in June 2020; the remaining three ungrouted specimens delivered in December 2020); (ii) inspecting the inner duct condition using a high-resolution endoscope camera to check for debris or damaged ducts; (iii) inserting the strands into the duct; and (iv) deploying the instrumentation to monitor the post-tensioning level and specimen behavior. Figure 3.9 illustrates the steps conducted prior to the post-tensioning procedure by the contracted specialists.



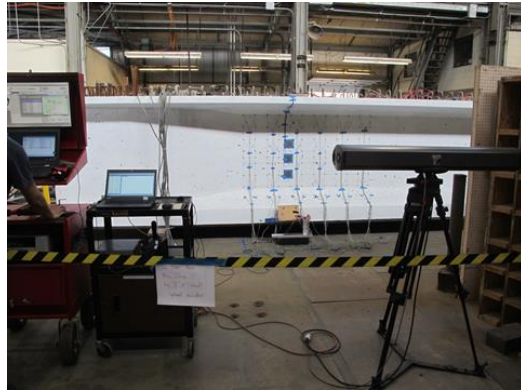
(a)



(b)



(c)



(d)

Figure 3.9 Preparation for Post-Tensioning Procedure: (a) Delivery of Prestressed Girder; (b) Inspection of Each Duct before Strands Placement; (c) Inserted Strands; and (d) Instrumentation during Post-Tensioning

The following section describes the post-tensioning procedure performed by Structural Technologies specialists: (i) install the post-tensioning hardware with stressing equipment and stress multi-strands; (ii) cut the redundant bundle of strands and install the cap with a grouting tube set; (iii) produce grouting mix; (iv) conduct the fresh material test; (v) inject pressurized grout; (vi) produce samples to determine the material properties; and (vii) conclude post-tensioning procedure. Figure 3.10 illustrates the post-tensioning and grouting procedures.

Stressing Procedure

For the post-tensioning of the test specimens, the research team chose the multistrand system (Model: ECI 6-19 Stressing Anchorage) manufactured by VSL. Based on the post-tensioning design, 19 low-relaxation seven-wire strands were placed into each duct, allowing extra length for a center-hole ram installation. After the multi-strand placement, the technicians removed the strand ends to assemble each anchor head efficiently, as shown in Figures 3.10(a) and (b). Figure 3.10(c) shows the wedge installation, performed through striking into the hole of the anchor head using a metal pipe, to minimize the slack between the anchor head and the wedge. A stressing “button” was placed between the anchor head and the center-hole ram to prevent excessive set losses during the post-tensioning process, as shown in Figure 3.10(d). After the completion of setting hardware and equipment, the technicians tensioned each strand to 20% of the target stress level, equivalent to 23 ksi uniformly. After the initial stressing, as shown in Figure 3.10(e), the final stressing was conducted up to the designed prestress level of 202 ksi ($0.75 f_{pu}$).

Producing the Grouting Mix

Following the stressing, all redundant strands were cut away for installing the grouting cap with the tube vents as shown in Figures 3.10(f) and (g). After the grouting hardware was completely secured at the designed location, the grouting mix (Euco Cable Grout PTX) was used for all grouted post-tensioned specimens. Before technicians injected the flowable grouting mix into the ducts, the research team performed the fresh material test to satisfy TxDOT requirements, including testing the mix temperature, performing a Schupak Pressure Bleed test, a fluidity test, and a mud balance test. All test results complied with DMS-4670 in the TxDOT manual (2014). Notably, due to the ambient temperature when producing the grouting mix, ice and liquid nitrogen were used to keep its temperature below 85°F set by TxDOT (2014), as shown in Figure 3.10(h). All grouting processes followed the PTI M55 (2013) as recommended by TxDOT.

Grouting Procedure

Once every grouting property met the standard, the technicians pumped the fresh grouting mix into one end vent. They continued to pump the grout until more than two gallons of grout (based on Post-Tensioning Institute [PTI]) spilled from the opposite end vent. The injection procedure ensured the proper amount of grout was inserted in the duct, eliminating entrapped air, as shown in Figure 3.10(j). After the technicians inspected for grout leakage, all vents were closed and curing commenced. At the same time, three by six-inch cylindrical samples were produced for compressive strength tests; the results yielded over 3 ksi at seven days and 5 ksi at 28 days, satisfied by TxDOT (2014).



(a)



(b)



(c)



(d)



(e)



(f)

Figure 3.10 Post-Tensioning Procedure: (a) Cutting Strands before Inserting Anchor Head; (b) Inserted Anchor Head; (c) Installation of Wedges; (d) Installation of Center-Hole Ram; (e) Post-Tensioning Strands; and (f) Completion of Post-Tensioning



(g)



(h)



(i)



(j)



(k)

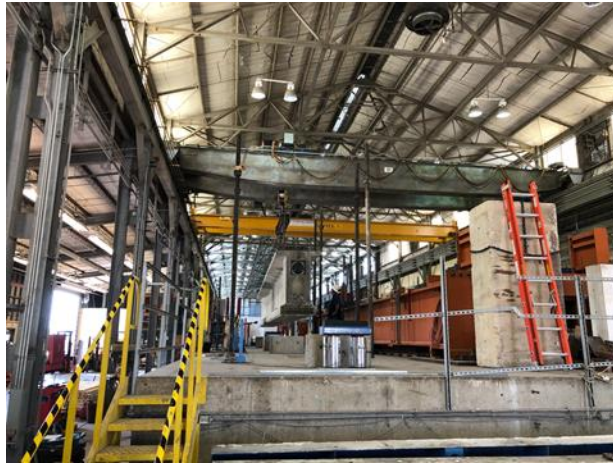


(l)

Figure 3.10 (cont.) Post-Tensioning Procedure: (g) Installation of Grouting Cap with Vents; (h) Grouting Mix Preparation; (i) Material Test before Grouting; (j) Inserting Grouting Mix; (k) Sample Fabrication for the Future Material Test; and (l) Completion of Post-Tensioning and Grouting

3.2.5. CIP Deck Concrete

The cast-in-place deck was intended to replicate field conditions more closely. In addition, it served to increase the moment capacity, thus ensuring a shear-governed failure mode during the structural test. The total weight of the composite girder with CIP deck concrete exceeded the lifting capacity of the two cranes at FSEL. As a result, the CIP deck concrete was placed when the post-tensioned girder was transferred to the designated structural area without any further logistics necessary until the end of the test. According to this logistic plan, only one post-tensioned specimen was installed in the test area, as shown in Figure 3.11(a). Figure 3.11(b) shows the CIP deck concrete placement with an eight-inch steel side form. Moreover, four by eight inch cylindrical concrete samples were produced for compressive tests to determine the concrete strength before the structural test.



(a)



(b)

Figure 3.11 Installation of (a) Supports and (b) CIP Deck Concrete

3.3. Instrumentation during Fabrication

3.3.1. Overview

In TxDOT Project 0-6652-1 (Moore et al., 2015), vibrating wire gauges (VWG) manufactured by Geokon (Model: 4200), as shown in Figure 3.12, were used successfully to monitor the internal strains of the test specimens. For that reason, the same VWGs were selected and installed in the test specimens for estimating prestress losses and measuring the expansion of the web during the structural test. For the purpose of estimating prestress losses, the VWGs were connected to a data acquisition (DAQ) system equipped with datalogger, analyzer, and multiplexer to record and monitor the strains in the girder since construction. The internal VWG monitoring started before prestressing release and continued until the end of the structural test. This section presents the as-built locations of the VWGs, the configuration of the DAQ system, and the process of monitoring test specimens at the precast facility.

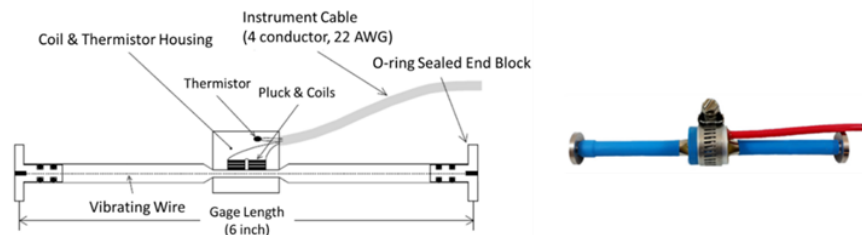


Figure 3.12 The Model 4200 of vibrating wire gauge (Geokon 2017)

3.3.2. Installation of DAQ System

The embedded VWGs play a pivotal role in obtaining the internal concrete strains. Three VWGs were placed longitudinally in the test region and at the mid-span of the test girders, as shown in Figure 3.13(a). The VWGs at the mid-span section in particular provided essential information for estimating the prestress losses, incorporating the effects of elastic shortening, creep, and drying shrinkage between the period of prestress transfer and structural test.

Another important objective of the embedded instrumentation was to evaluate the web expansion that potentially occurs around the duct in the web region. To accomplish this, either four or six VWGs (depending on the type of duct profile) were embedded in the out-of-plane direction, as shown in Figure 3.13(b). Figure 3.13(c) depicts the location of the embedded VWGs installed along the length of the test specimens. The total number of VWGs for each girder ranged from 8 to 16, depending on the test specimen design. Supplemental details about the instrumentation are provided in Appendix E.

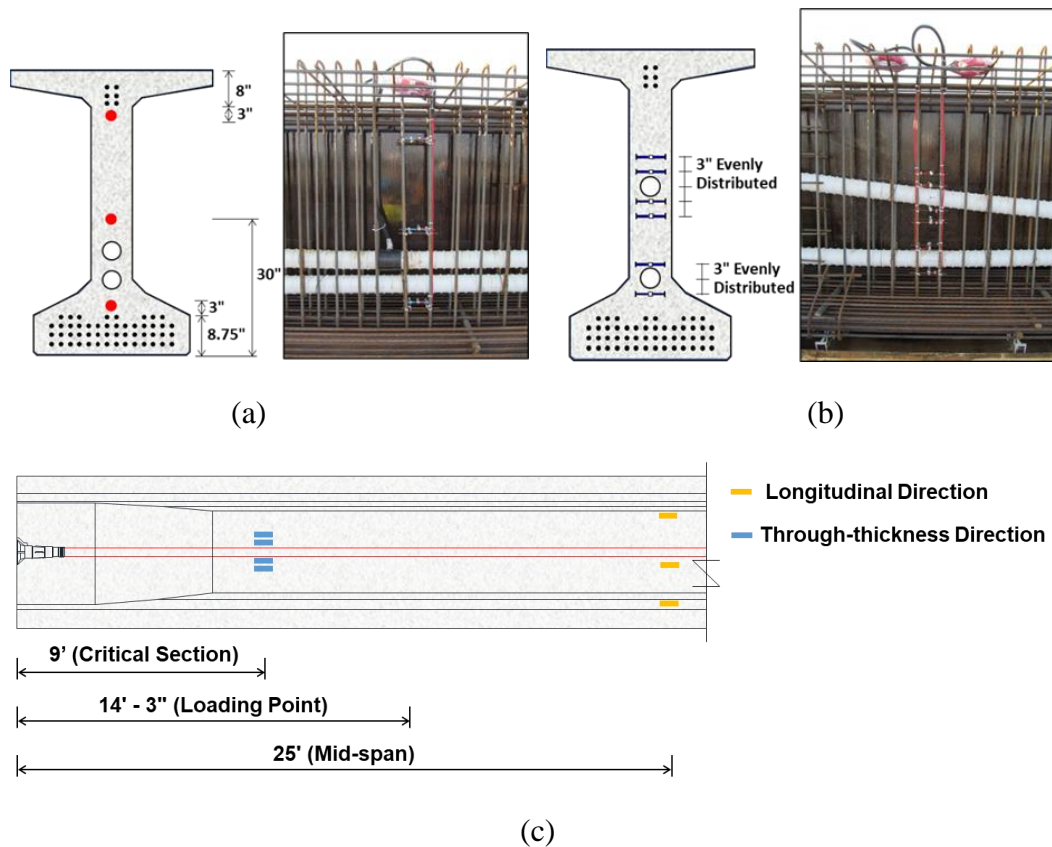


Figure 3.13 Locations of Embedded VWGs: (a) Longitudinal Direction of VWGs (i.e., Tx62-PSG & PSU); (b) Out-of-Plane Direction of VWGs (i.e., Tx62-PSG & PSU); and (c) VWGs along the Length of Test Specimen (i.e., Tx62-0SG & 0SU)

3.3.3. Configuration of DAQ System

This research used VWGs mainly because of the gauge's ability to measure long-term strain events. Since VWGs use the natural frequency of the internal wire, which provides constant reading along the monitoring timeline, the initial reference reading can be used to capture the long-term behavior of the target specimen. In order to utilize this type of gauge, a DAQ system manufactured by Campbell Scientific was configured by the research team for this project. This system consists of a datalogger (CR3000) with multiple peripherals (e.g., analyzer, multiplexers) to measure and record the VWGs. The system is powered by a solar array and housed in enclosures for protection from the environment, as shown in Figure 3.14. Figure 3.15 shows a schematic used for connecting the external DAQ components with the embedded VWGs in the test specimens.

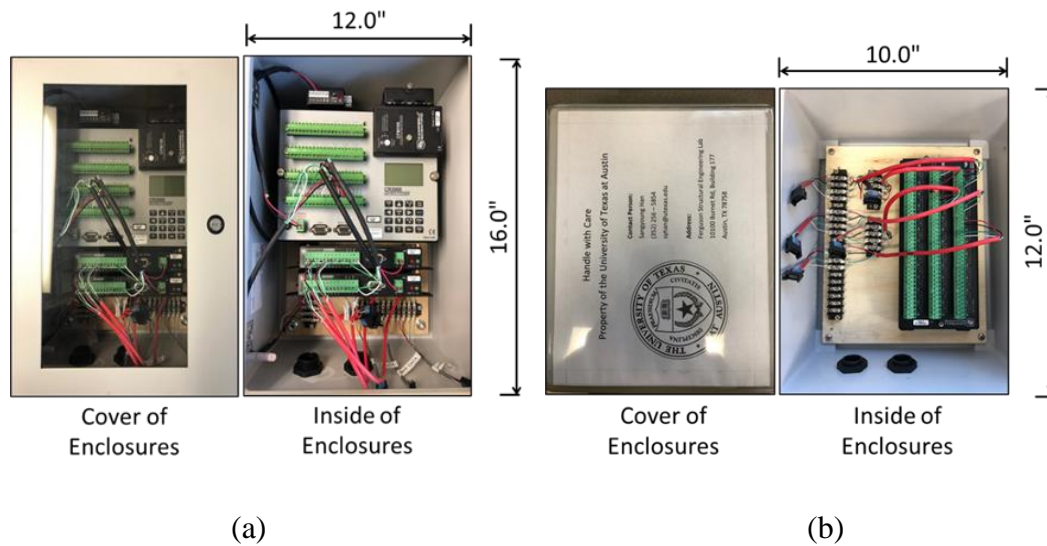


Figure 3.14 Fully Equipped Enclosures for Field Monitoring: (a) Enclosure with a Data Logger (Model: CR 3000) and Two Analyzers (Model: AVW 200) and (b) Enclosure with a Multiplexer (Model: AM 16/32B)

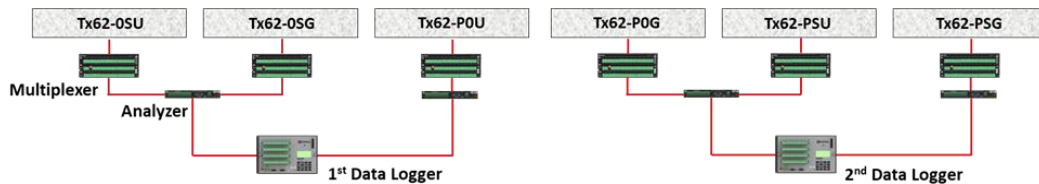


Figure 3.15 Configuration of the DAQ System for Field Monitoring

3.3.4. Monitoring Test Specimens at VPP

The DAQ system was employed at the precast facility after fabrication and continued to monitor the gauges in the girders while in storage (see Figure 3.16). The DAQ system recorded the longitudinal strains at prestress release to pick up the effects of elastic shortening. The test specimens continuously experienced time-dependent deformation due to drying shrinkage and creep. To monitor such deformation, the DAQ system was relocated to the storage area near the test specimens and continuously recorded the embedded gauges at one-hour intervals.



(a)



(b)



(c)

Figure 3.16 Logistics Plan for Production and Storage Areas of Fabricated Test Specimens: (a) Overhead View of Key Logistics Areas; (b) Fabricated Test Specimens in Storage Area; and (c) Protected DAQ System with Solar Panels

3.4. Summary of Fabrication

The main objective of Chapter 3 was to summarize the fabrication of the six test specimens and plans to deploy a DAQ system to monitor the early-age time-dependent prestress loss. The research team coordinated the fabrication in the precast plant from February 26 through March 10, 2020. The main activities are summarized as follows:

- Fabrication of the test specimens was successfully completed without any issues.
- After the prestressed girders were fabricated in the precast plant, the test specimens were transferred to FSEL to complete the remaining construction steps of post-tensioning, CIP concrete deck placement, and CIP overlay concrete repair for the structural test.

Chapter 4. Experimental Program

4.1. Structural Test Configuration and Protocol

In this experimental program, six test specimens were fabricated and twelve shear tests were conducted. The structural test layout and test protocol are outlined herein. Since the specimen dimensions were similar to those in Project 0-6652-1 (Moore et al., 2015), the structural testing setup of this research followed Moore et al.'s testing setup to ensure the desirable failure mode and to compare the test results directly, as shown in Figure 4.1.

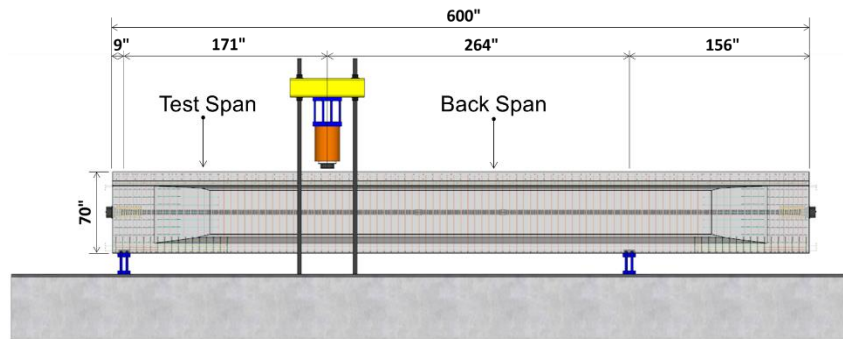
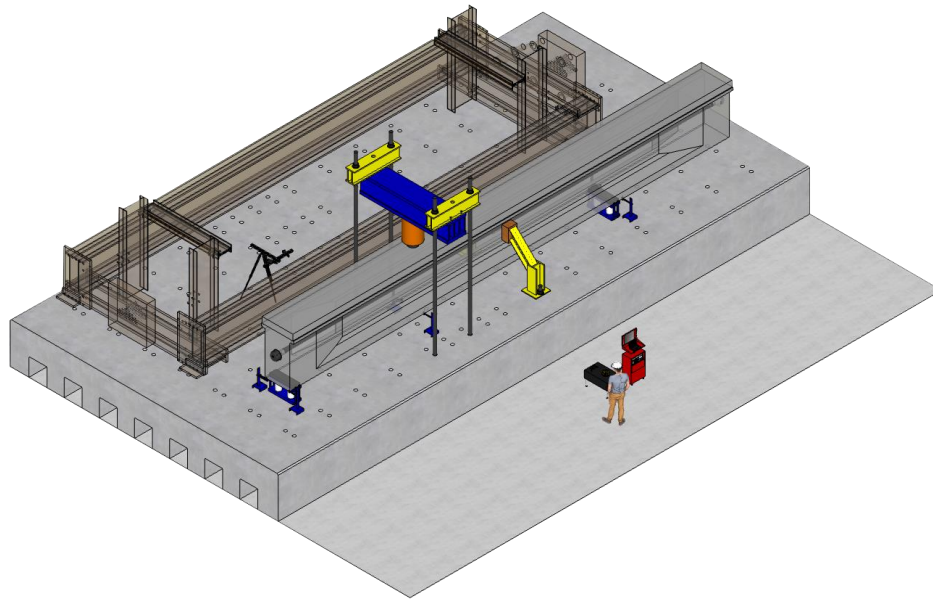


Figure 4.1 The Design of Shear Structural Test Schematic

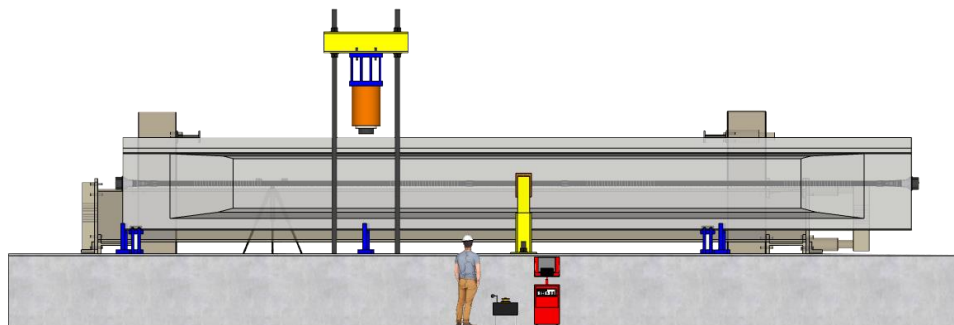
The ultimate load level to fail the test specimens was estimated with the AASHTO LRFD (2020) shear provision to be less than 1,800 kip, validated by the previous test results (Moore et al., 2015). Furthermore, an additional 20% was added to the test setup capacity to account for potential overstrength. Thus, the test frame was designed for 2,000 kip (e.g., hydraulic ram, pressure nozzle). The strength of the loading frame was also verified by its calculated resistance using AISC provision in terms of sectional flexural capacity, sectional shear capacity, and welding strength (AISC, 2017). Figure 4.2 exhibits the structural setup and monitoring area designed for this project, and Figure 4.3 includes the rendering of testing setup.



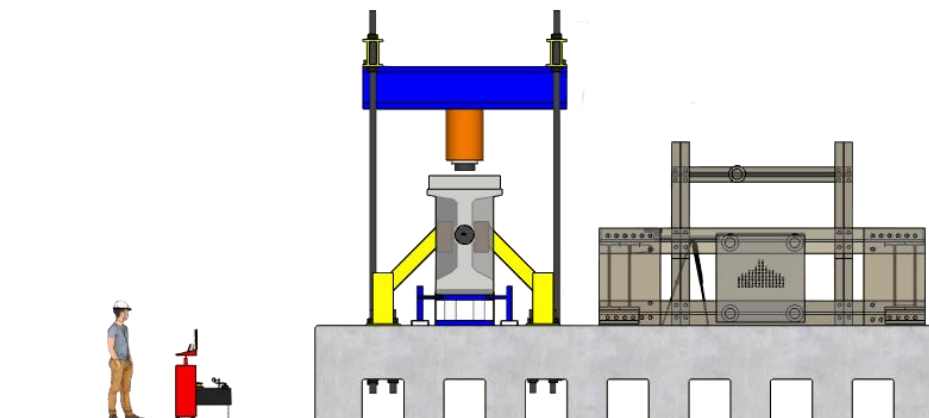
Figure 4.2 As-Built Structural Schematic: (a) Overall Structural Setup with the Test Specimen and (b) Designed Monitoring and Controlling Area during the Test



(a) Isometric View



(b) Front Elevation View



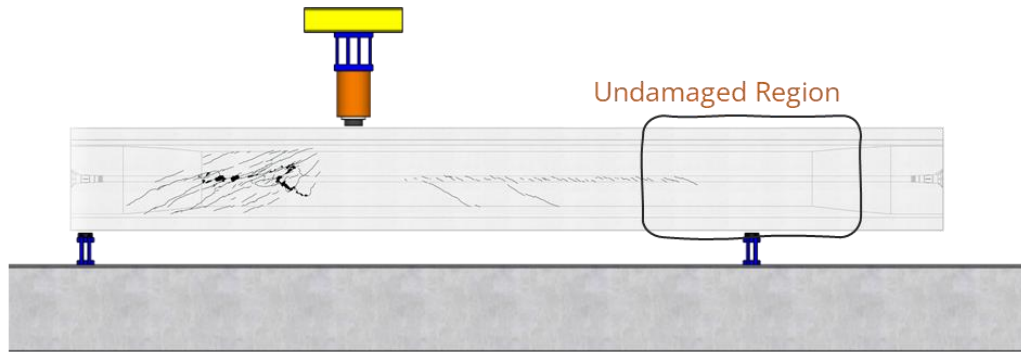
(c) Side Elevation View

Figure 4.3 Rendering of Structural Test (Elevated Slab in FSEL)

Each of the two tests was conducted per one test specimen, which had the same testing layout, by relocating the loading plate and supports to the opposite end of the untested region, as shown in Figure 4.4.

The load was applied monotonically until shear failure occurred. The load was applied in a 50-kip increment until the first diagonal shear cracking detection. After cracking detection, the loading was applied in a 75-kip increment. At each increment, the loading was paused to perform the cracking survey according to each loading level. Due to safety issues, the research team stopped taking crack measurements after the development of the dominant shear crack. The loading was then increased until the test specimen experienced failure. After ultimate failure, the applied load was removed, and the cracking survey resumed on the specimen surface. Figure 4.4 depicts the surveyed cracking development.

1st Test: CIP deck in the elevated slab



2nd Test: relocated loading frame & supports

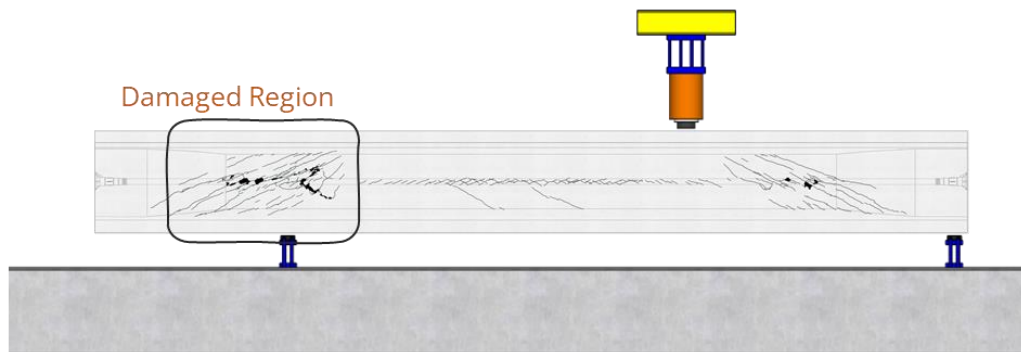


Figure 4.4 The Location of Loading Plate and Bottom Supports Cause Two Shear Failures and Corresponding Cracks in One Test Specimen

The total force experienced by the test specimen includes the applied load, the girder self-weight, and the weight of the loading frame during the structural test. In order to compute the shear force, the total forces were monitored from the load cells at two supports. AASHTO LRFD takes the location of the critical shear section for the girder determined as the effective shear depth (d_v) from the edge of bearing pad (65 in.); however, this is located within the end-block (the general beam section starts 90 in. from the end). A more practical approach to determining the critical section relates to the failure cracks, based on a visual inspection of Moore et al.'s test results (2015). Figure 4.5 shows where the most vulnerable area for shear force, and the critical section was determined to be approximately 1.5 feet from the termination of the end-block. This determined critical section of the test specimen serves as the critical location for the calculation of shear force and the various instrumentation applied to the specimens. The experimentally determined critical section from Moore et al. (2015) is reasonably close to the location of govern failure crack in this study.

The software Mastan2 was used to calculate the refined shear diagram due to the sum of the shear force due to the self-weight of the girder at the critical section, the weight of the load frame transmitted through the “test region” side support, and the maximum applied load transmitted to the support during testing, as shown in Figure 4.6.

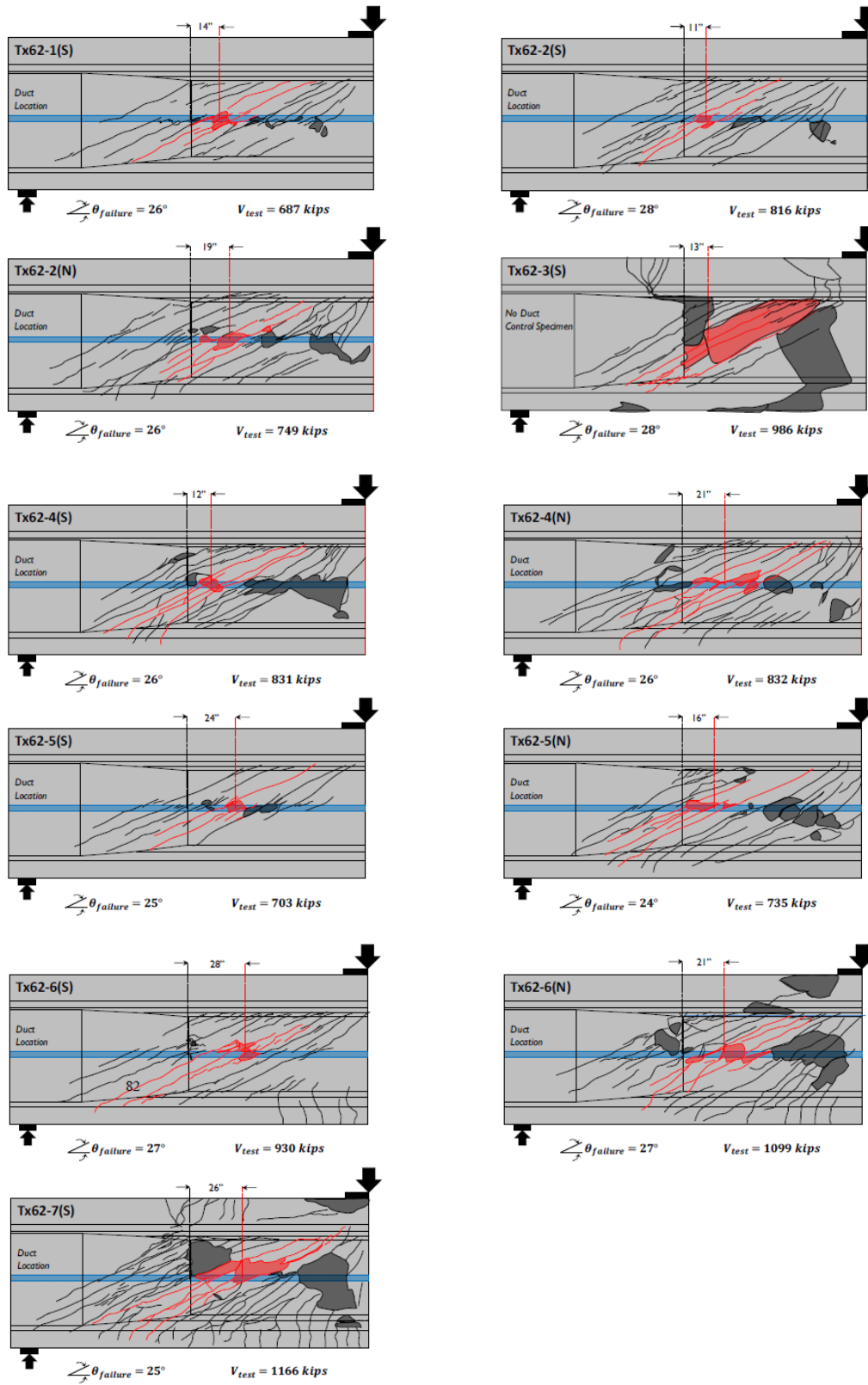


Figure 4.5 The Governed Failure Cracks of Moore et al.'s Specimens in Red (Moore et al., 2015)

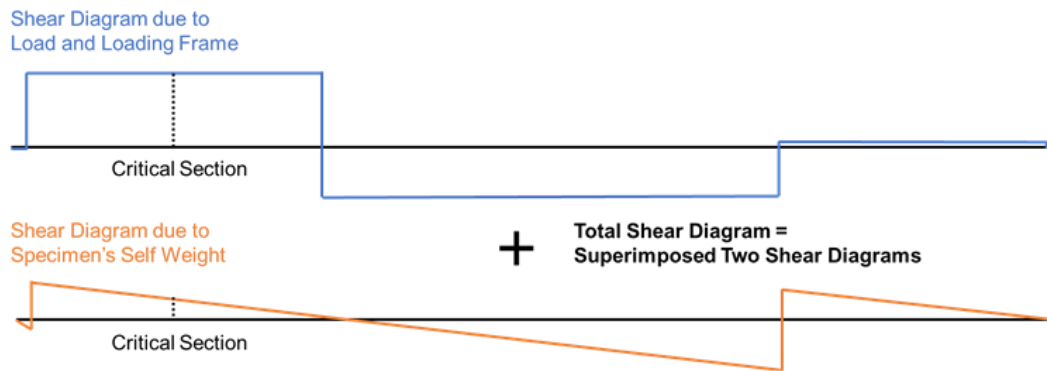


Figure 4.6 The Corresponding Shear Diagram from Applied Load, Loading Frame, and Self-Weight

4.2. Instrumentation during Structural Test

To achieve the project objectives, the research team's monitoring plan deployed various types of instrumentation systems, including: (i) an Agilent DAQ system connecting a pressure transducer, load cells, linear-potentiometers (L-pot) and electrical resistance-based strain gauges; (ii) a Campbell DAQ system connecting external and internal VWGs; and (iii) non-contact measurement system (e.g., motion capture system). This section presents the configuration of each DAQ system and what was expected from each system. Figure 4.7 illustrates the overall instrumentation deployment in the designated test area (i.e., elevated slab in FSEL).

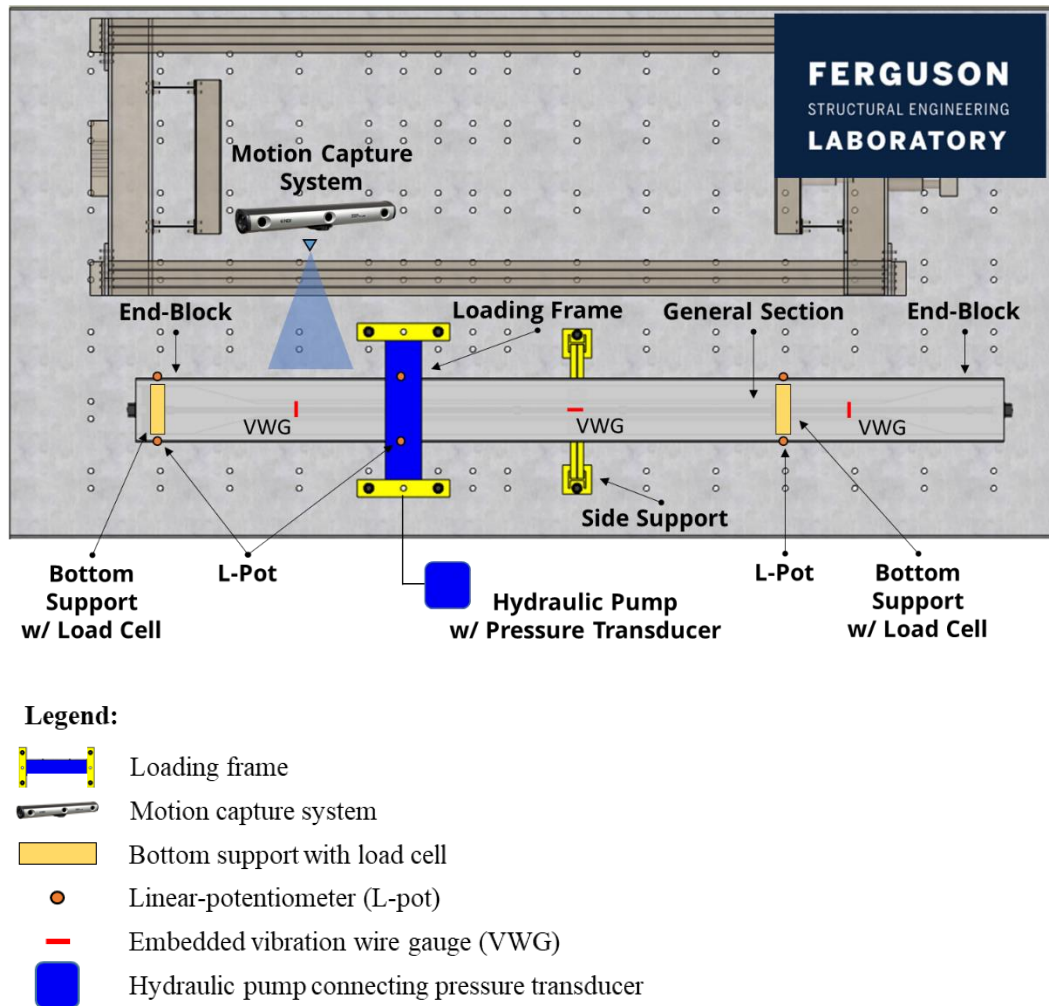


Figure 4.7 The Overall Plan View of Structural Testing Schematic and Locations of Instrumentation

4.2.1. Agilent DAQ System

Two of the critical data points analyzed were the applied total load and corresponding deflection of the test specimen. Figure 4.7 shows the locations of loading and deflection measurements by load cells and L-pots. The load cells located at the two supports recorded the total load during the structural test, which was simultaneously validated with the monitored ram pressure. The net deflection was determined by the continuous readings of each L-pots, as shown in Figure 4.8(a). This collected data of load and deflection were used for determining the shear strength and the stiffness of the test girder.

The transverse reinforcement in the web area at the critical section was expected to yield as the specimen approached failure. This critical section provided the overall structural responses and failure mode observation, which were essential for analysis. Therefore, the research team focused on capturing the structural responses in the critical section using the instrumentation applied, such as the rosette surface strain gauge and L-pot for measuring web expansion, as shown in Figure 4.8(b) as well as VWG and motion capture system addressed in the following Section 4.2.2 and 4.2.3, respectively.

In addition, the research team monitored the tendons behavior in ungrouted ducts during the structural test to determine the stress level due to the applied load. Before post-tensioning, the research team attached the electrical resistance-based strain gauge to several strands for monitoring the strain level during the structural test, as shown in Figure 4.8(c).

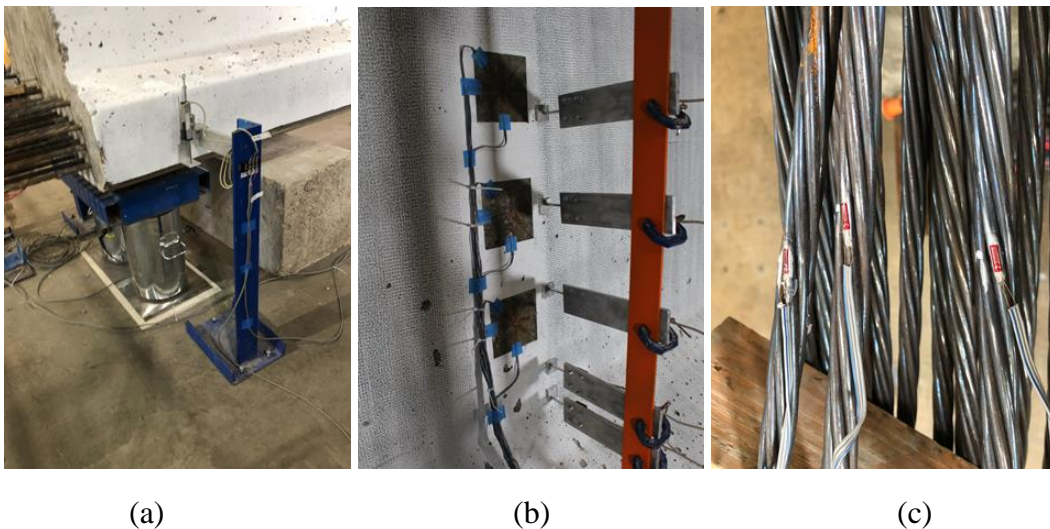


Figure 4.8 Instrumentation Used during Structural Testing: (a) Load Cell for Total Load and L-Pot for Deflection; (b) Surface Strain Gauge and Inverted U-Frame for Web Responses; and (c) Electrical Resistance-Based Strain Gauge Applied to Strands

4.2.2. Campbell DAQ System

The team installed the VWG to measure long-term strain evolution. The VWG uses the natural frequency of the internal wire, which provides constant reading along the monitoring timeline. As such, the initial reference reading can be used to capture the long-term behavior of the target specimen. To utilize this unique type of gauge, a DAQ system was configured by the research team. It consisted of dataloggers with multiple peripherals to measure and record the VWGs, as shown in Figure 4.9.

Embedded VWGs had an instrumental role in recording the internal concrete strains. Three VWGs were placed longitudinally at the mid-span of test girders, as shown in Figure 4.10(a). The VWGs at the mid-span section in particular provided essential information for estimating the prestress losses, incorporating the effect of elastic shortening, shrinkage, and creep between the period of prestress transfer and structural test. For example, the DAQ system recorded the longitudinal strains at prestress release to monitor the effect of elastic shortening. Further, the test specimens continuously experienced time-dependent deformation due to shrinkage and creep. To monitor such deformations, the DAQ system, as shown in Figure 4.9(a), was relocated from the precast plant to FSEL.

Another important objective of the embedded gauges was to evaluate the web expansion around the duct in the web region. To accomplish this, either four or six VWGs were embedded in the out-of-plane direction, as shown in Figure 4.10(b). Because the web expansion developed in a relatively short period compared to the developing prestress loss, another datalogger system that can capture a high-frequency sampling rate was required. The CR6 datalogger was employed to meet this need during the structural test, as shown in Figure 4.9(b).

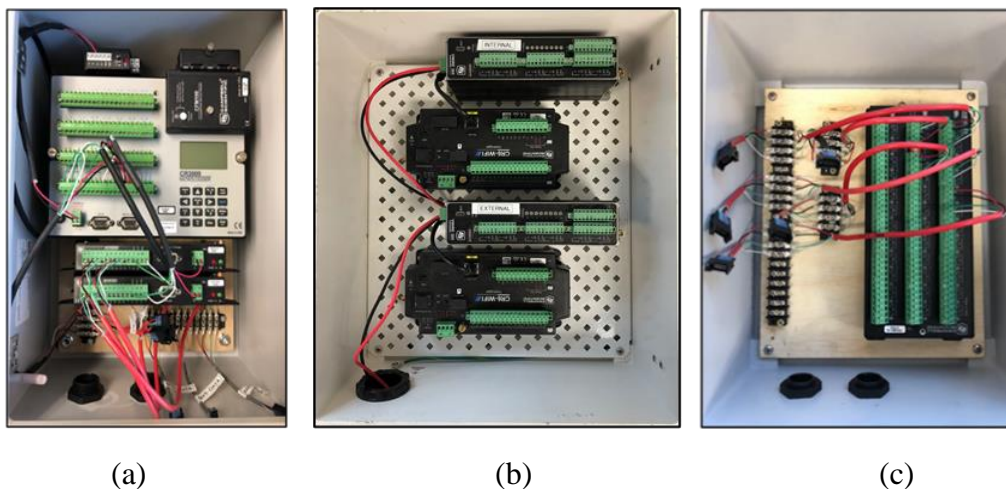


Figure 4.9 Fully Equipped Enclosures for Field Monitoring: (a) Enclosure with a CR 3000 Datalogger and Two AVW 200 Analyzers; (b) Enclosure with CR 6 Datalogger; and (c) Enclosure with AM 16/32B Multiplexer Model

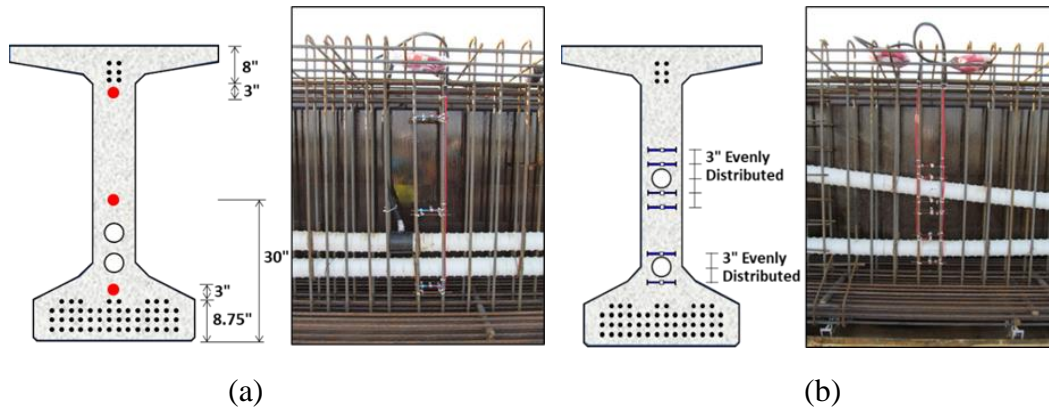


Figure 4.10 Cross-Sectional View of the Locations of Embedded VWGs: (a) Location of Longitudinal Direction of VWGs (Tx62-PSU & PSG) and (b) Location of Out-of-Plane Direction of VWGs (Tx62-PSU & PSG)

4.2.3. Motion Capture System

To enrich the variety of data, the research team employed vision systems to monitor the critical section in addition to the L-pots and electrical resistance-based strain gauges deployed in the same region. The motion capture system tracks a marker attached to the surface of the critical section, as shown in Figure 4.11. Motion capture systems have the advantages of calculating three-dimensional deformations and assessing broader areas than other established gauges. The motion capture system was intended to enlarge the monitoring region through comparison and validation with the strain gauges.

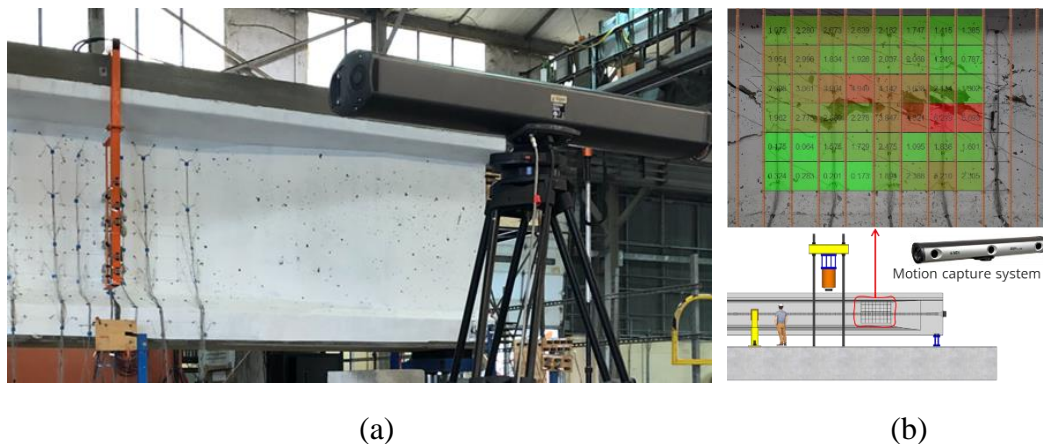


Figure 4.11 Motion Capture System Used for Monitoring during the Structural Test: (a) a Camera with Motion Capture System Markers Applied on the Web Surface and (b) Sample Data after Post-Processing

4.3. Experimental Results and Observations

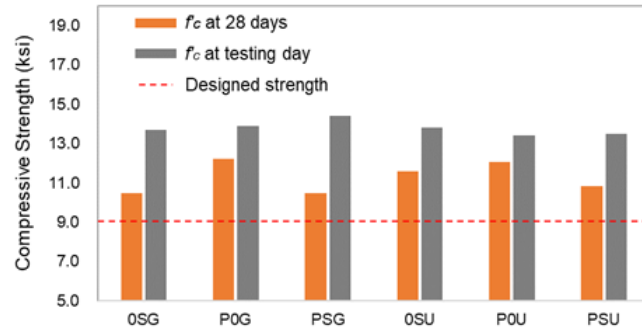
This section presents the experimental program along with the comparison between the shear test results and AASHTO LRFD shear resistance estimation. This comparison allowed the research team to assess the shear behavior of precast girders with either grouted or ungrouted ducts. This section addresses the determined input properties used to calculate AASHTO LRFD shear design and the comparison of the test results to shear strength estimation. Finally, this report discusses the comparison of tested capacity to AASHTO LRFD estimation in terms of shear resistance.

4.3.1. Input Properties for AASHTO Shear Design

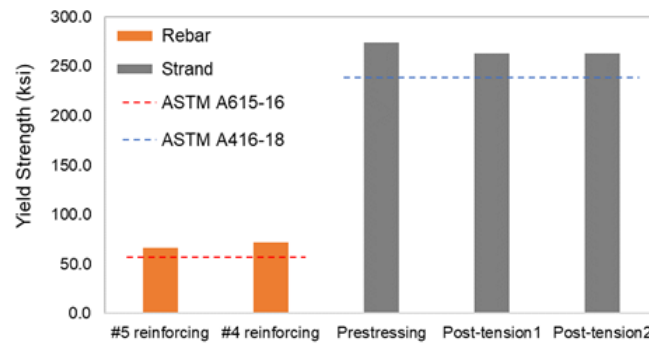
4.3.1.1. Material Properties

The research team conducted a thorough sampling of the concrete material to examine the fresh properties (ASTM C1611/C1611M, 2021) and to later perform the hardened material test (ASTM C39, 2014). Four by eight inch cylindrical concrete samples were produced at one of the batch plants for concrete materials test at 28 days and on the structural test day, as shown in Figure 4.12(a).

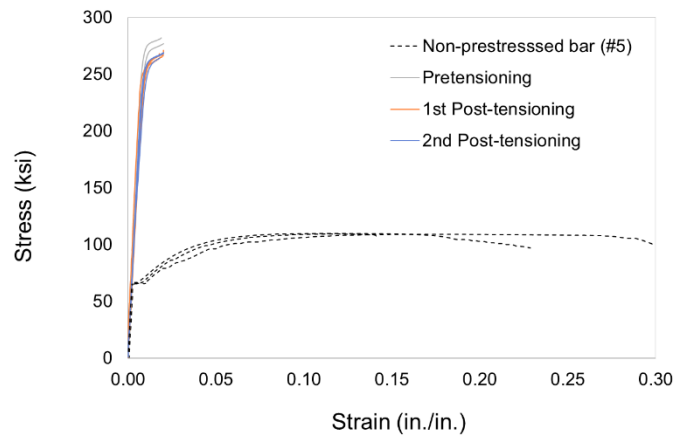
During the fabrication of the test specimens, samples from the non-prestressed reinforcing bars and the 0.6-in. seven-wire strands (low-relaxation) were also collected. The material test service company, Metallurgical Engineering Services, conducted the uniaxial tension test on the collected samples. Figure 4.12(b) shows the average yield strength of three samples, that satisfied the ASTM standards for reinforcing bars (ASTM A615, 2020) and for 0.6-in. seven-wire strands (ASTM A416, 2018), respectively.



(a)



(b)



(c)

Figure 4.12 The Results of Material Tests: (a) the Compressive Test Results of Concrete at 28 Days and Test Day; (b) the Yield Strength of Reinforcing Bars and 0.6-In. Seven-Wire Strands for Pretensioning and Post-Tensioning; and (c) Stress-Strain Response of Reinforcing Bars and Strand

4.3.1.2. Prestress Loss

To better predict the behavior of spliced post-tensioned girder, it is imperative to quantify the time-dependent prestress loss in strands. Figure 4.13(a) illustrates the methodology employed to measure the sectional strain profile, and then to determine the prestress loss, following the Garber Model (2013), validated in Project 0-6652-1 (Moore et al., 2015). The VWGs monitor the strain development from the prestress transfer to the first test for each girder specimen. The collected strain data were used to calculate the stress variation between the time of prestress transfer and the structural test to determine the prestress loss in the bottom strands. This method using VWGs calculates the prestress loss at important events such as prestress transfer, post-tensioning, and deck casting with respect to elapsed time.

AASHTO LRFD provides a prestress loss estimation that accounts for the effects of elastic shortening due to pretensioning and post-tensioning, shrinkage, creep, deck casting, and stress relaxation. Figure 4.13(b) compares the AASHTO LRFD estimation and the prestress loss calculated from the data collected before the test. As shown in the comparison, the differences are within 10% for all test specimens. This validates the determined prestress loss measured by VWGs and serves as one of the parameters used to calculate AASHTO LRFD shear resistance. The detailed procedure to estimate the prestress losses is provided in Appendix F.

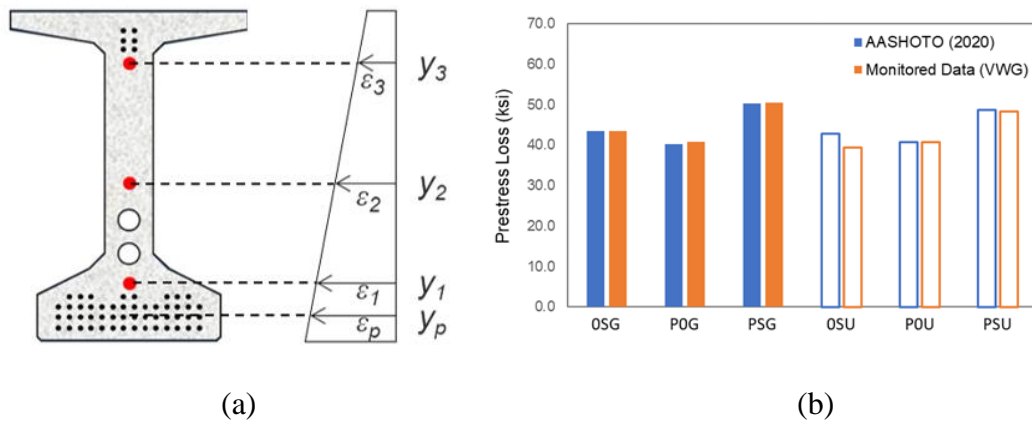


Figure 4.13 Prestress Loss of Test Specimen: (a) Garber Model to Determine the Prestress Loss based on Embedded VWGs and (b) the Final Gauge-Measured Prestress Loss Compared to the AASHTO LRFD Estimation

4.3.2. Failure Mechanism

In general, the timing, location, and cracking patterns provide valuable insight into the structural behavior during the test. All test girders behaved and failed in a similar manner. First, hairline cracks were observed at the duct location that further developed along the length of the girder as the applied load increased. At approximately 80% of the ultimate load, a dominant shear crack developed from the center of the web to the top and bottom flanges in the test span. Finally, the test specimens failed due to concrete compression failure in the vicinity of the post-tensioning duct, a result otherwise known as web crushing. Cracking development and ultimate failure mode were consistent in the grouted and ungrouted post-tensioning ducts. Figure 4.14 illustrates the three different cracking modes related to load and deflection. In addition, Figure 4.15 shows load-deflection plots and failure crack patterns for all 12 tests.

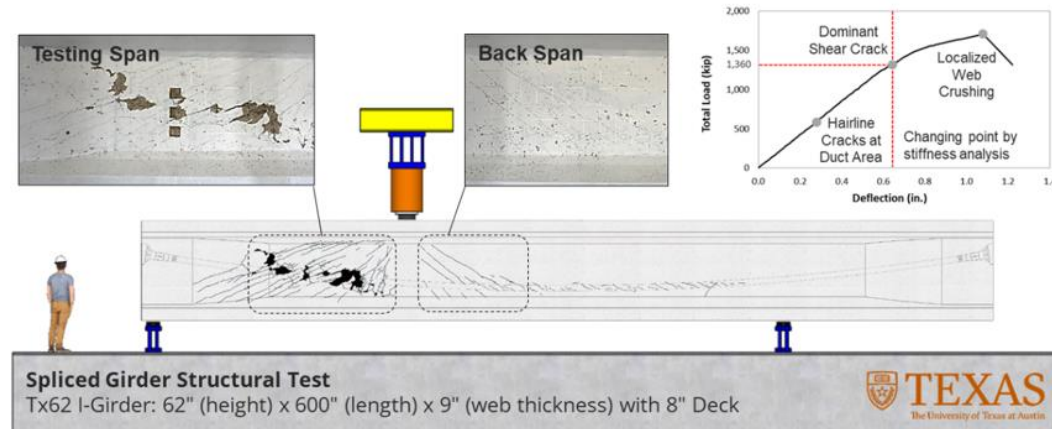
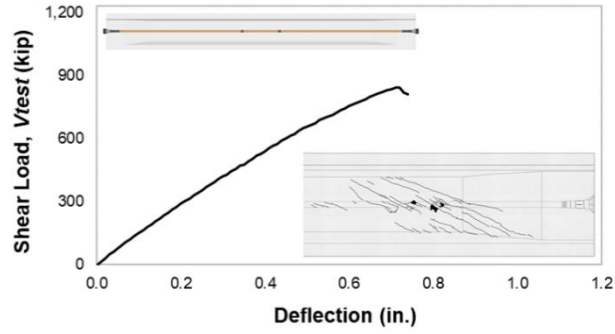
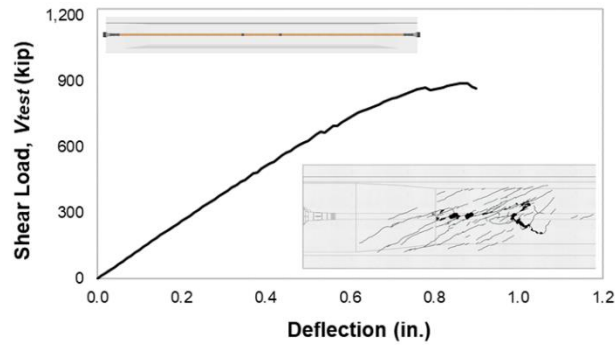


Figure 4.14 Structural Setup and Three Distinct Cracking Modes Related to Loading and Deflection

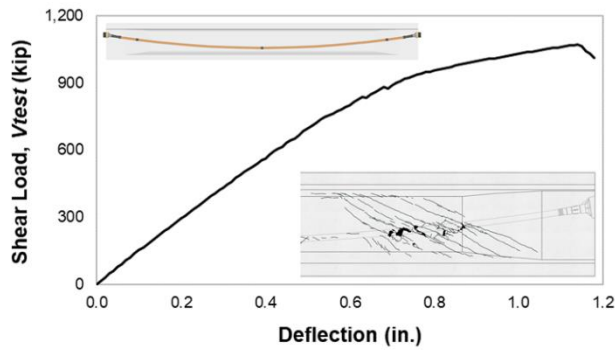
Figure 4.16 shows the cracking survey conducted along the length of the girder. As mentioned previously, the same three cracking modes, such as hairline crack, diagonal crack, and localized web crushing, can be observed in each shear test span. With respect to the diagonal cracking propagation, each specimen containing the same profile of post-tensioning duct experienced a similar cracking pattern, average crack spacing, and angle of diagonal cracks. This information provided valuable insight regarding the shear resistance provided by the concrete component (V_c), which is evaluated in detail in Chapter 5.



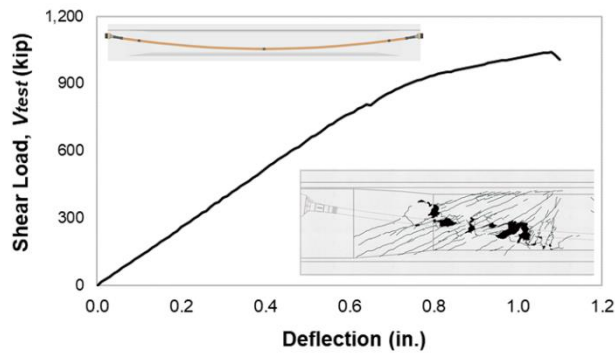
(a) Tx62-0SG (1st test)



(b) Tx62-0SG (2nd test)

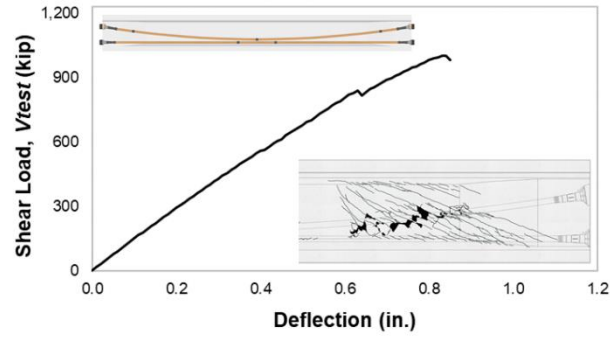


(c) Tx62-P0G (1st test)

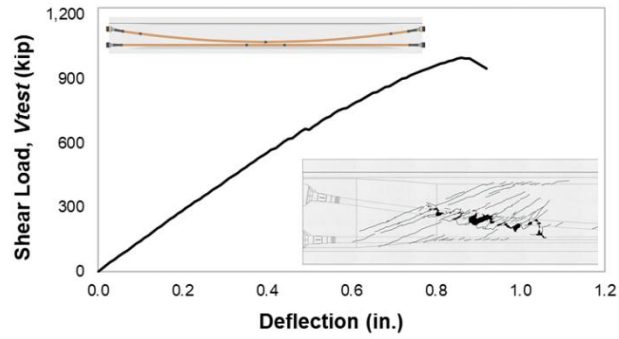


(d) Tx62-P0G (2nd test)

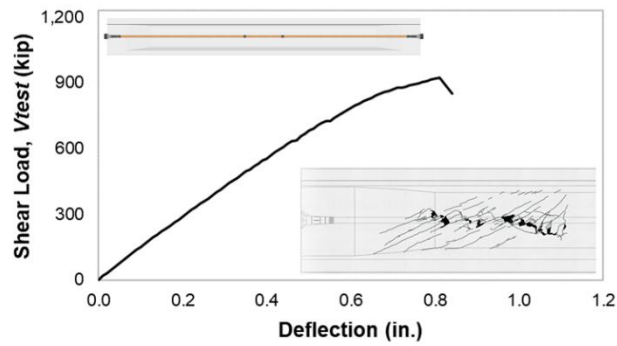
Figure 4.15 Shear Load-Deflection Plots of All Test Specimens with Surface Cracks



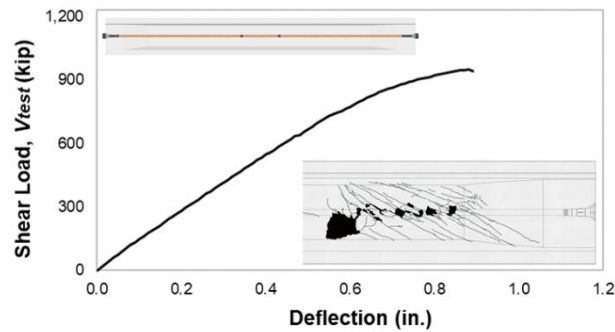
(e) Tx62-PSG (1st test)



(f) Tx62-PSG (2nd test)

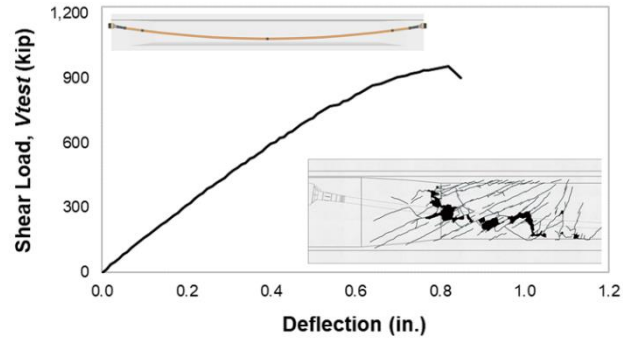


(g) Tx62-0SU (1st test)

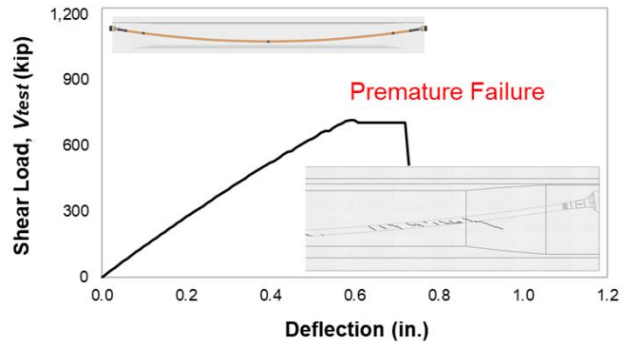


(h) Tx62-0SU (2nd test)

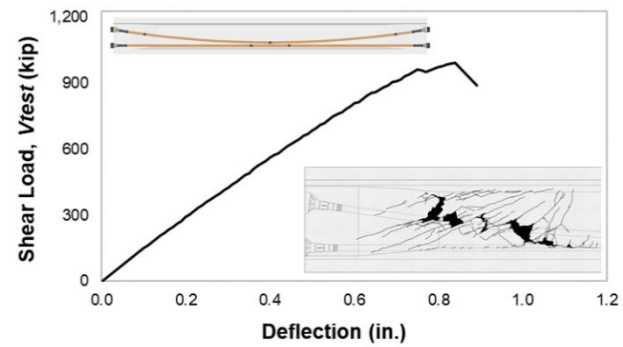
Figure 4.15 (cont.) Shear Load-Deflection Plots of All Test Specimens with Surface Cracks



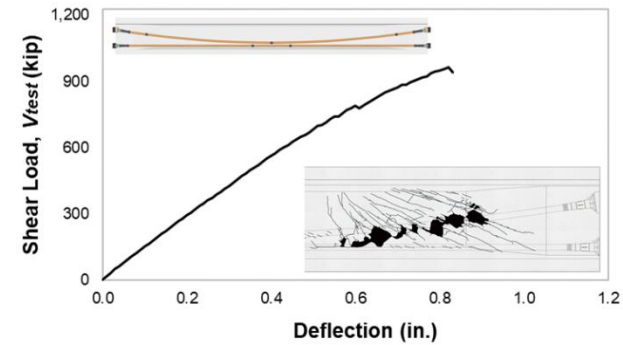
(i) Tx62-P0U (1st test)



(j) Tx62-P0U (2nd test)

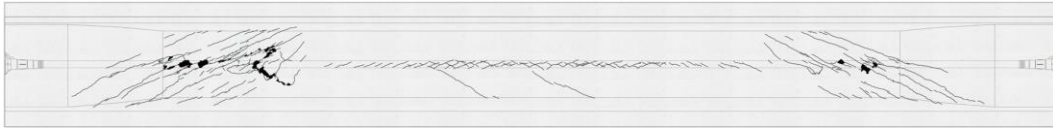


(e) Tx62-PSU (1st test)



(f) Tx62-PSU (2nd test)

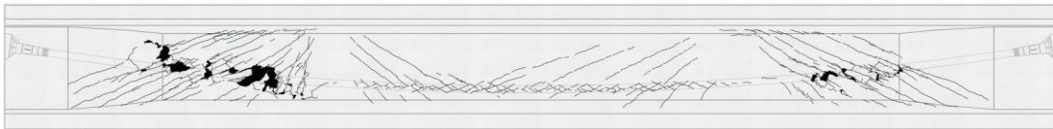
Figure 4.15 (cont.) Shear Load-Deflection Plots of All Test Specimens with Surface Cracks



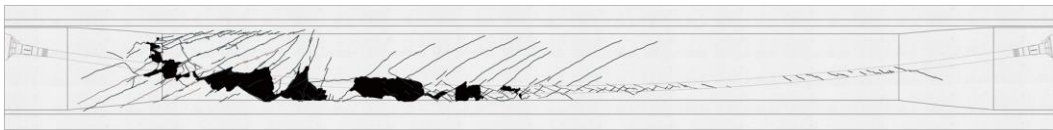
(a) Tx62-0SG



(b) Tx62-0SU



(c) Tx62-P0G



(d) Tx62-P0U



(e) Tx62-PSG



(f) Tx62-PSU

Figure 4.16 Surface Cracking Survey along the Girder Length after Two Combined Tests

The research team dissected the tested specimens at the critical section as an additional visual inspection to further analyze the cross-sectional behavior and identify potential particularities specific to specimens containing grouted or ungrouted ducts. Figure 4.17 shows the visual inspection for the developed cracking patterns such as diagonal shear crack, localized web crushing, and splitting cracks (Appendix G provides the internal cracking survey at the critical section from all 12 tests). More importantly, the internal cracking survey revealed the internal cracks that developed around the duct. This internal cracking behavior was the result of the splitting stresses in the vicinity of the duct, the embedded gauges quantifying this behavior. The detailed discussion of internal cracking will be provided in the following section.

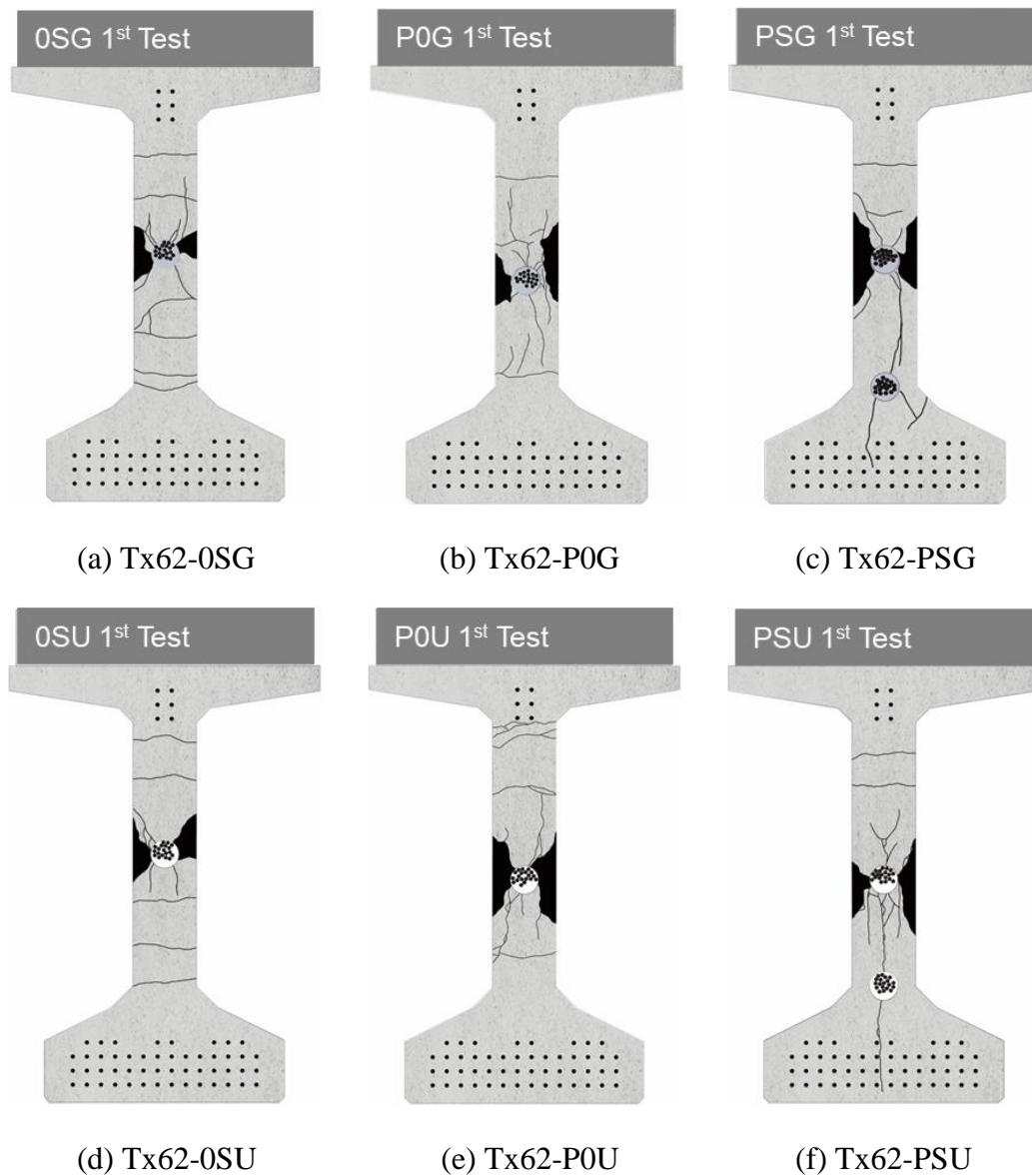


Figure 4.17 Internal Cracking Survey at Critical Section

4.3.3. Web Behavior

4.3.3.1. Web Behavior in the Out-of-Plane Direction

The presence of post-tensioning ducts in the web region of a T_x62 girder introduces a sectional discontinuity that influences the stress distribution around the duct and affects the shear behavior and capacity of the girder. Figure 4.18 depicts the early studies that addressed the phenomenon and shows a deviation of the compressive stress flow in the vicinity of a post-tensioning duct with stiff grout. The through-thickness tensile stresses develop where the compressive stresses start to deviate towards the grouted duct area because the grout was assumed to typically be stiffer than the surrounding concrete. However, in a section with an empty duct, the compressive stresses flow around the empty duct and through-thickness tensile stresses develop in the immediate vicinity of the duct. In both cases, through-thickness tensile stresses are induced by the deviation of compressive stresses, which eventually resulted in a reduction in the shear capacity of the girder (Muttoni et al., 2006; Wald et al., 2017).

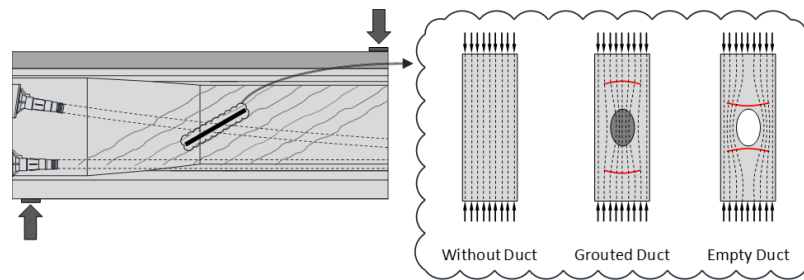


Figure 4.18 Internal Compressive Stress Flow in Thin Web of Post-Tensioned Girder and Concrete Panel Analogy of the Specimens without Duct, Grouted Duct, and Empty Duct (Adopted from Moore et al., 2017)

However, the previous study on the panel-based analogy has not investigated the actual structural boundary conditions. Moore et al. (2015) stated that the principal cause for the results from the panel-based test contradicting those from the large-scale test is the different governing failure mechanism. As such, all panel-based tests by Wald et al. (2017) reported the splitting failure to out-of-plane direction, as shown in Figure 4.19 due to the compressive-controlled boundary conditions. Figure 4.20 illustrates this structural boundary condition regarding the increase of compressive area with the constant tensile area as the thickness of the panel increases. The test setup with this boundary condition is unlikely to simulate the actual shear mechanism of the I-girder, highly resulting in governed splitting failure similar to the concrete test of splitting tensile strength (ASTM C496 1996). The research team firmly recommend applying the shear key into panel-based test setup introduced by Vecchio and Collins (1986) to simulate the actual shear mechanism of the I-girder.



Figure 4.19 Splitting and Crushing Failure Mechanisms of Panel-Based Specimens (Wald et al., 2017)

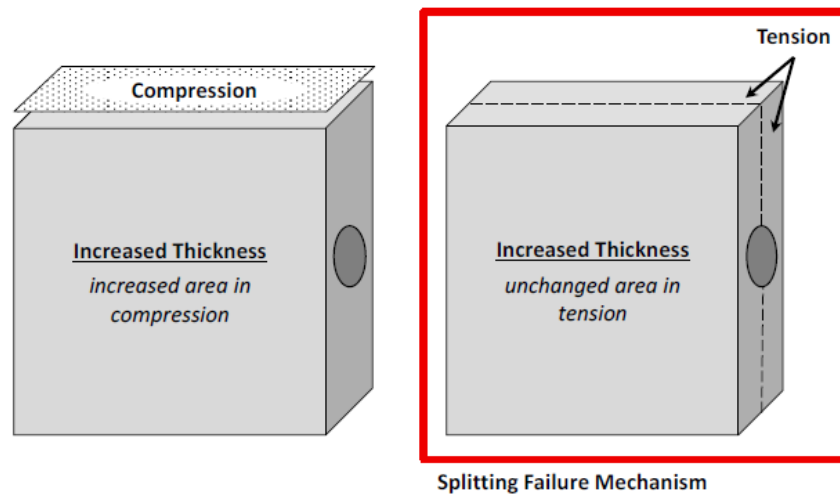
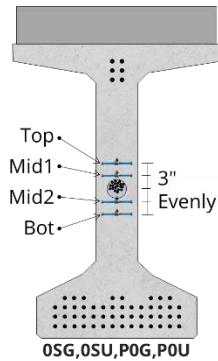
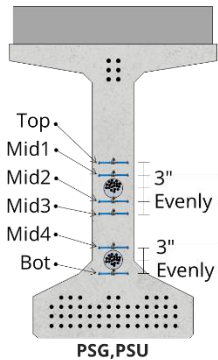


Figure 4.20 Cross-Sectional Area with the State of Compression and Tension in Terms of Increased Thickness (Moore et al., 2015)

Table 4.1 presents the measured tensile strain development at each gauge during the structural test. Note that “out-of-range (OR)” indicates that the increasing tensile strain exceeded the gauge’s measurement range. Around the duct area, where the strain measurements were taken, VWGs clearly report the increasing tensile strain in the out-of-plane direction. Most importantly, two locations close to the duct at the middle of web height (i.e., Mid 1, Mid 2) exceedingly expanded to the out-of-plane direction, which explained the localized web crushing regardless of duct condition. This observation contradicts the previous study’s established panel analogy, as shown in Figure 4.18 (Moore et al., 2017). This will be discussed in detail in Section 5.3.

Table 4.1 Web expansion at the critical section determined by VWGs

Measurement Location	ID	Specimen State	Load (kip)	Bot ($\mu\epsilon$)	Mid 4 ($\mu\epsilon$)	Mid 3 ($\mu\epsilon$)	Mid 2 ($\mu\epsilon$)	Mid 1 ($\mu\epsilon$)	Top ($\mu\epsilon$)
 OSG, OSU, POG, POU	OSG	Before shear crack	1000	-11	-	-	48	56	7
		Starting nonlinear	1180	-8	-	-	223	200	16
		Ultimate failure	1376	4	-	-	459	450	18
	POG	Before shear crack	1000	-21	-	-	53	34	-2
		Starting nonlinear	1451	347	-	-	1489	1781	1223
		Ultimate failure	1750	OR*	-	-	OR*	OR*	OR*
	PSG	Before shear crack	1000	-31	-26	-19	43	43	5
		Starting nonlinear	1277	-13	-27	-12	862	799	16
		Ultimate failure	1630	4	127	1682	OR*	OR*	OR*
 PSG, PSU	OSU	Before shear crack	1000	-12	-	-	49	206	10
		Starting nonlinear	1208	-10	-	-	353	758	26
		Ultimate failure	1500	1646	-	-	OR*	OR*	849
	POU	Before shear crack	1000	-22	-	-	92	35	2
		Starting nonlinear	1345	341	-	-	OR*	1025	45
		Ultimate failure	1560	2061	-	-	OR*	OR*	1066
	PSU	Before shear crack	1000	-43	-30	-26	68	47	-3
		Starting nonlinear	1378	-23	-5	-21	424	622	23
		Ultimate failure	1625	-18	55	OR*	OR*	OR*	OR*

* OR (out-of-range) indicates that the tensile strain in the out-of-plane direction exceeded the gauge’s measurement range.

4.3.3.2. Web Behavior in the In-Plane Direction

In addition to measuring physical displacements, the research team monitored the strains during the structural test using the Optotrak Certus motion capture system, an optical measurement system manufactured by NDI, as detailed in Section 4.2.3. This motion capture system tracks the position of infrared light-emitting diodes referred to as “markers.” These data were post-processed and used to investigate the web area’s strain distribution, which aided in identifying the controlled failure mechanism over the course of the structural test. For this project, the markers were installed to form a six-inch grid within the test region. The recorded displacements of the markers were used to estimate the average strain of each six by six-in. quadrilateral element.

The plots in Figure 4.21 show the vertical strain development with respect to the applied load. This observation was used to evaluate the behavior of transverse reinforcement. Note that data were only collected for four specimens, Tx62-0SG, 0SU, P0G, and PSU, due to an unexpected instrumentation malfunction for specimens of Tx62-P0U and PSG. Thus, this study will discuss the available motion capture data from Tx-0SG, 0SU, P0G, and PSU only. In this plot, all 9 lines are shown with a six-inch uniform spacing. Note that line 1 is located next to the general section, and Line 9 is located next to the end-block, with the other lines in between (the reference of the line number in Figure 4.22).

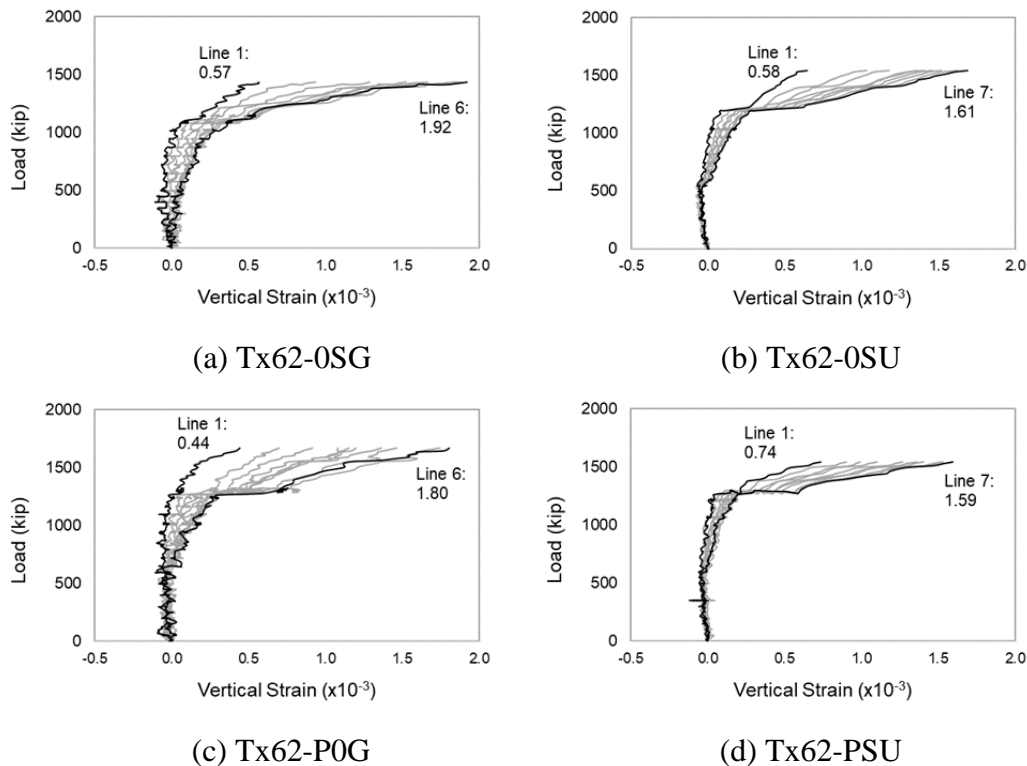


Figure 4.21 Vertical Strain Development at the Critical Section during the Structural Test

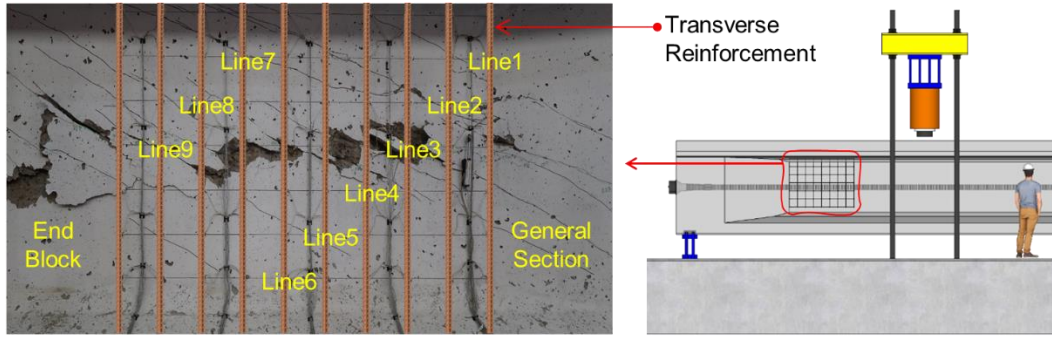


Figure 4.22 Vertical Strain Development at the Critical Section during the Structural Test

In post-processing, the data collected from the markers was subdivided from the quadrilateral elements defined by four markers into two triangles, each defined by three markers. The shape functions from constant strain triangle elements estimate the strain based on the nodal displacements. Finally, an area-weighted average of the two triangles determines the average strain in the quadrilateral region. These post-processed data were used to quantify the state of the cracked concrete component as shown in Figure 4.23. Note that red indicates high strain and green indicates low strain.

	← General Section				End-Block →			
Top	2.36	2.77	2.84	2.50	2.15	2.15	2.59	2.20
	2.86	1.77	2.51	2.61	1.73	0.77	0.35	0.84
	3.76	4.86	4.91	6.11	3.83	3.19	3.29	2.32
	0.68	1.11	1.77	5.01	5.29	4.21	3.72	4.24
	0.72	1.00	1.38	1.31	0.97	3.00	2.20	2.90
Bot	0.38	0.22	1.07	2.04		3.12	3.11	3.57

	← General Section				End-Block →			
Top	-0.97	-0.87	-0.88	-0.73	-0.70	-0.69	-0.60	-0.62
	-0.90	-0.64	-0.99	-0.56	-0.83	-0.57	-0.45	-0.58
	-0.71	-1.21	-1.72	-0.96	-1.40	-0.95	-0.77	-0.88
	-0.53	-0.51	-0.62	-0.64	-1.36	-1.32	-0.84	-1.16
	-0.29	-0.40	-0.68	-1.04	-0.72	-0.80	-0.23	-0.75
Bot	-0.17	-0.30	-0.51	-0.27		-0.24	-0.20	-0.40

(a) Tx62-0SG

	← General Section				End-Block →			
Top	1.97	2.28	2.87	2.64	2.16	1.75	1.42	1.38
	3.05	3.00	1.83	1.93	2.04	2.07	1.25	0.79
	2.40	3.06	3.90	4.95	4.14	3.64	2.13	1.30
	1.96	2.78	2.59	2.28	3.85	4.82	6.22	5.69
	0.17	0.06	1.57	1.73	2.47	1.09	1.84	1.60
Bot	0.32	0.28	0.20	0.17	1.89	2.39	3.21	2.31

	← General Section				End-Block →			
Top	-0.86	-0.93	-0.95	-0.71	-1.08	-0.75	-0.94	-0.73
	-1.06	-1.02	-0.76	-0.44	-0.69	-0.72	-0.70	-0.65
	-0.73	-0.83	-0.75	-0.89	-0.86	-1.15	-0.88	-0.89
	-0.73	-0.90	-0.55	-0.86	-0.96	-1.63	-0.91	-1.19
	-0.37	-0.46	-0.58	-0.84	-0.80	-0.73	-0.65	-0.82
Bot	-0.25	-0.33	-0.34	-0.38	-0.38	-0.54	-0.50	-0.27

(b) Tx62-0SU

	← General Section				End-Block →			
Top	2.22	2.60	1.90	2.40	2.49	1.26	0.98	0.13
	1.92	1.63	2.59	3.22	2.79	1.60	2.24	2.10
	2.67	2.94	2.02	2.76	4.01	2.30	1.35	1.21
	0.89	1.80	2.14	2.92	2.95	3.89	4.08	3.10
	1.06	1.32	0.36	1.30	1.31	3.41	3.13	2.01
Bot	1.18	1.93	1.34	0.29	0.35	2.97	2.75	2.36

	← General Section				End-Block →			
Top	-1.17	-0.89	-0.77	-0.90	-0.58	-0.73	-0.63	-0.66
	-0.68	-0.47	-0.72	-0.52	-0.67	-0.67	-0.66	-0.70
	-0.52	-0.77	-0.72	-0.82	-1.08	-0.89	-0.78	-0.70
	-0.44	-0.64	-0.52	-0.88	-0.80	-0.49	-0.61	-1.16
	-0.13	-0.20	-0.19	-0.51	-0.50	-0.72	-0.90	-0.91
Bot	-0.09	-0.07	-0.19	-0.22	-0.13	-0.48	-0.58	-0.44

(c) Tx62-P0G

	← General Section				End-Block →			
Top	2.13	2.07	2.43	2.12	2.46	2.45	1.61	1.23
	2.37	2.38	2.11	1.41	1.46	1.17	1.10	1.38
	0.90	2.48	3.14	3.84	3.67	0.99	0.71	0.70
	1.90	2.72	3.34	3.52	5.03	6.29	6.06	5.83
	0.97	1.18	0.55	2.53	2.76	2.99	2.85	1.64
Bot	0.43	0.54	0.52	0.77	0.56	0.98	2.08	2.71

	← General Section				End-Block →			
Top	-0.71	-0.61	-1.03	-0.75	-0.76	-0.62	-0.85	-0.63
	-0.73	-0.73	-0.66	-0.74	-0.62	-0.53	-0.72	-0.70
	-0.81	-1.01	-1.09	-1.40	-0.80	-1.10	-1.09	-1.02
	-0.69	-0.79	-1.00	-0.41	0.11	-1.22	-1.48	-1.41
	-0.56	-0.62	-0.73	-0.83	-0.71	-1.22	-1.34	-1.04
Bot	-0.29	-0.40	-0.57	-0.63	-0.69	-0.81	-0.79	-0.57

(d) Tx62-PSU

Figure 4.23 Determined Principal Strain of ε_1 (Left Column) and ε_2 (Right Column)

4.3.4. Behavior of Specimen with UngROUTED Ducts

The structural testing program was designed to conduct two tests on each specimen, one at each end of the girders. After the first test was performed, the setup was adjusted, and the instrumentation used for the first test was relocated to the other end of the girder to conduct the second test. The shear span-to-depth ratio (i.e., a/d) of 2.4 was maintained for both tests. The second test was successful for all grouted specimens, the intended shear-governed failure mode developed in the test span. The behavior observed during the second test, closely matched the behavior during the first test. However, a premature failure occurred during the second test in the back span of the first ungrouted specimen of Tx62-P0U— a/d of 3.8 in the back span (additional span length information for this structural setup is provided in Section 4.1). This necessitated a concrete repair in subsequent tests.

The structural test was designed to apply a shear force of approximately 61% of the total load in the test span, while the back span was subjected to 39% of the total load. Moreover, the specimen with ungrouted duct resulted in the axial force in the damaged region from the first test (i.e., shortening behavior). These combined forces increased the effect of shortening on the damaged region and caused additional web crushing in the vicinity of the duct. Evidence to support this, as shown in Figure 4.24(a), is the loss of post-tensioning during the second test, which did not occur in the first test. This indicates the girder had been experiencing the shortening behavior by axial force in the damaged region. Finally, the damaged region failed to carry additional axial and shear forces.

After overlay repair concrete was applied to the damaged region, the repaired test specimen of Tx62-0SU continued to carry the axial and shear forces until the completion of the second test, as shown in Figure 4.24(b).

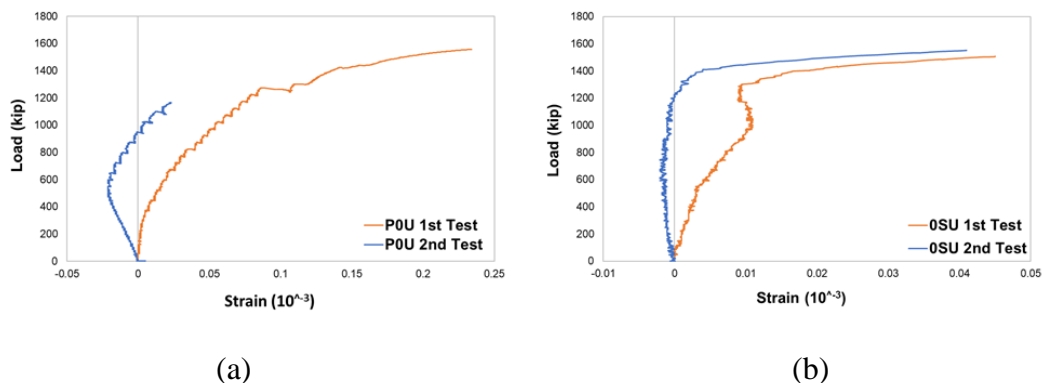


Figure 4.24 Behavior of Post-Tensioning Strands and Corresponding Loads during the Test: (a) Post-Tensioning of Tx62-P0U and (b) Post-Tensioning of Tx62-0SU

Therefore, after the premature failure during the second test of the first ungrouted girder, a CIP overlay repair concrete was applied in the damaged region for all remaining ungrouted specimens before performing the second test. This repair plan increased the cross-sectional thickness of the damaged region, thereby resisting the combined shear and axial force and mitigating the shortening effect on the girder. To increase the web thickness, double layers of transverse rebars were anchored into the holes of the top and bottom flanges using Hilti Epoxy HIT-HY 220R, as shown in Figure 4.25(a). Prior to the CIP concrete application, the steel forms on each side were closed and external vibrators were installed on the forms. Figure 4.25(b) shows the removal of side forms after repair concrete placement. After the second test was successful, the repair plan was replicated for the remaining specimen.



Figure 4.25 CIP Overlay Repair Concrete Placement: (a) Anchored Rebar Cage and (b) Completion of Repair Concrete Placement on Each Damaged Side

4.3.5. Summary of Test Results

4.3.5.1. Service Level Cracking

The serviceability of structural components shall be considered with the structural performance at the service level of loading in the aspects of cracking, deformation, and concrete stresses according to AASHTO LRFD (2020). Based on the notion of this provision, an early study by Birrcher et al. (2009) provided an experimental-based methodology to determine the serviceability performance subjected to in-plane shear loading by using the prestressed concrete member such that the ratio of the shear resistance factor (ϕ) to the load factor (η) is equal to the ratio of the service level load to the nominal capacity. This study will review Birrcher et al.'s similar approach to determine the serviceability of post-tensioned concrete members. The ratio of service level load to nominal capacity is determined as:

$$\phi \cdot \text{Nominal Capacity} \approx \eta \cdot \text{Service Level Load} \quad \text{Equation 15}$$

rearrange as:

$$\frac{\phi}{\eta} \approx \frac{\text{Service Level Load}}{\text{Nominal Capacity}} \quad \text{Equation 16}$$

where ϕ is the shear resistance factor of 0.9 and η is the load factor defined as a function of the load case and the distribution of the loads. This study uses the suggested η factor equal to 1.4 based on the assumptions of (1) Strength I—basic load combination relating to the normal vehicular use of the bridge without wind—in AASHTO LRFD (2020) governs design, 1.25 DL + 1.75 LL and (2) 75% of the service load is DL with 25% of the service load is LL.

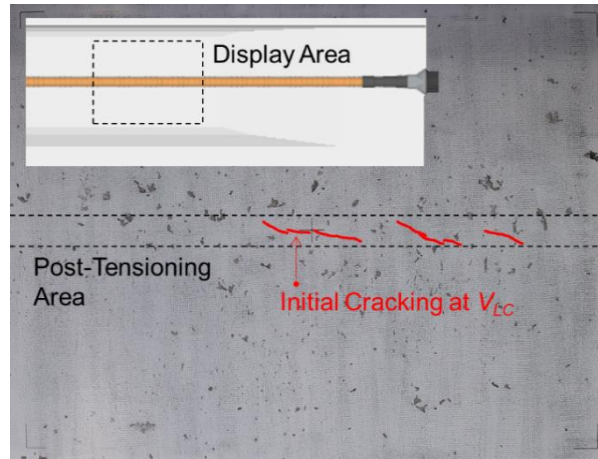
Using Equation 15, Birrcher et al. (2009) reported the proposed model to compute the ratio of service level load to experimental capacity can be calculated as:

$$\frac{V_n}{V_{test}} \cdot \frac{\phi}{\eta} = \frac{1}{1.3} \cdot \frac{0.9}{1.4} \approx 0.5 \quad \text{Equation 17}$$

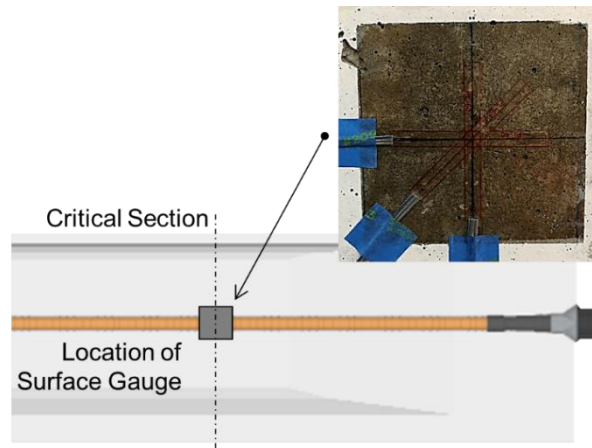
where V_n is the nominal shear resistance, V_{test} is the shear strength from the test. In this study, the ratio of the nominal shear resistance to ultimate strength equals 1.3 for grouted duct case, which can be found in Section 4.4. The computed ratio of approximately 0.5, related to the relationship between the experimental ultimate shear capacity and the nominal capacity of a section, is the service level load as a function of V_{test} .

The aforementioned assumptions are applied to calculate this value, and the change in any of these assumptions can alter this ratio. However, this approach serves as a good reference for the service level determined by the experimental results. In this study, the determined service load level is compared to the shear loading level to cause the first cracking (referred to as V_{LC}) to evaluate the service level of shear behavior in the post-tensioned concrete members.

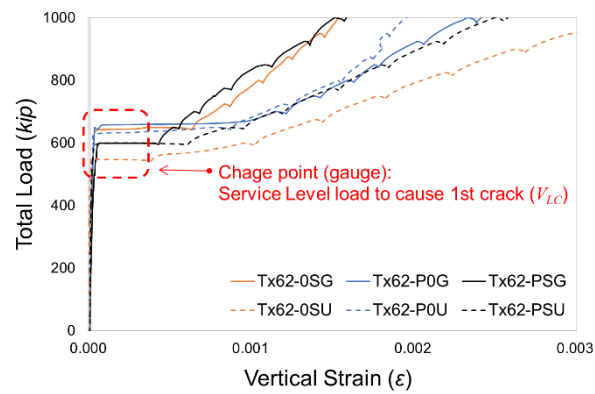
As mentioned in Section 4.3.2, all post-tensioned test specimens regardless of duct conditions experienced initial hairline cracks at the duct area, as shown in Figure 4.26(a) that occurred at a shear force level of (V_{LC}). To refine the serviceability analysis, the research team monitored the occurrence of cracking within the testing span using the strain development of the surface gauge, as shown in Figure 4.26(b). Figure 4.26(c) shows the vertical strain development containing the change point of distinctly elevated strain. This change point of shear loading level (V_{LC}) is validated by the visual inspection for the occurrence of initial hairline crack as illustrated in Figure 4.26(a). This information will clearly explain the serviceability of post-tensioned girder, which will discuss as follows.



(a)



(b)



(c)

Figure 4.26 The Analysis of Service Level Loading: (a) Initial Cracking at the Critical Section; (b) Attached Surface Gauges; and (c) Vertical Strain Development

Table 4.2 presents the analysis of serviceability methodology in terms of the shear force for the service level crack (V_{LC}) based on the change point by using the surface gauge, the ratio of V_{LC} to V_{Test} , and normalized shear stress. The serviceability performance of post-tensioned concrete girders was inferior to the predicted behavior using Birrcher et al.'s method (2009). More importantly, the normalized shear stress of both grouted and ungrouted specimens indicated similar stress levels to trigger the onset of the diagonal shear cracks in the post-tensioning duct area. In other words, no difference in serviceability performance was observed regardless of the duct condition.

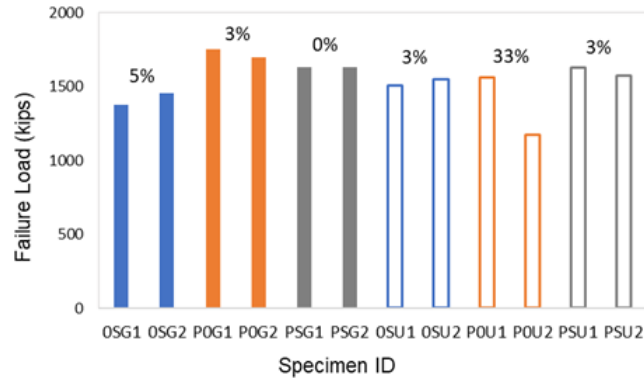
Table 4.2 Service level cracking for grouted and ungrouted specimens

		V_{LC} (kip)	V_{Test} (kip)	V_{LC}/V_{Test} (Ratio)	*Normalized shear stress
Grouted specimens	Tx62-0SG	403	855	0.47	0.18
	Tx62-P0G	418	1082	0.39	0.19
	Tx62-PSG	383	1011	0.38	0.16
Ungrouted specimens	Tx62-0SU	352	961	0.37	0.15
	Tx62-P0U	411	966	0.43	0.18
	Tx62-PSU	381	1005	0.38	0.17

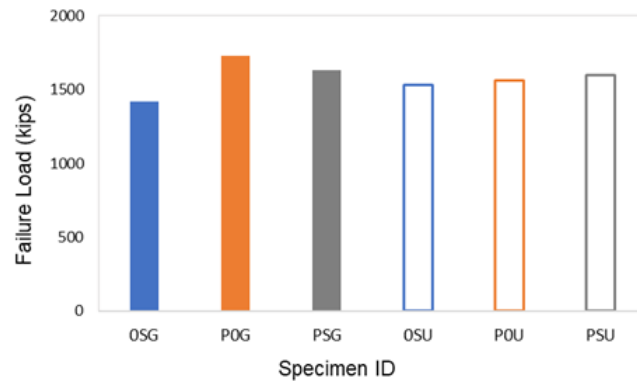
* Normalized shear stress calculated as $(V_{LC}-V_P)/(b_w d_v \sqrt{f'_c})$

4.3.5.2. Ultimate Level

As described in Section 4.1, the research team conducted 12 tests on six test specimens in the experimental program. Figure 4.27(a) shows the failure load of each test. Note that, as expected, the failure loads obtained from each pair of tests were within 5% of each other. For clarity, the average failure load from each pair of tests, as shown in Figure 4.27(b), will be used for the comparison with AASHTO LRFD shear resistance. However, Tx62-P0U experienced premature failure during its second test, and it was the first ungrouted test specimen to do so. Thus, only the first test result for Tx62-P0U was used for further analysis.



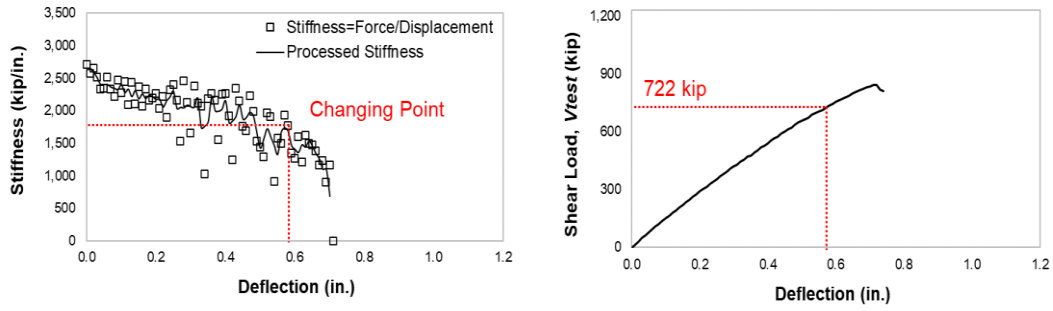
(a)



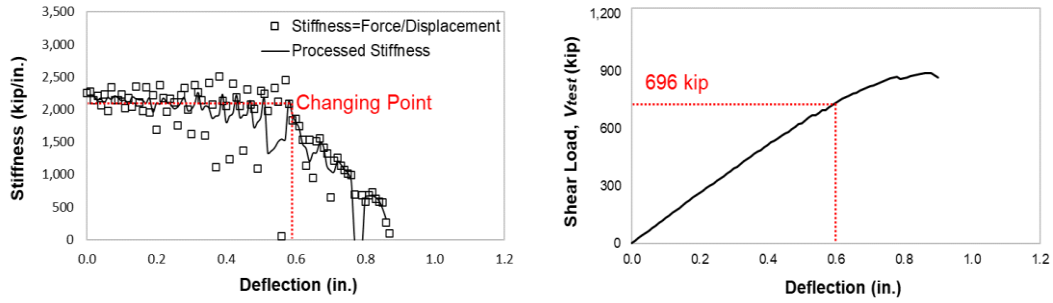
(b)

Figure 4.27 Summary of Failure Loads from the 12 Tests: (a) Failure Load from Each of the 12 Tests and (b) Average of Two Tests' Failure Load for Each of the Six Tested Specimens

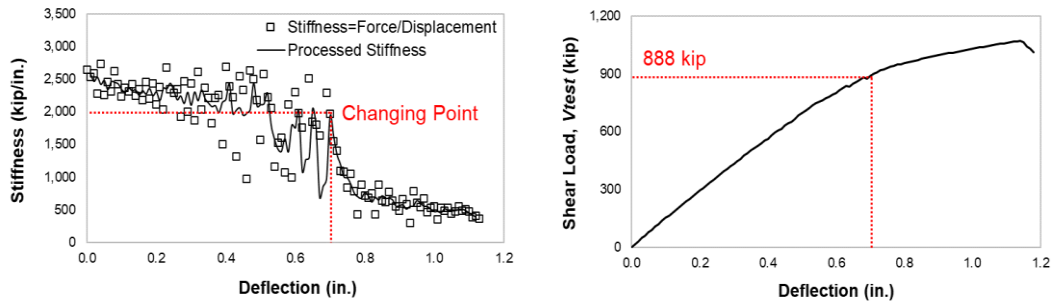
Figure 4.28 shows the load-deflection plots along with the stiffness analysis of all tested specimens. The stiffness analysis determined the specimen's change point from linear to nonlinear behavior, calculated by dividing the applied force by the corresponding deflection. This change point matched the onset of a fully developed diagonal shear crack, consistently occurring at load levels of approximately 80% of the ultimate load.



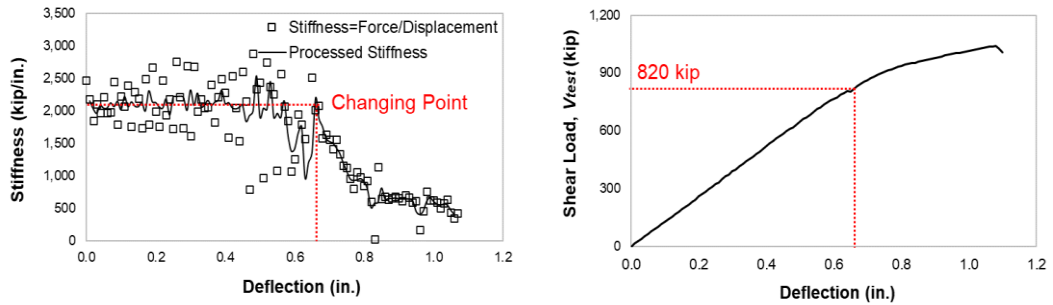
(a) Tx62-0SG (1st test)



(b) Tx62-0SG (2nd test)

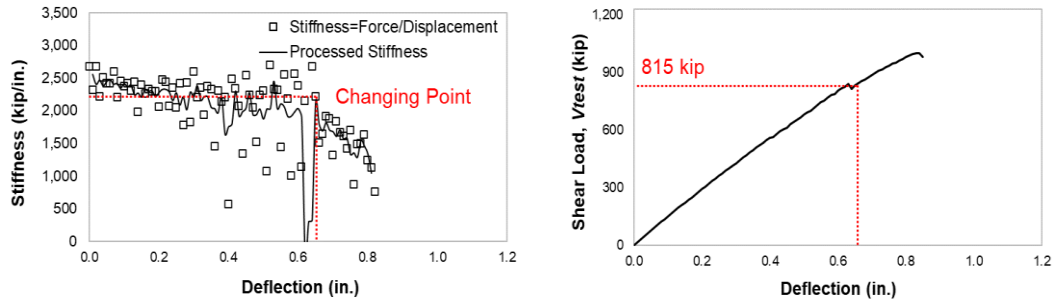


(c) Tx62-P0G (1st test)

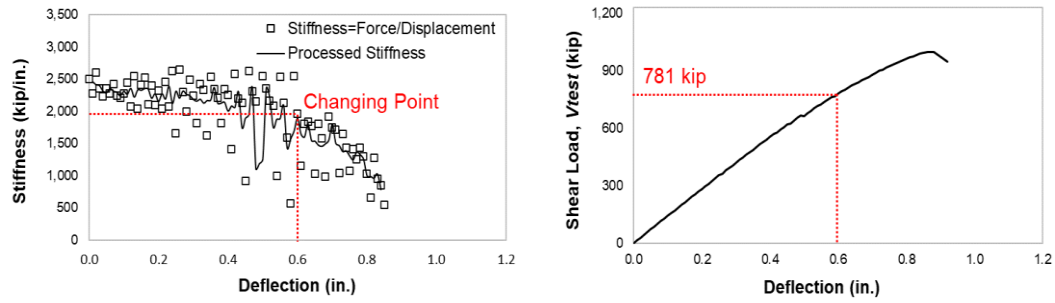


(d) Tx62-P0G (2nd test)

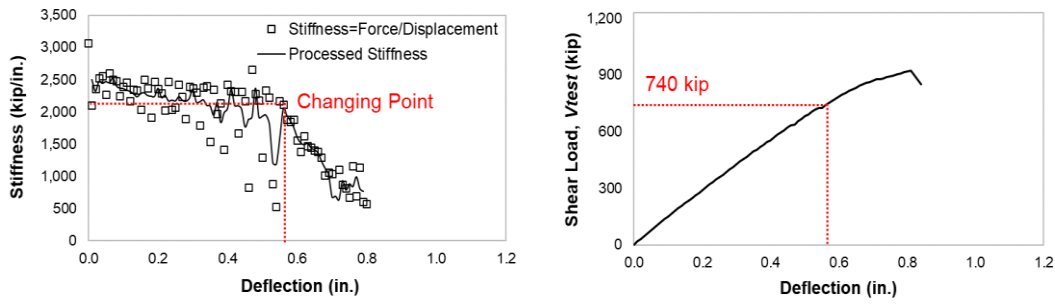
Figure 4.28 Stiffness Analysis to Define Nonlinear Behavior (Left Column) and Shear Force Behavior (Right Column) with Respect to Deflection



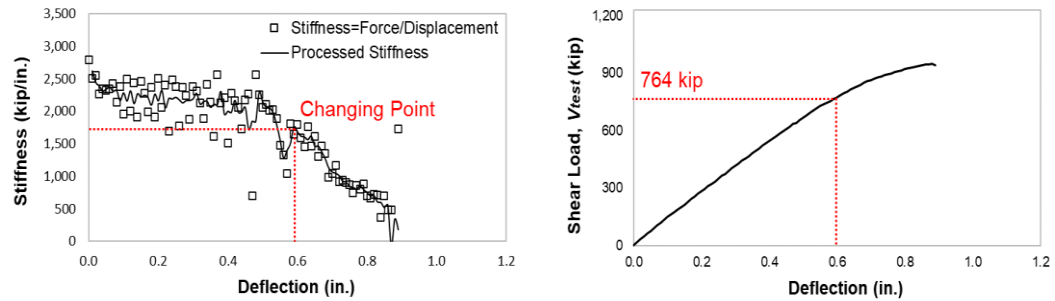
(e) Tx62-PSG (1st test)



(f) Tx62-PSG (2nd test)

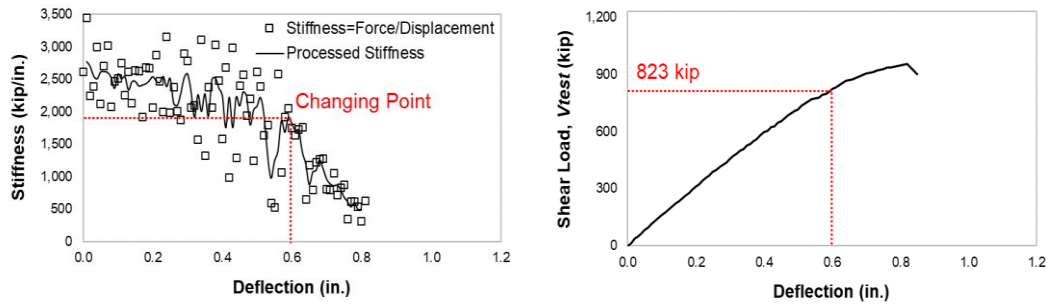


(g) Tx62-0SU (1st test)

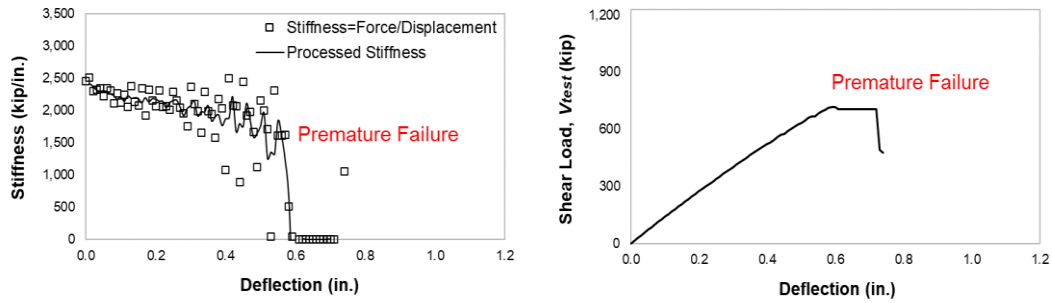


(h) Tx62-0SU (2nd test)

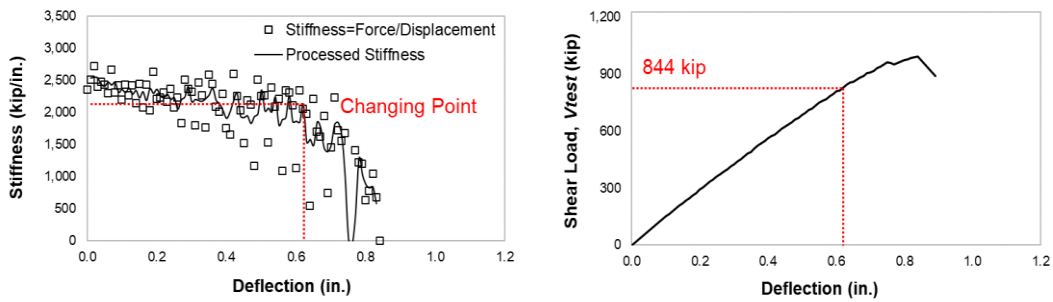
Figure 4.28 (cont.) Stiffness Analysis to Define Nonlinear Behavior (Left Column) and Shear Force Behavior (Right Column) with Respect to Deflection



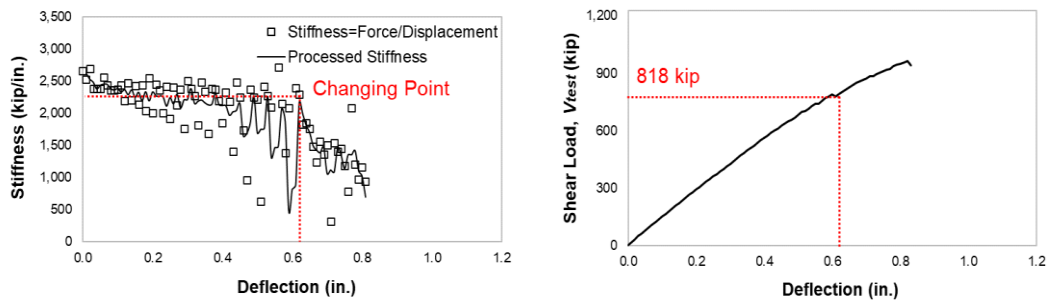
(i) Tx62-P0U (1st test)



(j) Tx62-P0U (2nd test)



(k) Tx62-PSU (1st test)



(l) Tx62-PSU (2nd test)

Figure 4.28 (cont.) Stiffness Analysis to Define Nonlinear Behavior (Left Column) and Shear Force Behavior (Right Column) with Respect to Deflection

It is beneficial to normalize the ultimate shear stress by using Equation 18.

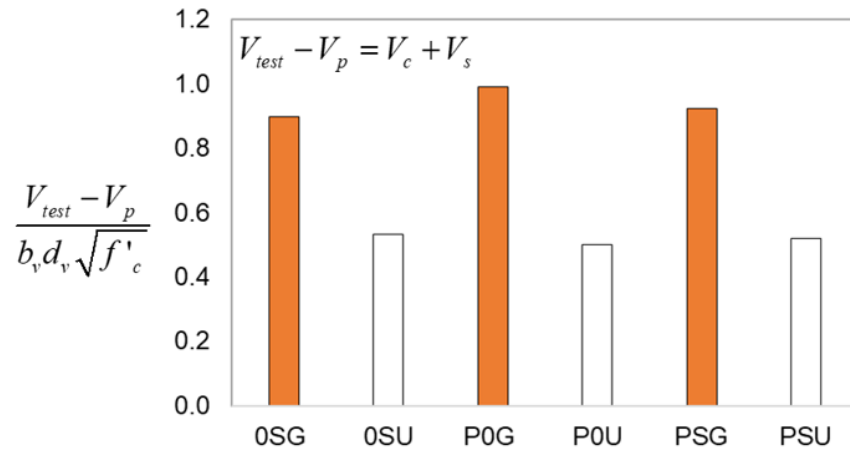
$$v_{normal} = \frac{V_{test} - V_p}{b_v d_v \sqrt{f'_c}} \text{ or } \frac{V_{test} - V_p}{b_w d_v \sqrt{f'_c}} \quad \text{Equation 18}$$

where V_{test} is the maximum shear force carried by the test specimen, V_p is the vertical component of the prestressing force, b_v is the effective web width, b_w is the gross web width, and d_v is the effective shear depth.

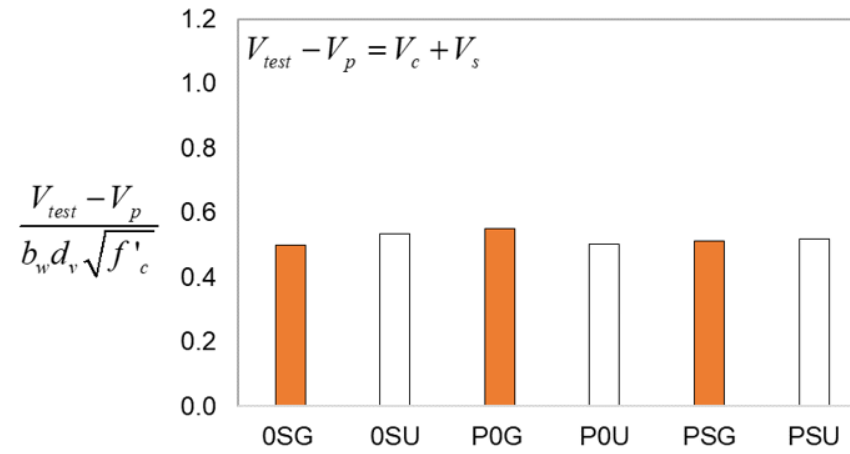
The coefficient of effective web width (k) plays a pivotal role in determining the shear behavior of the post-tensioned concrete member. For example, the current edition of AASHTO LRFD (2020) establishes different values for k based on the filler condition of the duct due to the different internal stress flows, as shown in Figure 4.18. Accordingly, Figure 4.29(a) shows the normalized shear stress calculated using the effective web width (b_v), which applies the appropriate values of k to the specimens containing grouted and ungrouted ducts, respectively. It clearly indicates that, using the current AASHTO LRFD procedure, higher shear stress levels are calculated for the specimens with grouted ducts compared to the ungrouted ones. Figure 4.29(b) shows the normalized shear stress calculated using the gross web width (b_w) regardless of duct condition. Remarkably, all test specimens are calculated to develop a similar level of normalized shear stress.

In Section 4.3.2, the survey of the cracking in the web revealed well-distributed, fan-shaped shear cracks for all test specimens. This indicates that the whole web engages in the shear force resistance mechanism. As the cracked concrete component carries shear through the aggregate interlock force at the crack interfaces, similar patterns of diagonal cracking could expect a similar shear resistance from the effect of aggregate interlock on the cracks based on the aforementioned shear resistance in Section 2.2. In this shear mechanism, the same coefficient of effective web width correction factor should be considered to take into account the cracking of the web area that develops during shear loading.

All in all, the use of the gross web width to estimate the normalized shear stress contradicts this project's intention to establish the effective web widths for the specimens containing grouted and ungrouted ducts in AASHTO LRFD. To better understand the shear mechanism of post-tensioned concrete members and to determine the coefficient of k , the web behavior will be further analyzed in Chapter 5.



(a)



(b)

Figure 4.29 Normalized Ultimate Shear Stress: (a) Using the Effective Web Width (b_v) and (b) Using the Gross Web Width (b_w)

4.3.6. Experimental Shear Capacity versus AASHTO LRFD

One of the primary goals of this project was to update the shear strength reduction factor, referred to as λ_{duct} , in AASHTO LRFD for post-tensioning girders with ungrouted duct conditions. The shear strength, V_{test} , was calculated at the critical section based on the measured ultimate load from each test. The collected shear design properties, such as prestress loss, material, and geometry conditions, were used to calculate the nominal shear strength, V_n , using the current AASHTO LRFD (2020). Appendix H presents the detailed procedure used to estimate V_n .

Table 4.3 presents the comparison between the experimental shear strength capacity, V_{test} , and the calculated capacity using the AASHTO LRFD shear design, V_n . Moreover, information on reduction factors, such as the web width reduction factor, k , duct diameter correction factor, δ , and shear strength reduction factor, λ_{duct} , are provided to evaluate the current version of shear strength design according to the AASHTO LRFD provisions. Since the primary purpose of this procedure is to evaluate the shear capacity of test girders, the load and resistance factors were taken as 1.0.

The calculated capacities of the specimens with grouted ducts were on average 30% larger compared to the experimental capacities. This level of conservatism is generally regarded as adequate for shear-critical specimens. On the other hand, the calculated capacities for the specimens with ungrouted ducts produced capacity estimates with a smaller safety margin, less than 10% on average. Therefore, the associated shear strength reduction factors need to be revised to provide consistent levels of conservatism with the grouted case.

Table 4.3 Test result Summary with a ratio of test result to nominal shear resistance

Specimen ID	k Web Width Reduction	δ Duct Diameter Correction	λ_{duct} Shear Strength Reduction	V_n Nominal Shear Resistance	V_{test} Test Results	V_{test}/V_n Ratio
Tx62-0SG	0	2	0.605	694	879	1.27
Tx62-P0G	0	2	0.605	766	1,066	1.39
Tx62-PSG	0	2	0.605	809	1,009	1.25
Tx62-0SU	1	0	1.000	906	948	1.05
Tx62-P0U	1	0	1.000	934	966	1.03
Tx62-PSU	1	0	1.000	1,027	990	0.96

4.4. Summary of Experimental Program

The main objective of Chapter 4 was to summarize the results of the structural tests conducted. The research activities and findings are summarized as follows:

- To better understand the specimens' structural behavior, various gauges were deployed to measure load, deflection, web deformation, prestress loss, and sectional behavior. All data were successfully collected.
- The research team found that all tested specimens experienced a similar failure mechanism regardless of the duct condition.

Chapter 5. Development of Design Recommendations

5.1. Overview

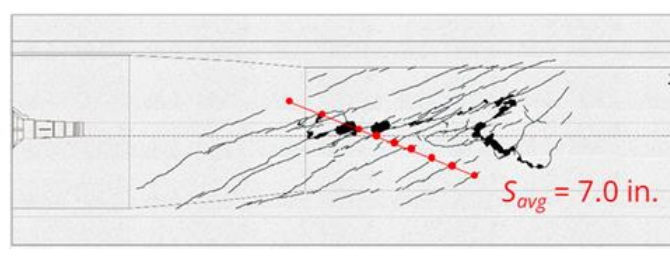
The objective of Chapter 5 is to present the development of shear design recommendations for the post-tensioned girders that incorporate the effect of grouted and ungrouted ducts on the shear resistance mechanism. The proposed changes to the shear design of post-tensioned members are based on the experimental observations summarized in Chapter 4 of this report, as well as the analysis of relevant data available in the literature (Moore et al., 2015). The experimental program undertaken was developed to address the dearth of knowledge with respect to the performance of post-tensioning systems containing ungrouted ducts. The program involved the design, fabrication, and structural test of six large-scale specimens incorporating the following main variables: (i) three different duct layouts (straight, parabolic, hybrid) and (ii) grouted and ungrouted ducts.

The experimental program was successfully completed, and all specimens exhibited similar cracking patterns such as hairline cracks in the duct region, well-distributed diagonal shear cracks over the web, and localized web crushing at the duct region. Initially, hairline cracks were observed at the duct location, and they further developed along the length of the girder as the applied load increased. At approximately 80% of the ultimate load, a dominant shear crack developed from the center of the web to the top and bottom flanges in the test span. Finally, all test specimens failed due to concrete crushing in the vicinity of the post-tensioning duct. Cracking development and ultimate failure mode were consistent, whether the post-tensioning duct was grouted or ungrouted. The three cracking modes related to load and deflection are shown in Figure 4.14.

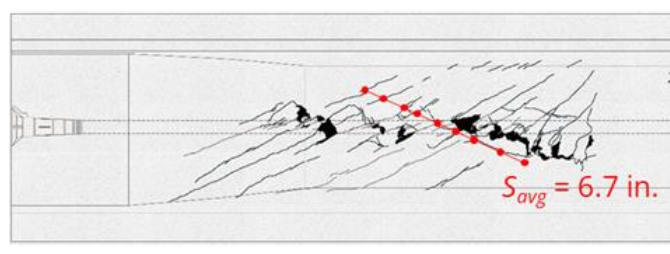
5.2. Proposed Modification for the Calculation of $V_{n1}=V_c+V_s+V_p$

5.2.1. Effective Web Width Factor, b_v

Figure 5.1 depicts the surveyed crack patterns for the specimens with straight grouted and ungrouted ducts. Well-distributed, fan-shaped diagonal cracks developed, which had similar average cracking spacings regardless of the duct condition. Similar cracking patterns were observed for all test specimens. This indicated that the entire web engaged in the shear force resisting mechanism and provided insight for the calculation of the concrete contribution to the nominal shear resistance.



(a) Tx62-0SG



(b) Tx62-0SU

Figure 5.1 Cracking Propagation and Average Cracking Spacing at the Ultimate Load Level

As mentioned in Section 4.3.3, the strains were monitored during the structural test using the Optotrak Certus motion capture system, shown in Figure 5.2(a). The average strains from the selected quadrilateral web region, sized 24 by 24 in., were used to calculate the residual tensile stresses in the cracked concrete component using the Collins-Mitchell model (Collins & Mitchell, 1987). Figure 5.2(b) shows the post-cracking tensile stresses calculated for specimens of Tx62-0SG, 0SU, P0G, and PSU, indicating similar performance. This leads the research team to conclude that there is virtually no difference in terms of the value of the average tensile strains and the concrete tensile stresses between specimens with grouted and

ungROUTED ducts. Therefore, the effective web width correction factor, k , in AASHTO LRFD should be updated to the value of 0.0 for both grouted and ungrouted conditions, to reflect the engagement of the gross web width (b_w), based on the aforementioned results and numerical analysis. Ultimately, the results presented in Section 4 support this hypothesis.

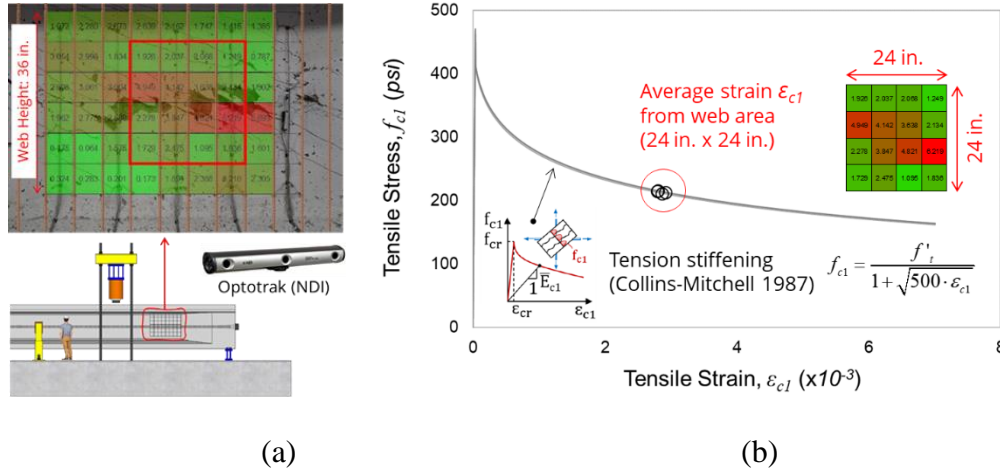


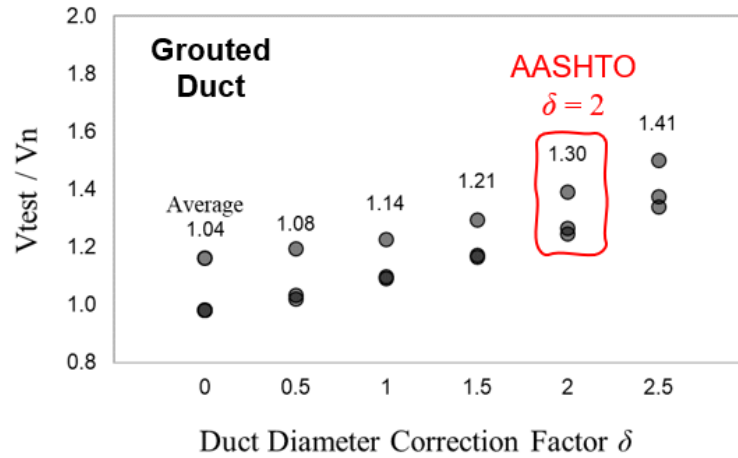
Figure 5.2 The State of Residual Tensile Stress Using Vision System: (a) Vision System Monitoring the Shear Span and (b) State of Tensile Stress at the Ultimate Load Level

In summary, the following conclusions can be made based on the development of cracks and the state of post-cracking concrete tensile stress:

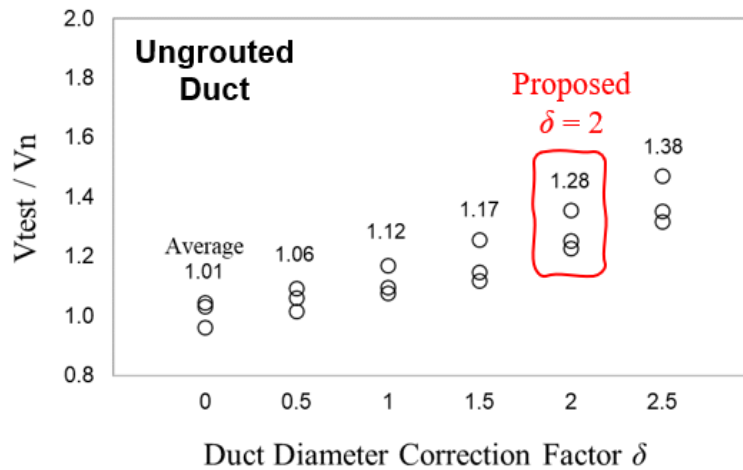
- The entire web engages the shear transfer mechanism, as indicated by the occurrence of well-distributed, fan-shaped diagonal shear cracks for specimens with either grouted or ungrouted ducts.
- No significant difference was observed between the specimens with grouted and ungrouted ducts with respect to the post-cracking tensile stresses of the concrete component.
- As such, the gross web width, b_w , should be used in the calculation of the concrete contribution to the shear strength capacity.

5.2.2. Duct Diameter Correction Factor, δ

Figure 5.3 shows the variation of the experimental-to-calculated ratios as a function of the duct diameter correction factor, δ , in the grouted and ungrouted ducts, respectively. For δ taken as 2.0, the same level of conservatism is achieved for specimens with ungrouted ducts as for those with grouted ducts.



(a)



(b)

Figure 5.3 Duct Diameter Correction Factor (δ) for: (a) the Current Edition of AASHTO LRFD for Grouted Duct and (b) the Proposed Modification for Ungouted Duct

Based on the changes proposed for the effective web width correction factor (k), the proposed value of 2.0 for the duct diameter correction factor (δ) ensures similar structural conservativeness in both grouted and ungrouted ducts.

5.3. Proposed Modification for the Calculation of $V_{n2}=0.25f'_c b_v d_v$

The nominal shear resistance (V_n) is calculated as the smaller value of two nominal shear resistance calculations, referred to as V_{n1} and V_{n2} as follows:

$$V_{n1} = V_c + V_s + V_p \quad \text{Equation 19}$$

$$V_{n2} = 0.25f'_c b_v d_v + V_p \quad \text{Equation 20}$$

The nominal shear resistance (V_{n2}) limits the shear stress level to $0.25f'_c$ to avoid compressive failure of the concrete, as suggested by Bentz et al. (2006). All test specimens experienced localized web crushing failure in the vicinity of the post-tensioning duct at the ultimate loading level, regardless of whether ducts were grouted or ungrouted, as shown in Figure 5.4. The current edition of AASHTO LRFD uses different values for k for grouted duct as the gross web width ($k = 0$) and ungrouted duct as the effective web width ($k = 1$). This approach is not in agreement with the test results that indicate similar failure mechanisms.

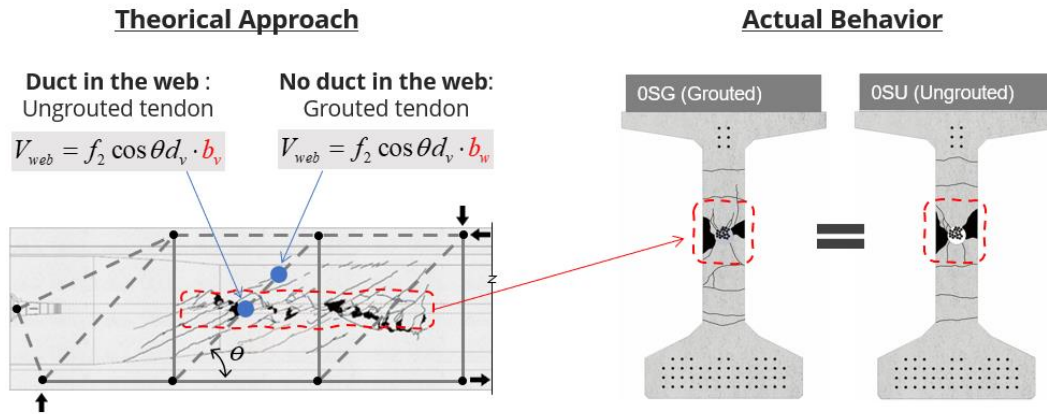


Figure 5.4 The Ultimate Failure Mode of Localized Web Crushing in Specimens with Grouted (Tx62-0SG) or Ungrouted (Tx62-0SU) Ducts

Specifically, the value of k is 0.0 for grouted ducts, as stiff grout is assumed to resist the intruding compressive stress. On the other hand, k is 1.0 for the ungrouted duct, since the empty duct is expected to redirect the internal stress flow, potentially decreasing the resistance of compressive force, as shown in Figure 5.5(a). Nevertheless, this assumed internal stress flow is only validated in the condition of elasticity and linear behavior, which implies no growth of macro-cracks in the concrete component.

The research team surveyed the cracking at the critical section by cutting the tested specimen, as shown in Figure 5.5(b). Three cracking patterns were reported: (i) the horizontal crack, which is the inclined shear crack; (ii) localized web crushing; and (iii) internal cracks around the duct due to the splitting force. When the internal cracks form around the duct, they decrease the bond strength between the duct and adjacent concrete. At the ultimate load level, accounting for the plasticity in the post-tensioned girder, this debonded condition redirects the internal compressive stress flow towards the outside of the cross-section, similar to the ungrouted duct. This plasticity mechanism approach is rational since the nominal shear resistance should be determined at the ultimate loading level.

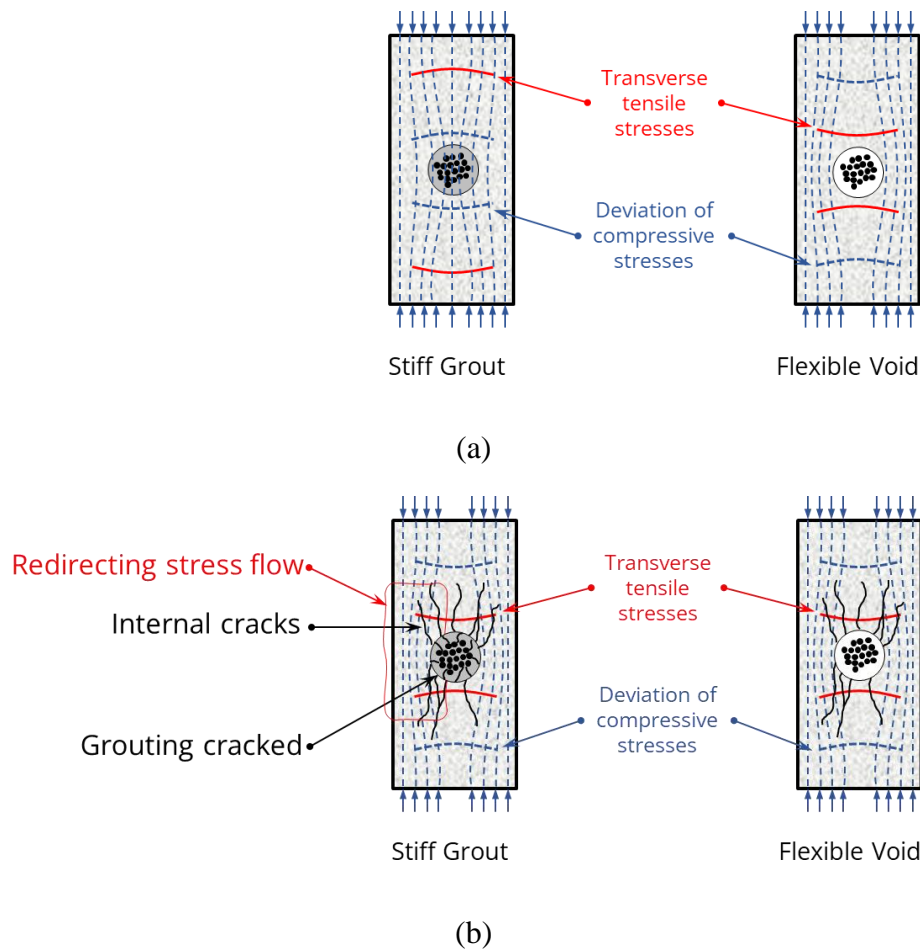
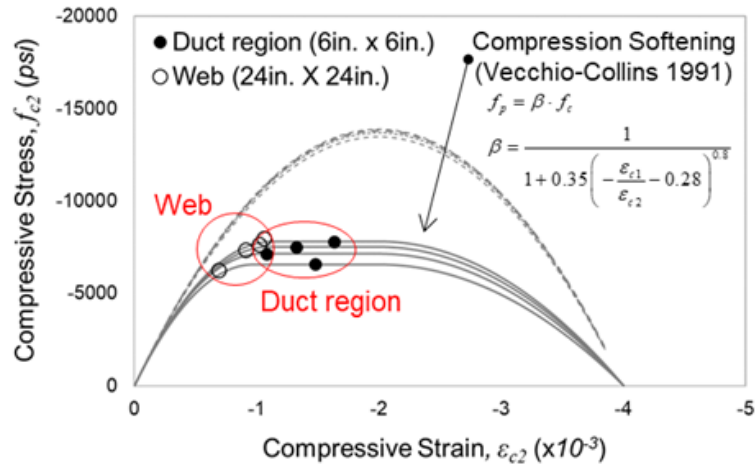


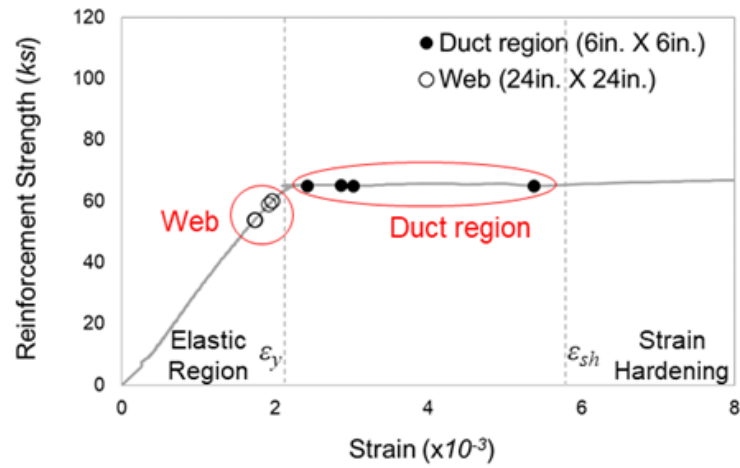
Figure 5.5 The Conceptual Theory of Internal Stress Flow for Grouted and Ungrounded Ducts: (a) Currently Adopted Mechanism Considering Elasticity (Muttoni et al., 2006; Moore et al., 2015) and (b) Proposed Approach Considering Plasticity at the Ultimate Load Level

The motion capture system data at the ultimate load level were used to calculate the principal strains (ε_1 and ε_2) in two quadratic regions: the web (24 x 24 in.) and the duct (6 x 6 in.) at the critical section. The Vecchio-Collins compressive softening model (Vecchio & Collins, 1993) was used to calculate the compressive stress of web and duct regions, respectively, as shown in Figure 5.6(a). This state of compressive stress indicates that the duct region is going to reach localized web crushing before the rest of the web region. Moreover, this analysis predicted similar failure modes regardless of the duct conditions, which aligns with the test results.

In the same manner, the strength contribution of the transverse reinforcement can be determined, as shown in Figure 5.6(b). Using the vertical strain (ε_y), the transverse reinforcement at the duct region is highly expected to yield based on the stress and strain curve from the material test of the reinforcing bar. The stress levels of the concrete and transverse reinforcement components show the failure mode was initiated by yielding of the transverse reinforcement and localized web crushing. This numerical analysis reflects the failure modes from the test results, as shown in Figure 5.4. It is important to note that Bentz et al. (2006) assumed small concrete compression strains (i.e., within the linear-elastic region) in their original derivation that led to Equation 2. However, Figure 5.6 shows that the estimated strains in the girder webs are in the nonlinear region. The condition of the duct for V_{n2} will be discussed in the following section, as this research proposes the effective web width correction factor (k).



(a)



(b)

Figure 5.6 The State of Stress Condition: (a) Concrete and (b) Transverse Reinforcement Component

As the allowable maximum shear stress level of $0.25f'_c$ was originally derived from panel tests without post-tensioning ducts, the research team needed to confirm that it would be appropriate for the estimation of the localized web crushing of post-tensioned girders. The original MCFT by Vecchio and Collins (1986) was simplified by Bentz et al. (2006), as shown in Figure 5.7(a), and this simplified MCFT was adopted by AASHTO LRFD. The upper shear stress limit, $0.25f'_c$, was developed assuming that the concrete was crushing, and the transverse and longitudinal reinforcement were yielding ($\varepsilon_y = \varepsilon_2 = \varepsilon_x = 0.002$), which resulted in the maximum shear stress of $0.28f'_c$. For lower longitudinal strain values (ε_x), the maximum shear stress was estimated to be $0.32f'_c$ (Bentz et al., 2006). This maximum shear stress level range was validated through panel test results, and the coefficient of 0.25 was adopted as a conservative simplification, subsequently validated by Proestos et al. (2018). On the other hand, the effective web width (b_v) for specimens with ungrouted ducts ($k = 1$), has a different internal compressive stress profile due to the duct's geometrical discontinuity, compared to the same value of the gross web width (b_w), as shown in Figure 5.7(b). Thus, there is potentially a risk for unconservative designs. The research team therefore evaluated the influence of the shear stress level limit on the proposed modifications to the AASHTO LRFD shear design provisions using the test results from this project.

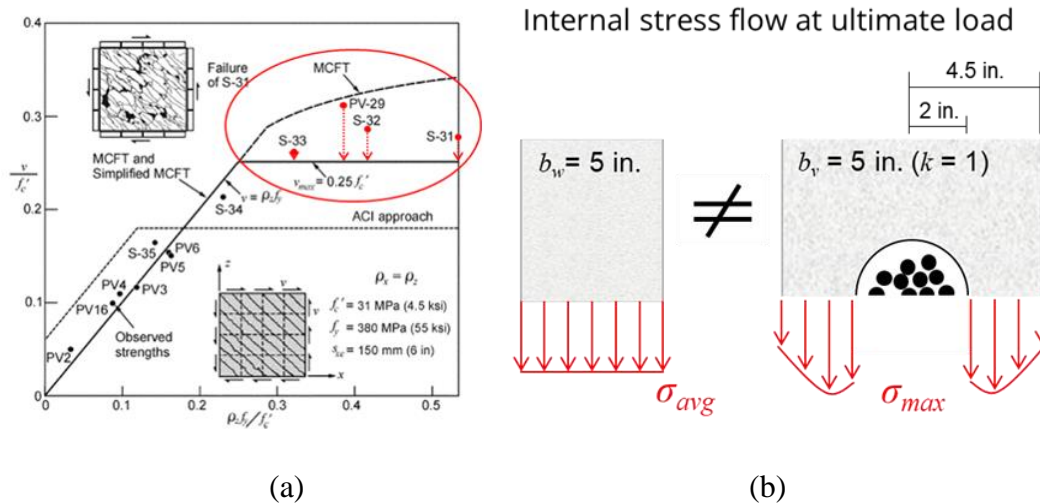


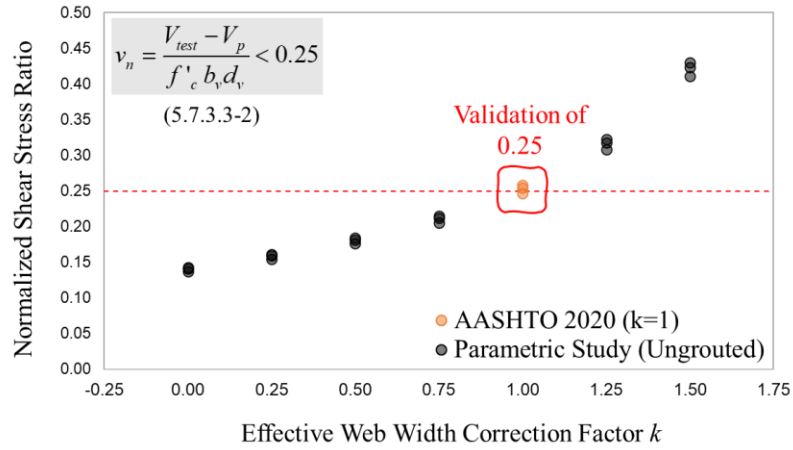
Figure 5.7 Theory Related to Web Crushing: (a) the Simplified MCFT (Reproduced by Bentz et al., 2006) and (b) the Concept of Effective Web Width Factor

The test data from the large-scale specimens provide justification for design coefficients in pursuit of the aforementioned purposes of the effective web reduction coefficient factor (k) and the shear stress level of $0.25f'_c$ for web crushing. Using the shear strength (V_{test}) from the test, the shear stress (v_{test}) can be calculated:

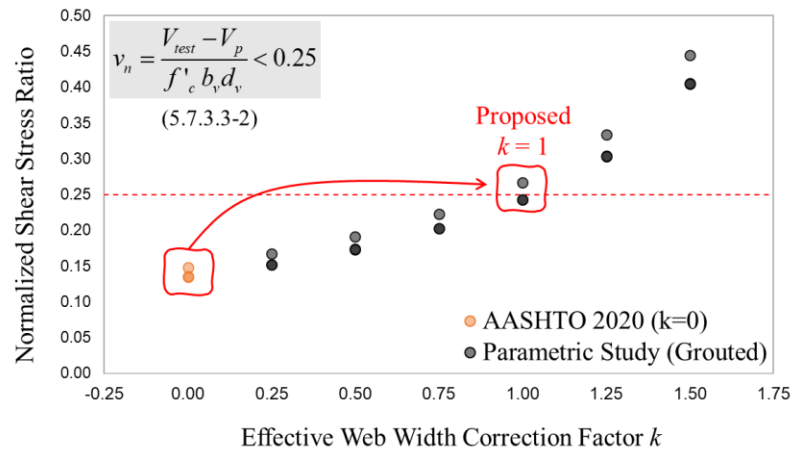
$$v_{test} = \frac{V_{test} - V_p}{b_v d_v} < 0.25f'_c \quad \text{Equation 21}$$

Figure 5.8 shows the results of a parametric study performed to determine the effective web width correction factor, k . The shear stress level for specimens with ungrouted ducts has a value equal to $0.25f'_c$ when $k = 1.0$, corresponding to the current AASHTO LRFD value for k . Based on the internal stress profile shown in Figure 5.5, a value of 1.0 for k is reasonable for an ungrouted duct, reflecting the localized web crushing in the test specimen.

On the other hand, the shear stress levels calculated for the specimens with grouted ducts using the current edition of AASHTO LRFD ($k = 0$) are below the value of $0.25f'_c$. These results disagree with the failure mode observed during the test, web crushing at the onset of transverse reinforcement yielding. To address this issue, the research team proposes to use a value of 1.0 for k , leading to calculated normalized shear stress levels in the range of $0.25f'_c$, as per Figure 5.8(b). This recommendation also aligns with the internal stress flow, as shown in Figure 5.5, considering plasticity in the concrete girder containing the post-tensioning duct.



(a) Specimens Containing UngROUTED Duct



(b) Specimens Containing Grouted Duct

Figure 5.8 The Normalized Shear Stress Level Using the Structural Test with Respect to the Effective Web Width Correction Factor, k

The following conclusions can be drawn:

- The level of concrete compressive stress determined using the Vecchio-Collins compressive softening model (Vecchio & Collins, 1993) justifies the experimentally observed web crushing for specimens with either grouted or ungrouted ducts.
- The tested specimen containing ungrouted duct experiences the localized web crushing at the normalized shear stress level of $0.25f'_c$.
- When k equals 1.0, as proposed, the shear stress level at the failure of specimens with grouted ducts becomes similar to that of specimens with ungrouted ducts. This aligns well with the failure mode of localized web crushing.

5.4. Evaluation of Proposed Modifications

Table 5.1 presents a summary of the proposed modifications to the current edition of AASHTO LRFD. The proposed modifications have a similar approach to the shear design of post-tensioned systems with grouted and ungrouted ducts. They include: (i) the shear strength reduction factor, λ_{duct} , should be used in the calculation of the transverse reinforcement contribution, V_s , to the nominal shear resistance; (ii) the gross web width, b_w , should be used in the calculation of the concrete contribution, V_c , to the nominal shear resistance, V_{n1} ; and (iii) the upper limit on the nominal shear resistance ($V_{n2}=0.25f'_c b_v d_v$) should be calculated using the effective web width, b_v , reduced to account for the presence of the duct.

Table 5.1 Proposed modification for shear design of girders containing post-tensioned ducts

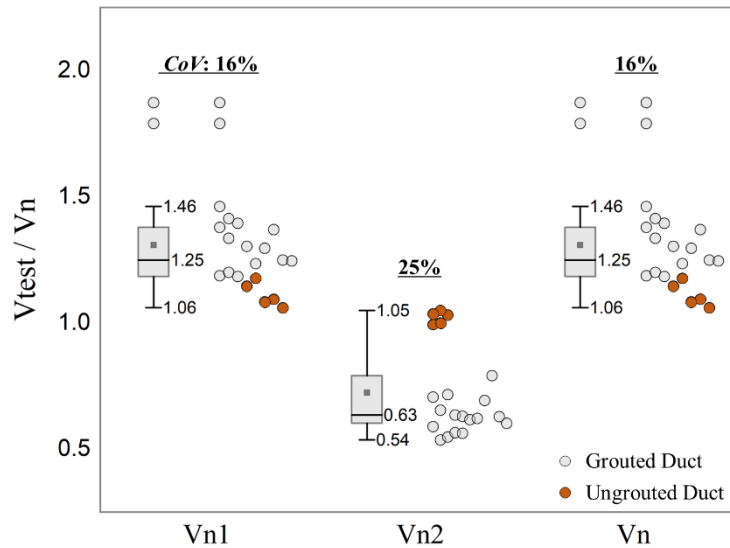
	AASHTO (2020)		Proposed Modification	
Nominal Shear Resistance V_n^\dagger	$V_{n1}=V_c+V_s+V_p$	$V_{n2}=0.25f'_c b_v d_v$	$V_{n1}=V_c+V_s+V_p$	$V_{n2}=0.25f'_c b_v d_v$
Effective Web Width Correction Factor, $b_v = b_w - k \cdot \phi_{duct}$	$k=0(\text{grouted})$ $k=1(\text{ungrouted})$	$k=0(\text{grouted})$ $k=1(\text{ungrouted})$	$k=0(\text{grouted})$ <u>$k=0$</u> [*] (ungrouted)	<u>$k=1$</u> [*] (grouted) $k=1(\text{ungrouted})$
Duct Diameter Correction Factor, $\lambda_{duct} = 1 - \delta \cdot \left(\frac{\phi_{duct}}{b_w} \right)^2$	$\delta=2(\text{grouted})$ $\delta=0(\text{ungrouted})$	Not Applicable	$\delta=2(\text{grouted})$ <u>$\delta=2$</u> [*] (ungrouted)	Not Applicable

*Proposed coefficient based on the results of this study in red with an underline.

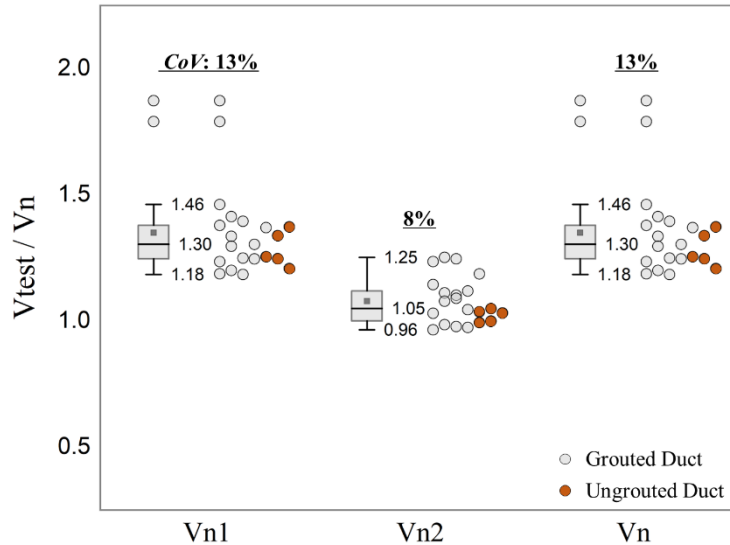
[†] V_n is determined by the lesser of V_{n1} and V_{n2} .

Figure 5.9 shows the comparison between the shear strength predictions obtained using the current AASHTO LRFD shear design equations and using the proposed modifications, in terms of experimental-to-calculated ratios. The results of both $V_{n1}=V_c+V_s+V_p$ and $V_{n2}=0.25f'_c b_v d_v$ are shown, and the lesser value, V_n , is given in the third column. The coefficient of variance (CoV) decreases for the predictions obtained employing the proposed modifications while maintaining a level of structural conservativeness similar to the current AASHTO LRFD equations. In addition, the results obtained for $V_{n2}=0.25f'_c b_v d_v$ employing the proposed modifications are in significantly better agreement with the experimental results, compared to the current AASHTO LRFD equation.

For all specimens, the calculated values for V_{n1} were lower compared to the values obtained for V_{n2} ; as such, the nominal shear resistances, V_n , have the values of V_{n1} . Overall, as indicated by the reduced CoV , the proposed modifications improve the reliability of the shear design equations of the post-tensioned concrete elements. Appendix I provides in-line revisions to the current edition of AASHTO LRFD (2020).



(a)



(b)

Figure 5.9 The Calculation of Nominal Shear Resistance using: (a) Current AASHTO LRFD Equations and (b) Proposed Modifications

5.5. Summary of Design Recommendations

The current AASHTO LRFD (2020) for the shear design of post-tensioned concrete members accounts for a reduction in the shear capacity due to the detrimental effect caused by the presence of ducts in the web region, varying based on the condition of the ducts. For grouted ducts, this is accomplished through a reduction in the contribution of the transverse reinforcement, while for ungrouted ducts, AASHTO LRFD (2020) uses a reduced effective web width in the shear design equations.

Chapter 5 aimed to develop updated design recommendations for post-tensioned members. To achieve this goal, the structural test results and shear models were thoroughly reviewed to shed light on the underlying similarities and differences between the shear responses of post-tensioned members containing grouted and ungrouted ducts. In conclusion, no significant shear strength difference was found between grouted and ungrouted ducts.

The research findings and conclusions from Chapter 5 are summarized as follows:

- The entire web engages the shear resistance mechanism, based on the occurrence of well-distributed, fan-shaped diagonal shear cracks for specimens with either grouted or ungrouted ducts.
- No significant difference was found between the grouted and ungrouted ducts with respect to the post-cracking tensile stresses within the concrete component.
- The gross web width, b_w , should be used in the calculation of the concrete component, V_c , to the shear strength capacity.
- The level of concrete compressive stress determined using the Vecchio-Collins compressive softening model justifies the experimentally observed web crushing for specimens with grouted or ungrouted ducts.
- The tested specimen containing ungrouted duct experienced localized web crushing at the normalized shear stress level of $0.25f'_c$.
- The normalized shear stress level of the specimen with grouted duct became similar to that of the specimen containing ungrouted duct with the proposed value of 1.0 for k . This is in accordance with the specimens exhibiting the same failure mode of localized web crushing.
- For the calculation of V_{n2} , the shear stress level in the specimen containing grouted duct becomes similar to that of the specimen containing ungrouted duct with the proposed value of 1.0 for k , which accords with the specimens having the same failure mode, localized web crushing.

Chapter 6. Summary and Conclusion

6.1. Summary

A comprehensive experimental program was undertaken to investigate the shear behavior of post-tensioned concrete members with ungrouted ducts, selecting the grouting conditions and duct layout as test variables. The experimental program involved the construction and testing of six Tx62 I-girder specimens. The research team coordinated the fabrication of the specimens at a local precast plant and engaged certified technicians to conduct the post-tensioning process. All required material properties were determined following adequate standards. The structural tests resulted in similar failure modes, initiated by localized web crushing, regardless of the duct condition and tendons profile. The extensive instrumentation that monitored the experimental behavior of the specimens provided valuable insight on the underlying mechanisms that governed the response. These tests serve as validation studies for the updated shear strength reduction factors proposed for implementation in AASHTO LRFD.

6.2. Proposed Changes to the AASHTO LRFD

The current AASHTO LRFD provisions for the shear design of post-tensioned concrete members account for a reduction in the shear capacity due to the detrimental effect caused by the presence of ducts in the web region, varying based on the condition of the ducts. The current shear design procedure was not found to align with the observed failure mechanism of the post-tensioned concrete members. This led to the following proposed modifications:

- The entire web engages the shear transfer mechanism, regardless of whether the specimen's ducts are grouted or ungrouted. As such, the gross web width (b_w) should be used in the calculation of the concrete component to the shear strength capacity for the V_{n1} equation of §5.7.3.3-1 (AASHTO, 2020).
- The normalized shear stress level of specimens containing grouted ducts is similar to that of specimens with ungrouted ducts when the value of k is 1.0, as proposed. This is in agreement with the observed failure mode, localized web crushing. Thus, when calculating the concrete contribution to the shear strength capacity in the V_{n2} equation of §5.7.3.3-2, the effective web width (b_v) should be reduced by the diameter of the duct (AASHTO, 2020).

- Based on the changes proposed for the effective web width correction factor (k), the proposed value of 2.0 for the duct diameter correction factor (δ) ensures similar structural conservativeness for both grouted and ungrouted ducts.

For sections containing at least the minimum amount of shear reinforcement, the nominal shear resistance of a concrete member shall be taken as (modifications shown in red with underline):

$$V_n = V_c + V_s + V_p \leq 0.25 f'_c b_v d_v + V_p \quad \text{Equation 22}$$

The concrete contribution to the shear strength of the member shall be taken as:

$$V_c = 0.0316 \beta \sqrt{f'_c} b_w d_v \quad \text{Equation 23}$$

and the transverse reinforcement contribution to the shear strength of the concrete member shall be taken as:

$$V_s = \frac{A_v f_y d_v (\cot \theta + \cot \alpha) \sin \alpha}{s} \cdot \lambda_{duct} \quad \text{Equation 24}$$

where:

$$\lambda_{duct} = 1 - \delta \cdot \left(\frac{\phi_{duct}}{b_w} \right)^2 \quad \text{Equation 25}$$

where δ is duct diameter correction factor, taken as 2.0 for grouted or ungrouted ducts.

Moreover, the effective web width can be determined as:

$$b_v = b_w - k \cdot \phi_{duct} \quad \text{Equation 26}$$

where k is the effective web width correction factor, taken as 1.0 for grouted or ungrouted ducts.

6.3. Concluding Remarks

The preliminary spliced girder research programs performed at the UT FSEL (Moore et al., 2015; Wald et al., 2017; Williams et al., 2015) led to the development of significant observations and findings that contributed to the development of the AASHTO LRFD general shear design for the post-tensioned concrete members by (i) updating effective web width (b_v); (ii) introducing strength reduction factor (λ_{duct}); and (iii) increasing maximum size of duct in the web. In addition, research performed at UT FSEL has led to further knowledge of (i) the different shear mechanisms between small panel tests and large-scale specimens and (ii) cast-in-place splice region design based on industry survey and structural testing.

However, the reduction factors in AASHTO LRFD were developed from a limited database that did not include ungrouted post-tensioning systems, resulting in incomplete code specifications. This lack of knowledge served as motivation for the study presented herein. This study's meticulous analysis of large-scale test data and the in-depth review of rational shear models shed light on the underlying shear mechanism of the post-tensioned concrete member, leading to the proposed modifications for the upcoming edition of AASHTO LRFD. Spliced girder research conducted at the UT FSEL will contribute to the optimized design tool for the precast industry better reaching its full potential.

References

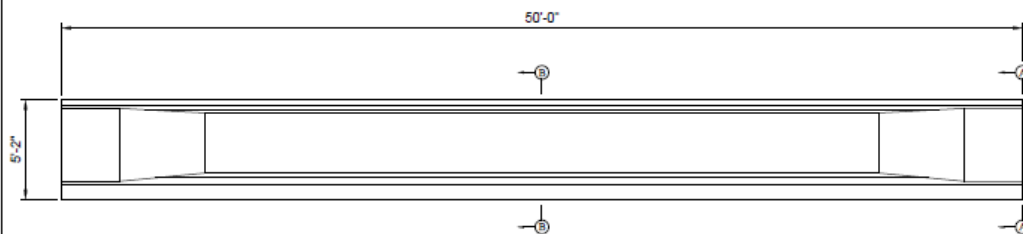
- AASHTO. (2020). *LRFD Bridge Design Specification* (9th ed.). Washington D.C.: American Association of State and Highway Transportation Officials.
- AISC. (2017). *Steel Construction Manual* (15th ed.). Chicago, IL: American Institute of Steel Construction.
- ASTM A416. (2018). *Standard Specification for Low-Relaxation, Seven-Wire Steel Strand for Prestressed Concrete*. West Conshohocken, PA: American Society for Testing and Materials.
- ASTM A615. (2020). *Standard Specification for Deformed and Plain Carbon-Steel Bars for Concrete Reinforcement*. West Conshohocken, PA: American Society for Testing and Materials.
- ASTM C1611/C1611M. (2021). *Standard Test Method for Slump Flow of Self-Consolidating Concrete*. West Conshohocken, PA: American Society for Testing and Materials.
- ASTM C39. (2014). *Standard Test Method for Compressive Strength of Cylindrical Concrete Specimens*. West Conshohocken, PA: American Society for Testing and Materials.
- Bentz, E. C., Vecchio, F. J., & Collins, M. P. (2006). Simplified modified compression field theory for calculating shear strength of reinforced concrete elements. *ACI Structural Journal*, 103(4), 614.
- Birrcher, D., Tuchscherer, R., Huizinga, M., Bayrak, O., Wood, S. L., & Jirsa, J. O. (2009). *Strength and Serviceability Design of Reinforced Concrete Deep Beams*. Austin, TX: Center for Transportation Research
- C1758M, A. C. /. (2011). *Standard Practice for Fabricating Test Specimens with Self-Consolidating Concrete*. West Conshohocken, PA: American Society for Testing and Materials.
- Castrodale, R. W., & White, C. D. (2004). *Extending Span Ranges of Precast Prestressed Concrete Girders*. Washington D.C.: National Cooperative Highway Research Program.
- Collins, M. P., & Mitchell, D. (1987). *Prestressed Concrete Basics*. Ontario: Response Publications.
- Collins, Michael P, & Mitchell, D. (1991). *Prestressed Concrete Structures*. Englewood Cliffs, NJ: Prentice Hall.
- Dolan, C. W., & Hamilton, H. R. (2019). *Prestressed Concrete*. Switzerland: Springer.
- FDOT. (2002). *New Directions for Florida Post-Tensioned Bridges*. Tallahassee, FL: Florida Department of Transportation.

- FDOT (2022). *Structures Manual*. Tallahassee, FL: Florida Department of Transportation.
- Garber, D., Gallardo, J., Deschenes, D., Dunkman, D., & Bayrak, O. (2013). *Effect of New Prestress Loss Estimates on Pretensioned Concrete Bridge Girder Design*. Austin, TX: Center for Transportation Research
- Geokon (2017) *Instruction Manual: Model 4200ER Extended Range Vibrating Wire Strain Gage*. Lebanon, NH.
- Hamilton, H. R., & Brenkus, N. (2013). *Long Spans with Transportable Precast Prestressed Girders*. Tallahassee, FL: Florida Department of Transportation.
- Hamilton, H. R., Rice, J. A., Abdullah, A. B. M., Bhatia, R., Brenkus, N., & Skelton, D. (2017). *Replaceable Unbonded Tendons for Post Tensioned Bridges*. Tallahassee, FL: Florida Department of Transportation.
- Kuchma, D. (2013). *Effect of Ducts on Shear Strength of Prestressed and Non-Prestressed Members [Interview] (15 June 2013)*.
- Mattock, A. (1979). Flexural strength of prestressed concrete sections by programmable calculator. *PCI Journal*, 24(1), 32–54.
- Moore, A. M., Williams, C. S., Massey, J. B., Bayrak, O., Ghannoum, W. M., & Jirsa, J. O. (2015). *Shear Behavior of Spliced Post-Tensioned Girders*. Texas Department of Transportation. Austin, TX: Center for Transportation Research
- Muttoni, A., Burdet, O., & Hars, E. (2006). Effect of duct type on the shear strength of thin webs. *ACI Structural Journal*, 103(5), 729–735
- Proestos, G. T., Bentz, E. C., & Collins, M. P. (2018). Maximum shear capacity of reinforced concrete members. *ACI Structural Journal*, 115(5), 1463–1473.
- PTI M55. (2013). *Specification for Grouting of Post-Tensioned Structure* (3rd ed.). Farmington Hills, MI: The Post-Tensioning Institute.
- Ritter, W. (1899). Die bauweise hennebique. *Schweizerische Bauzeitung*, 33(7), 59–61.
- TxDOT. (2014). *TxDOT Design Manual*. Austin, TX: Texas Department of Transportation.
- Vecchio, F. J., & Collins, M. P. (1993). Compression response of cracked reinforced concrete. *ASCE Journal of Structural Engineering*, 119(12), 3590–3610.
- Vecchio, Frank J, & Collins, M. P. (1986). The modified compression-field theory for reinforced concrete elements subjected to shear. *ACI Structural Journal*, 83(2), 219–231.

- Wald, D. M., Moore, A., Bayrak, O., & Jirsa, J. O. (2017). Compressive behavior of concrete panels containing steel and plastic ducts. *ACI Structural Journal*, 114(5).
- Williams, C., Moore, A., Al-Tarafany, D., Massey, J., Bayrak, O., Jirsa, J., & Ghannoum, W. (2015). *Behavior of the Splice Regions of Spliced I-Girder Bridges*. Austin, TX: Texase Department of Transportation.

Appendix A. Test Specimen Drawings

Detailed drawings of the six test girders constructed during the current study are provided in this appendix. The design of these girders outside of the end-block was guided by the current Tx62 standards, which can be downloaded from the Texas Department of Transportation website. Note that the figure number is not provided in this appendix due to the drawing template, which is different to other appendices.



BEAM ELEVATION, TYPICAL

SPECIMEN MATRIX				
SPECIMEN ID	DUCT LAYOUT	DRAWING NUMBER		FABRICATION SEQUENCE
TX62-0SG	STRAIGHT	P-1, P-2, P-5, P-9	P-3, P-6	1
TX62-0SU	STRAIGHT		P-3, P-6	2
TX62-P0G	PARABOLIC		P-3, P-7	3
TX62-P0U	PARABOLIC		P-3, P-7	4
TX62-P5G	PARABOLIC+STRAIGHT		P-4, P-8	5
TX62-PSU	PARABOLIC+STRAIGHT		P-4, P-8	6

GENERAL NOTES:

PRETENSIONED STEEL

- ALL STRANDS SHALL BE 0.6-INCH DIA. LOW RELAXATION STRANDS
- $F_{pu}=270$ KSI
- JACKING STRESS= $0.75F_{pu}=202.5$ KSI)

POST-TENSIONING DUCT

- SUPPLIED BY UT RESEARCH TEAM
- VSL PT-PLUS DUCT
- 4-INCH I.D. HDPE TUBE
- FRICTION FACTOR AND WOBBLE FRICTION COEFFICIENT ARE 0.23 AND 0.0002 FT^{-1}

ANCHORAGE DEVICES

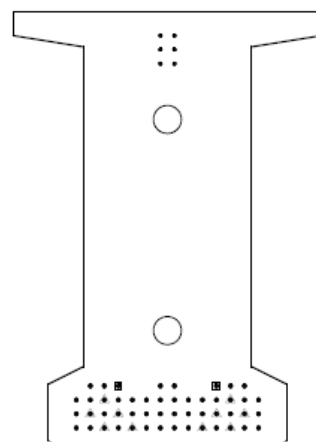
- SUPPLIED BY UT RESEARCH TEAM
- VSL TYPE ECI 8-19

REINFORCING STEEL

- ASTM A615, GR 60 STEEL
- $F_y=60$ KSI

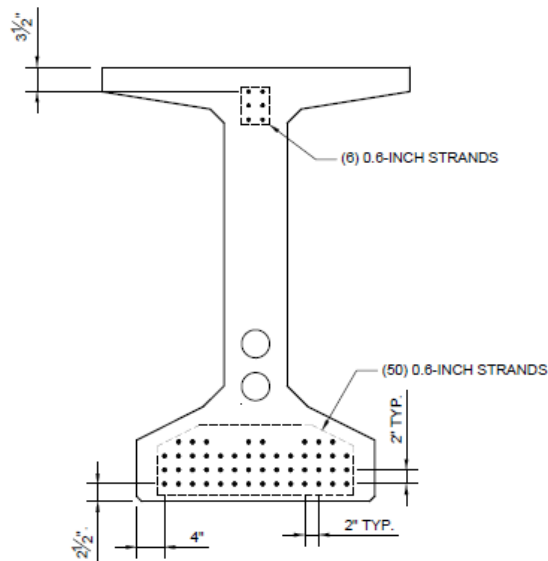
CONCRETE

- SELF COMPACTING CONCRETE (SCC)
- $FC'=10$ KSI (AT 28 DAYS)
- $FCI'=7.5$ KSI (AT RELEASE; ASSUMED IN CALCULATIONS)



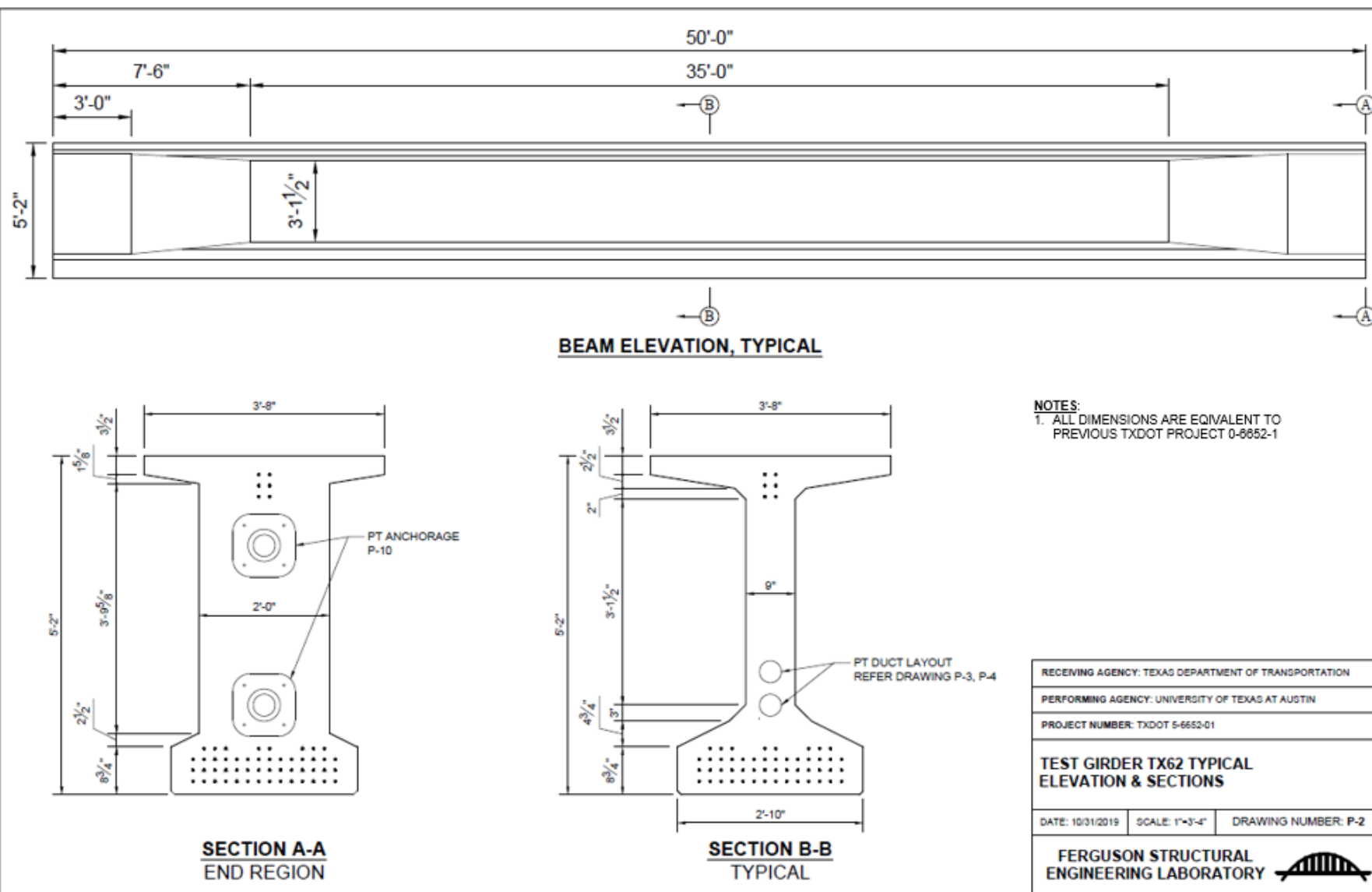
**SECTION A-A
DEBONDING LAYOUT**

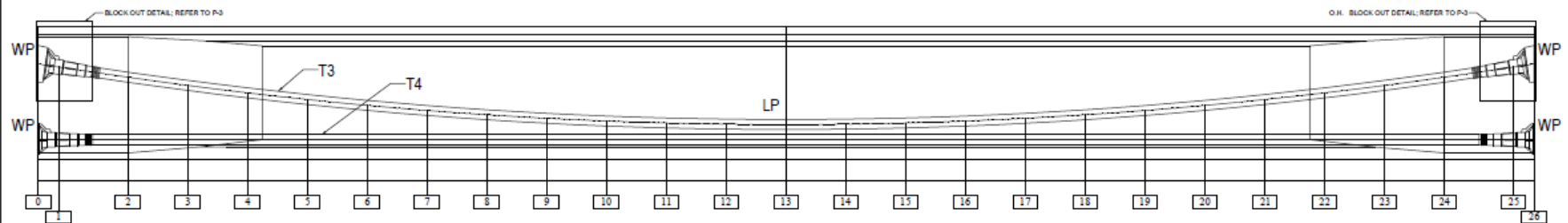
DEBONDING TERMINATES AT
 △ 3 FEET
 □ 6 FEET



**SECTION B-B
PRESTRESS LAYOUT**

RECEIVING AGENCY: TEXAS DEPARTMENT OF TRANSPORTATION		
PERFORMING AGENCY: UNIVERSITY OF TEXAS AT AUSTIN		
PROJECT NUMBER: TXDOT 5-6652-01		
TYPICAL SECTION AT END AND MID-SPAN		
DATE: 10/31/2019	SCALE: 1"=1'-4"	DRAWING NUMBER: P-1
FERGUSON STRUCTURAL ENGINEERING LABORATORY		





ELEVATION PT LAYOUT

TX62-PSG AND PSU

NOTES:

1. OTHER REINFORCEMENT AND INSERTS NOT SHOWN FOR CLARITY.
2. PARABOLIC TENDON LAYOUT WILL BE THE SAME FOR P0G, P0U, PSG AND PSU
3. STRAIGHT TENDON IN THIS DRAWING IS ONLY FOR PSG AND PSU

PROFILE		WP	AP													LP												AP	WP
Tendon ID	Node	0	1	1	2	3	4	5	6	7	8	9	10	11	12	13	14	15	16	17	18	19	20	21	22	23	24	25	26
	Distance from WP (ft)	0.00	0.68	0.68	3.00	5.00	7.00	9.00	11.00	13.00	15.00	17.00	19.00	21.00	23.00	25.00	27.00	29.00	31.00	33.00	35.00	37.00	39.00	41.00	43.00	45.00	47.00	49.32	50.00
T3	Y (in.)	47.00	45.69		41.47	38.18	35.20	32.54	30.18	28.14	26.42	25.01	23.91	23.13	22.66	22.50	22.66	23.13	23.91	25.01	26.42	28.14	30.18	32.54	35.20	38.18	41.47	45.69	47.00
	Y1 (in.)				39.47	36.18	33.20	30.54	28.18	26.14	24.42	23.01	21.91	21.13	20.66	20.50	20.66	21.13	21.91	23.01	24.42	26.14	28.18	30.54	33.20	36.18	39.47		
T4	Y (in.)	16.40		16.40	16.40	16.40	16.40	16.40	16.40	16.40	16.40	16.40	16.40	16.40	16.40	16.40	16.40	16.40	16.40	16.40	16.40	16.40	16.40	16.40	16.40	16.40	16.40	16.40	16.40
	Y1 (in.)				14.40	14.40	14.40	14.40	14.40	14.40	14.40	14.40	14.40	14.40	14.40	14.40	14.40	14.40	14.40	14.40	14.40	14.40	14.40	14.40	14.40	14.40	14.40	14.40	14.40

TENDON PROFILE NOTES

1. WP - WORK POINT
2. AP - ANCHOR POINT
3. LP - LOW POINT
4. Y - VERTICAL DISTANCE OF TENDON MEASURED FROM THE BOTTOM OF GIRDER TO THE CENTER LINE OF DUCT
5. Y1 - SUPPORT HEIGHTS MEASURED FROM THE BOTTOM OF GIRDER TO THE BOTTOM OF THE DUCT
6. DUCT SHOULD BE SUPPORTED EVERY 2 FEET

RECEIVING AGENCY: TEXAS DEPARTMENT OF TRANSPORTATION

PERFORMING AGENCY: UNIVERSITY OF TEXAS AT AUSTIN

PROJECT NUMBER: TXDOT 5-6652-01

**TEST GIRDER TX62-PSU & PSG
POST TENSIONING TENDON LAYOUT AND
PROFILE**

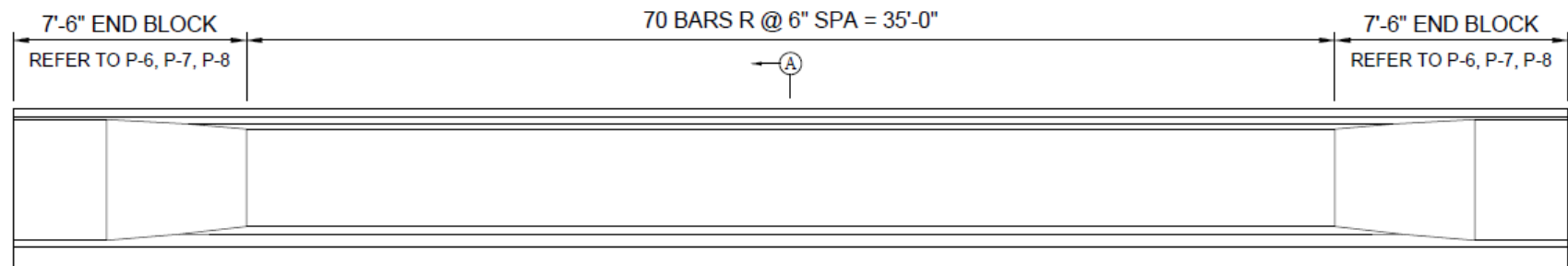
DATE: 10/31/2019

SCALE: 1"=3'-4"

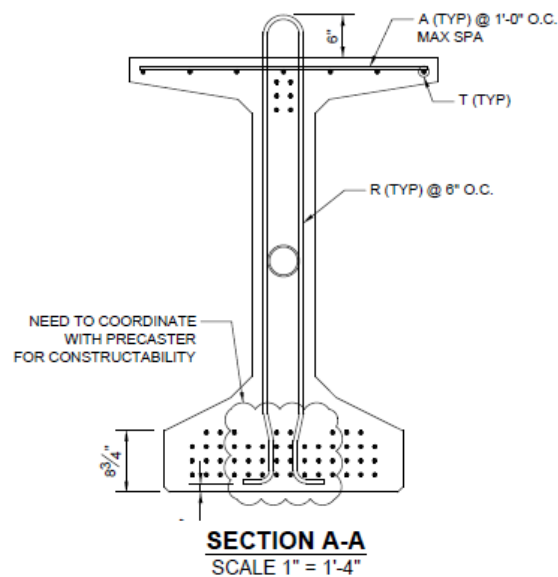
DRAWING NUMBER: P-4

**FERGUSON STRUCTURAL
ENGINEERING LABORATORY**

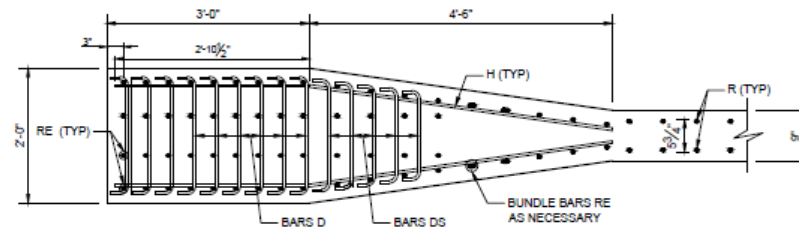
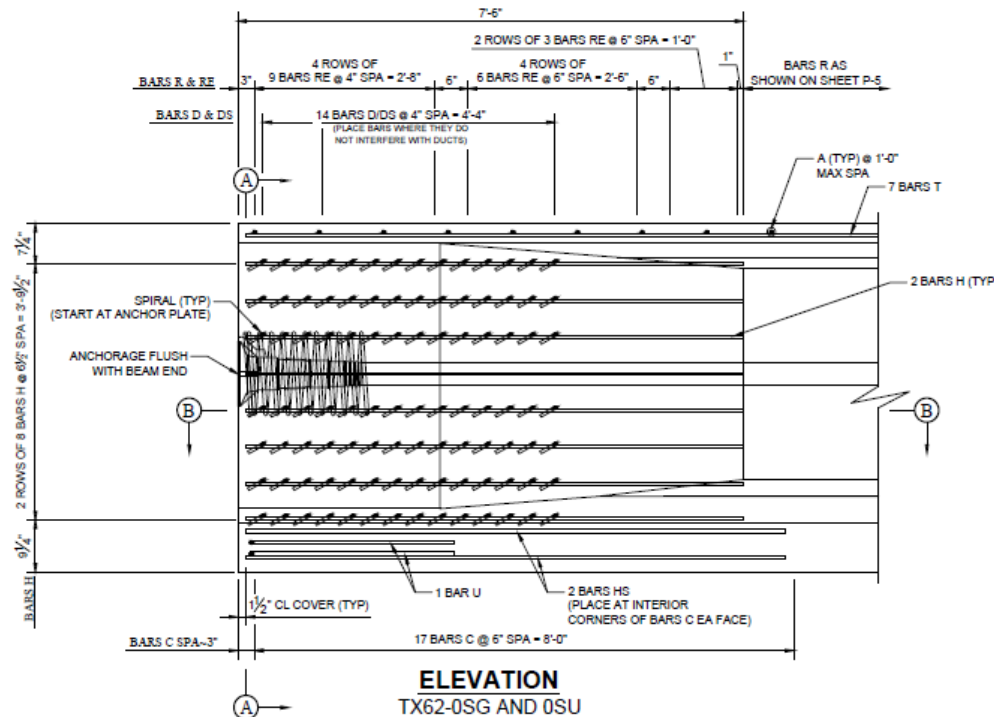




BEAM ELEVATION, TYPICAL

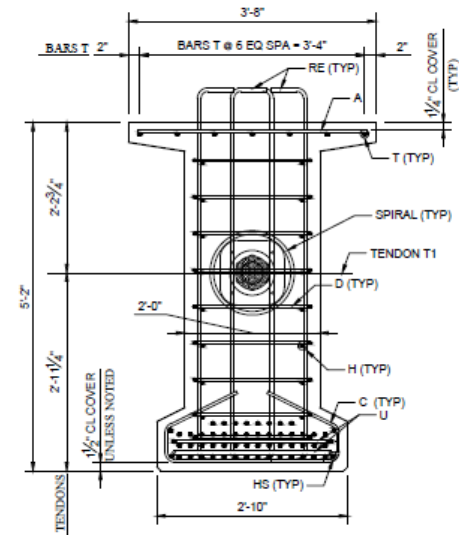



RECEIVING AGENCY: TEXAS DEPARTMENT OF TRANSPORTATION		
PERFORMING AGENCY: UNIVERSITY OF TEXAS AT AUSTIN		
PROJECT NUMBER: TXDOT 5-6652-01		
GENERAL SECTION DETAIL		
DATE: 10/31/2019	SCALE: 1"=3'-4"	DRAWING NUMBER: P-5
FERGUSON STRUCTURAL ENGINEERING LABORATORY		

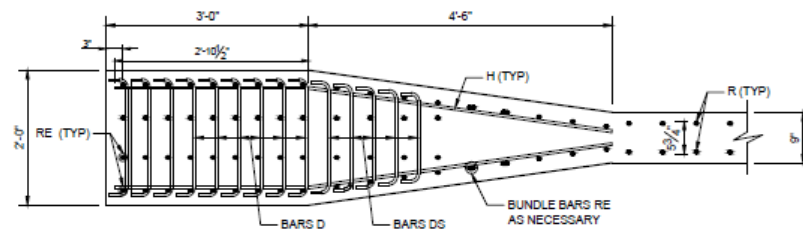
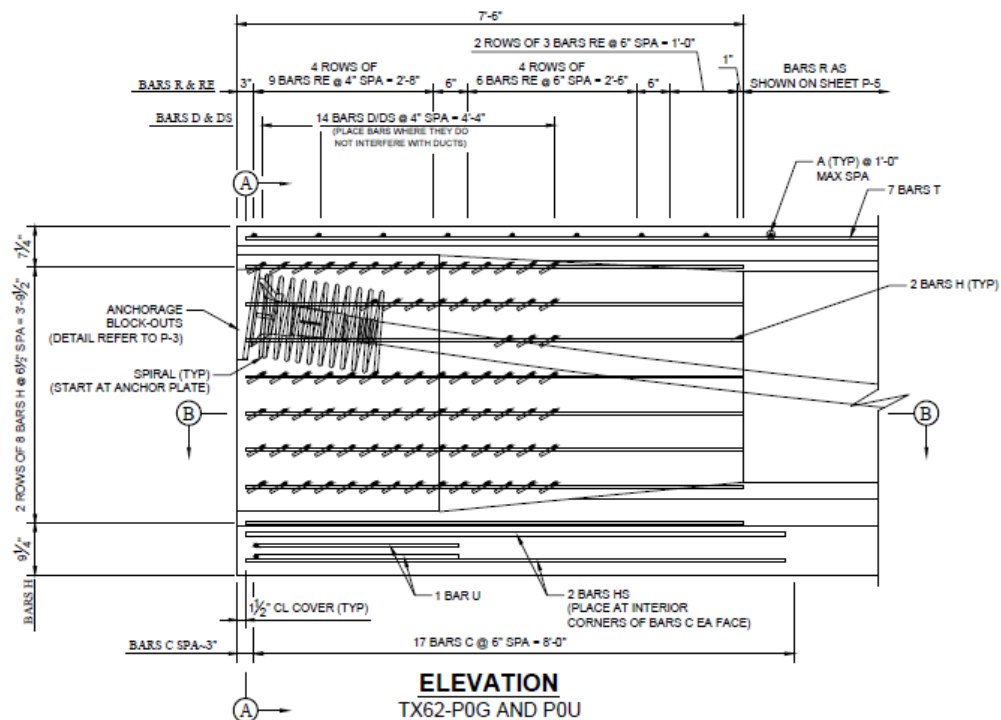


NOTES:

1. POST-TENSIONING DUCT LAYOUT REFER TO P-3
2. REINFORCEMENT BAR SCHEDULE REFER TO P-9




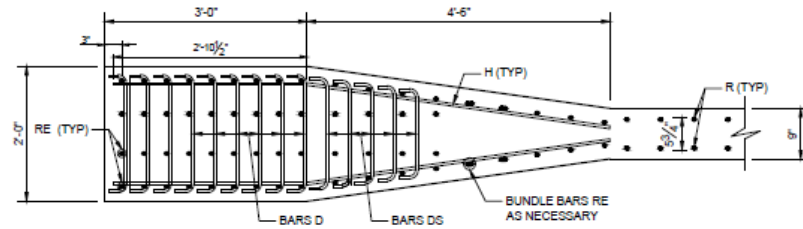
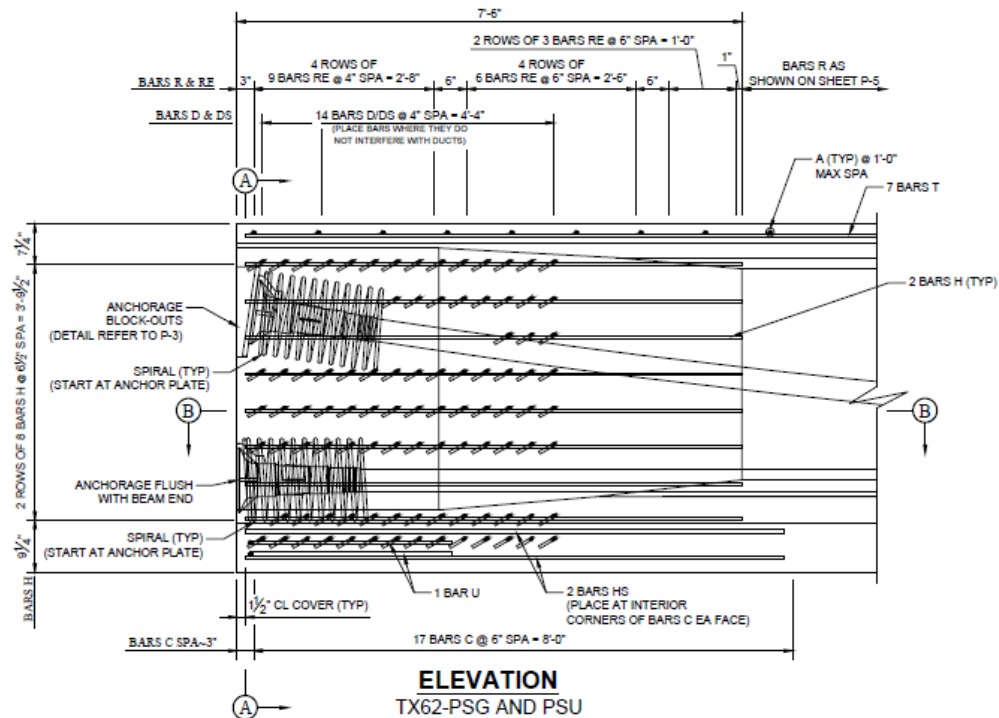
RECEIVING AGENCY: TEXAS DEPARTMENT OF TRANSPORTATION		
PERFORMING AGENCY: UNIVERSITY OF TEXAS AT AUSTIN		
PROJECT NUMBER: TXDOT 5-6652-01		
TEST GIRDER TX62-0SU & 0SG END BLOCK DETAIL		
DATE: 10/31/2019	SCALE: 1"=1'-8"	DRAWING NUMBER: P-6
FERGUSON STRUCTURAL ENGINEERING LABORATORY		



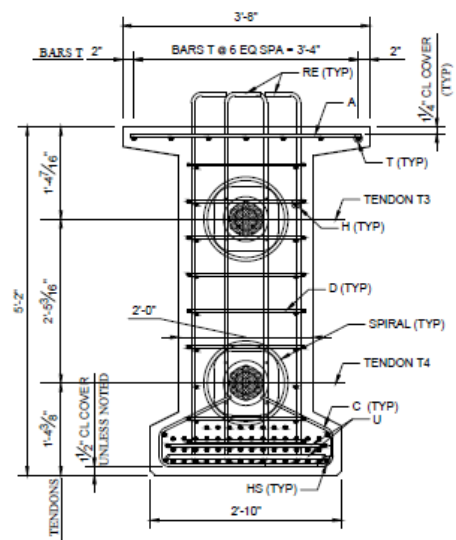
SECTION B-B

SECTION A-A

RECEIVING AGENCY: TEXAS DEPARTMENT OF TRANSPORTATION		
PERFORMING AGENCY: UNIVERSITY OF TEXAS AT AUSTIN		
PROJECT NUMBER: TXDOT 5-6652-01		
TEST GIRDER TX62-P0U & P0G END BLOCK DETAIL		
DATE: 10/31/2019	SCALE: 1"=1'-0"	DRAWING NUMBER: P-7
FERGUSON STRUCTURAL ENGINEERING LABORATORY		

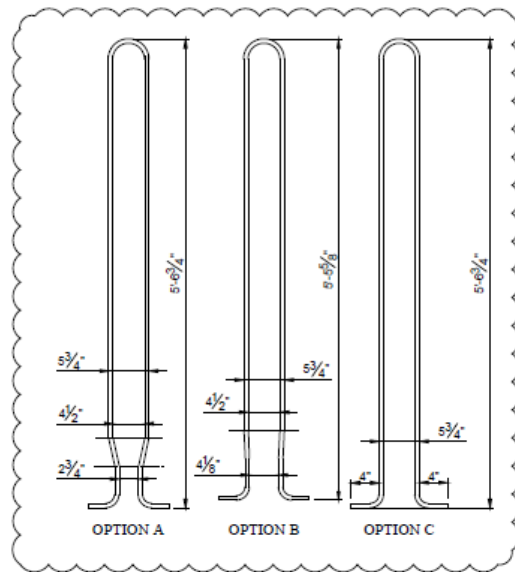


- NOTES:**
1. POST-TENSIONING DUCT LAYOUT REFER TO P-4
 2. REINFORCEMENT BAR SCHEDULE REFER TO P-9

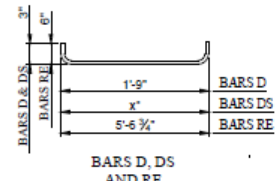


RECEIVING AGENCY: TEXAS DEPARTMENT OF TRANSPORTATION		
PERFORMING AGENCY: UNIVERSITY OF TEXAS AT AUSTIN		
PROJECT NUMBER: TXDOT 5-6652-01		
TEST GIRDER TX62-PSU & PSG END BLOCK DETAIL		
DATE: 10/31/2019	SCALE: 1"=1'-8"	DRAWING NUMBER: P-8
FERGUSON STRUCTURAL ENGINEERING LABORATORY		

REINFORCING STEEL		
BAR	SIZE	COMMENT
A	4	
C	4	
D	4	
DS	4	
H	4	
HS	5	
R	5	
RE	5	
T	5	
U	5	
SPIRAL	5	UT RESEARCH TEAM WILL SUPPLY



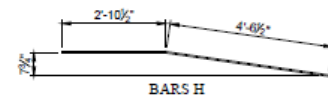
BAR S



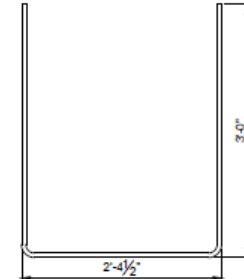
BAR S, DS AND RE

* DIMENSION "x" OF FIVE DS BARS: 1'-8", 1'-7", 1'-6", 1'-5", AND 1'-4"

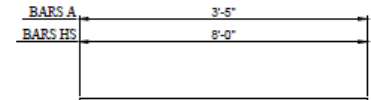
BAR S TO BE COORDINATED WITH PRECASTER PRIOR TO FABRICATION



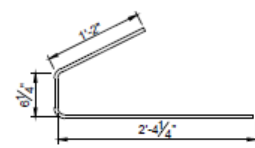
BAR S H



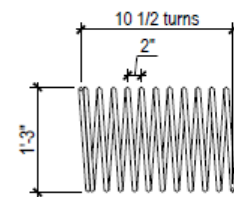
BAR S U



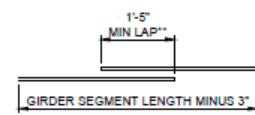
BAR S A AND HS



BAR S C



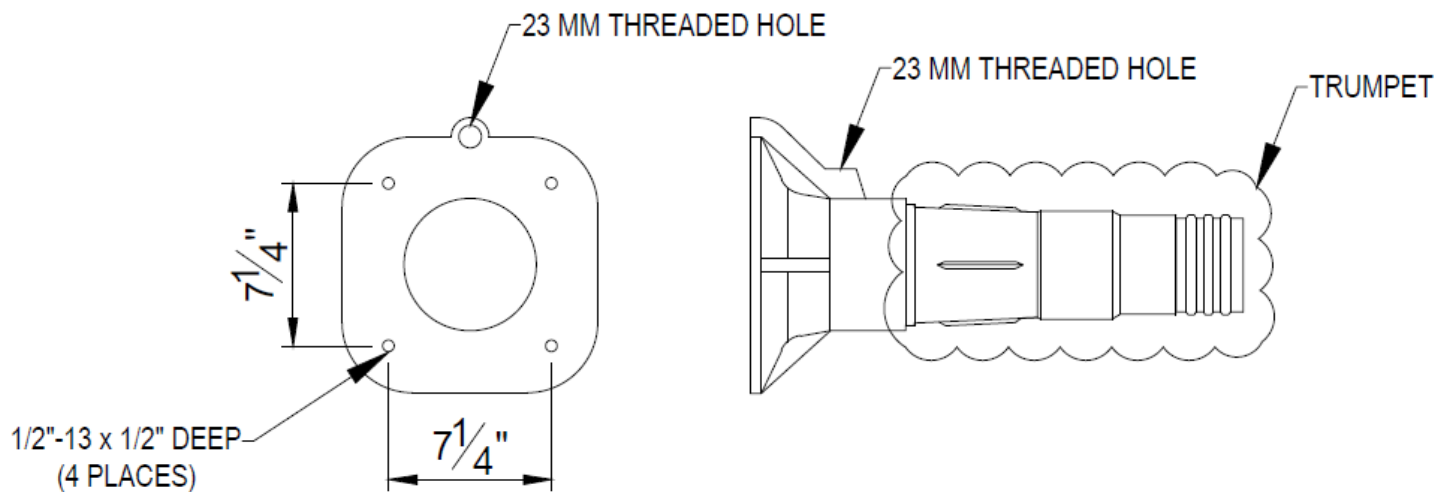
SPIRAL



BAR S T

** LAP BARS WHERE NECESSARY

RECEIVING AGENCY: TEXAS DEPARTMENT OF TRANSPORTATION		
PERFORMING AGENCY: UNIVERSITY OF TEXAS AT AUSTIN		
PROJECT NUMBER: TXDOT 5-6652-01		
REINFORCING BAR SCHEDULE		
DATE: 10/31/2019	SCALE: 1"=1'-4"	DRAWING NUMBER: P-9
FERGUSON STRUCTURAL ENGINEERING LABORATORY		



VSL TYPE ECI 6-19 BEARING PLATE AND TRUMPET

RECEIVING AGENCY: TEXAS DEPARTMENT OF TRANSPORTATION

PERFORMING AGENCY: UNIVERSITY OF TEXAS AT AUSTIN

PROJECT NUMBER: TXDOT 5-6652-01

VSL TYPE ECI 6-19 ANCHORAGE

DATE: 10/31/2019

SCALE: 1"=5"

DRAWING NUMBER: P-10

**FERGUSON STRUCTURAL
ENGINEERING LABORATORY**



Appendix B. Rendering of End-Block Reinforcement

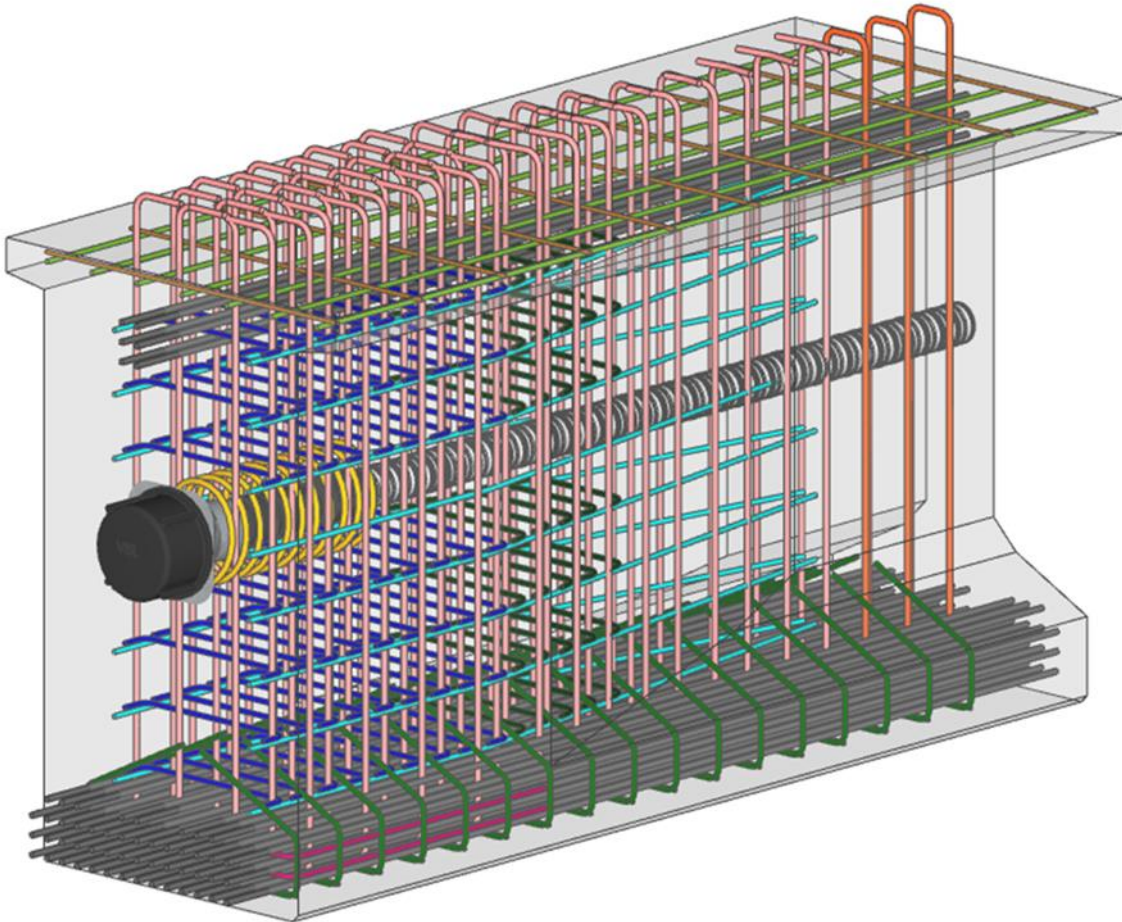


Figure B.1 Rendering of End-Block Reinforcement (Isometric View)

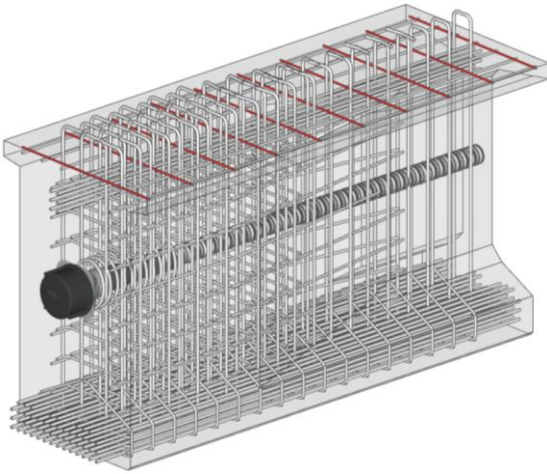


Figure B.2 A Bars

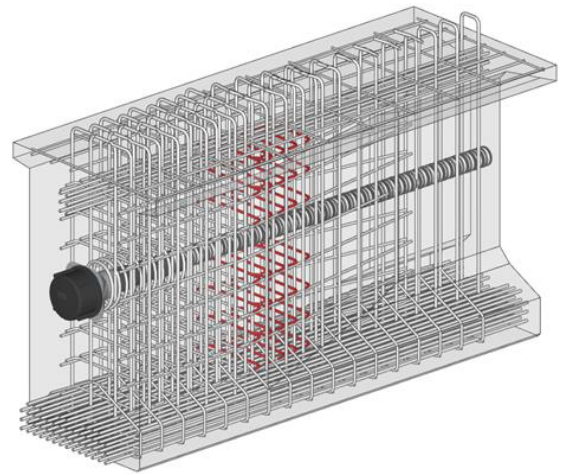


Figure B.5 DS Bars

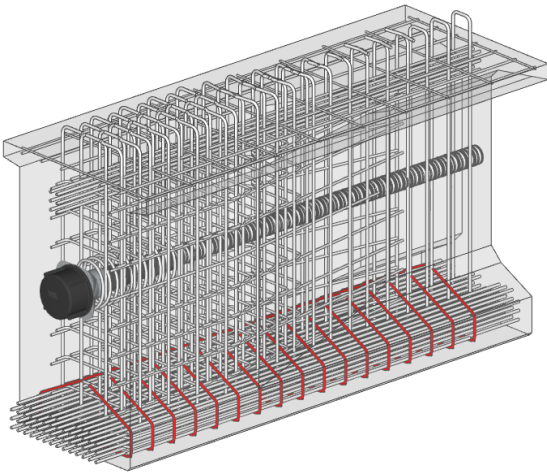


Figure B.3 C Bars

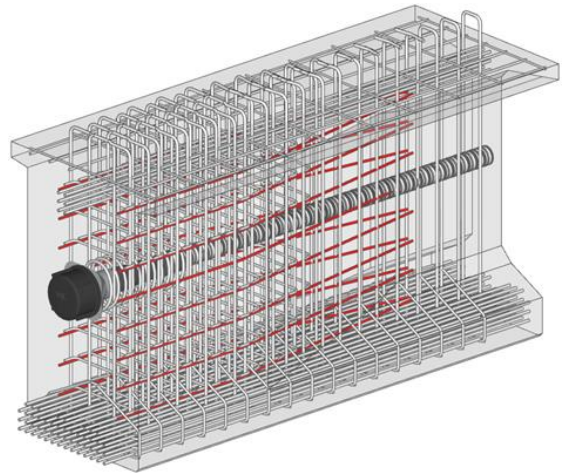


Figure B.6 H Bars

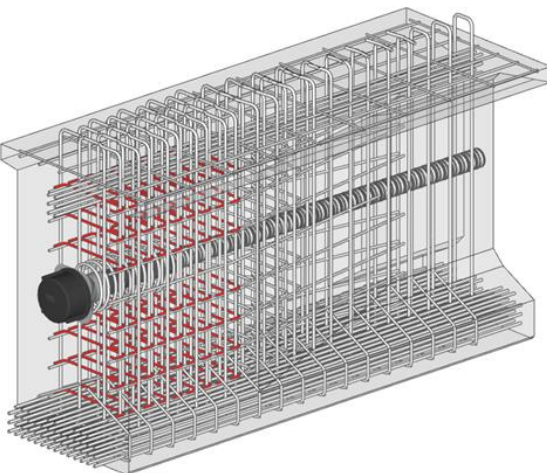


Figure B.4 D Bars

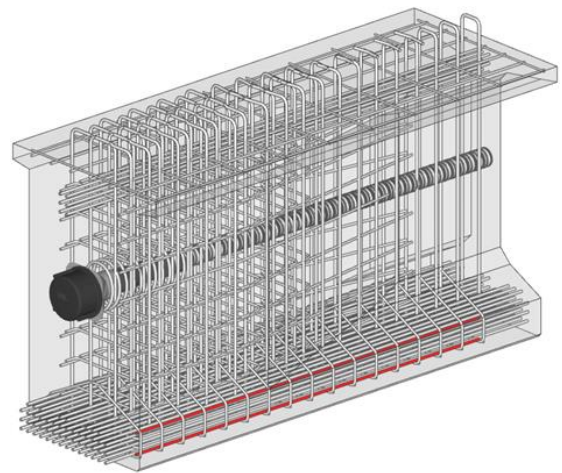


Figure B.7 HS Bars

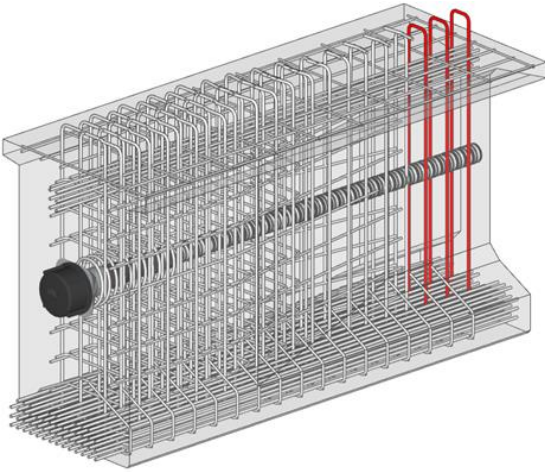


Figure B.8 R Bars

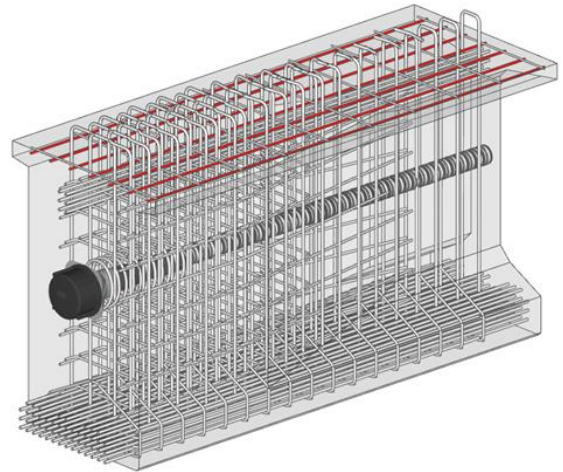


Figure B.11 T Bars

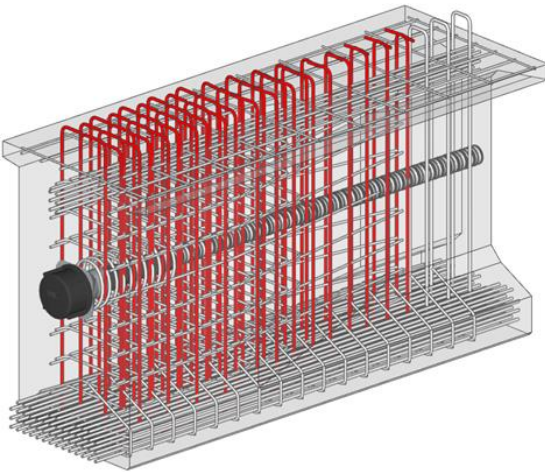


Figure B.9 RE Bars

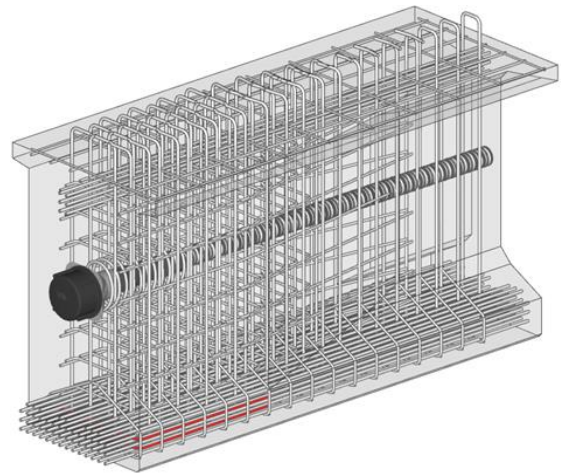


Figure B.12 U Bars

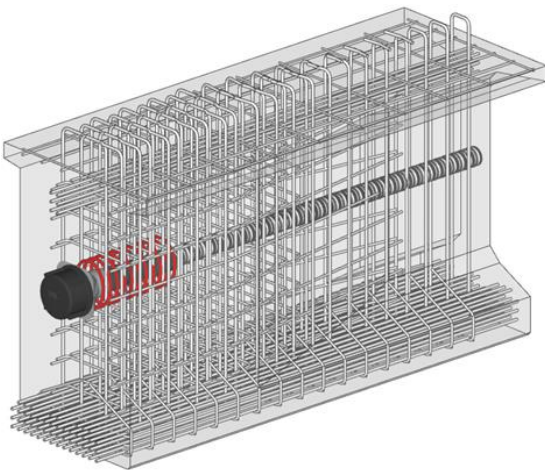


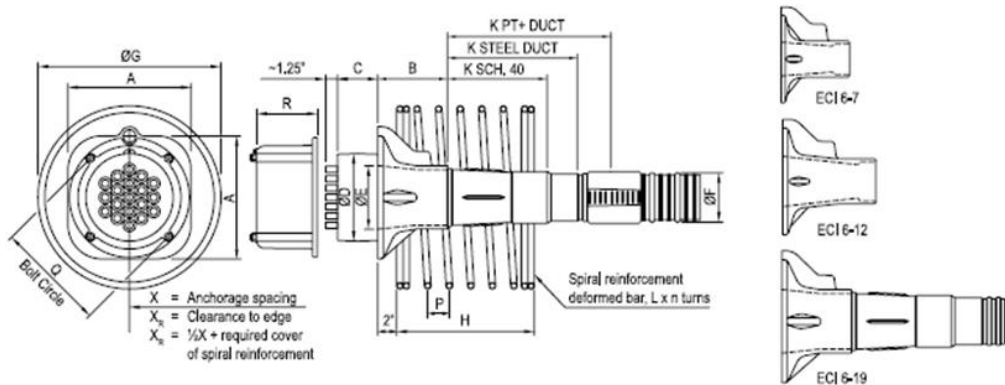
Figure B.10 Spiral

Appendix C. Post-Tensioning: Assemblies

C1. VSL Brochure for Type ECI Stressing Anchorage

VSL MULTISTRAND SYSTEMS:

Type ECI Stressing Anchorage



Tendon Unit	f _{ci} (psi)	Dimensions (Inches)														
		A	B	C	eD	eE	eF PT+ Duct	eF Steel Duct	eF SCH 40 Pipe	eG	H	K PT+ Duct	K Steel Duct	K SCH 40 Pipe	L	n
6-7	3500	8.54	6.69	2.37	5.33	3.31	2.87	2.88	3.00	11.00	12.00	No Trumpet on 6-7			#4	6.50
6-7	5500	8.54	6.69	2.37	5.33	3.31	2.87	2.88	3.00	11.00	12.00	No Trumpet on 6-7			#4	6.50
6-12	3500	9.88	8.66	3.00	6.85	4.62	3.58	3.24	3.50	13.00	14.00	No Trumpet on 6-12			#5	7.00
6-12	5500	9.88	8.66	3.00	6.85	4.62	3.58	3.24	3.50	13.00	13.50	No Trumpet on 6-12			#4	7.00
6-19	3500	11.42	6.91	3.75	8.13	5.90	4.57	4.10	4.50	17.00	19.00	15.19	12.09	9.29	#5	11.50
6-19	5500	11.42	6.91	3.75	8.13	5.90	4.57	4.10	4.50	15.00	17.00	15.19	12.09	9.29	#5	10.50



Notes:

Anchorage spacings are in accordance with test requirement of AASHTO (The Special Anchorage: Device Acceptance Test Procedure, AASHTO 2000).

For proper design and detailing of anchorage zones and related reinforcement, refer to the VSL Publication Detailing for Post-Tensioning.

Dimensions are valid for:

- f_{ci} (psi) is the nominal minimum concrete cylinder strength at the time of stressing.
- Maximum prestressing force may be applied when concrete reaches a cylinder strength of 3,500 psi (24 MPa) and 5,500 psi (38 MPa) respectively.
- Temporary overstressing to 80% of Guaranteed Ultimate Tensile Strength.
- Yield strength of spiral reinforcement: Grade 60 (400 MPa).
- Tie one and one-half turns of spiral at both ends.
- Additional orthogonal reinforcement may be required in the local anchorage zone as determined by design.
- Spirals may be replaced by suitable orthogonal reinforcement.
- Information for other concrete strengths and conditions is available from your local VSL Representative.
- Spiral reinforcement shall be centered on the anchorage assembly and be placed directly behind the bearing plate as indicated above.

VSL US Technical Data and Dimensions • ECI Multistrand 1207 • ©VSL Structures, LLC

C2. VSL Brochure PT Plus Duct

VSL MULTISTRAND SYSTEMS:

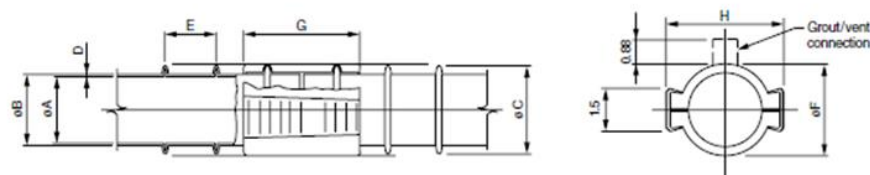
PT-Plus™ Duct



Ducts PT-Plus™ System Polypropylene (PP) Plastic Duct



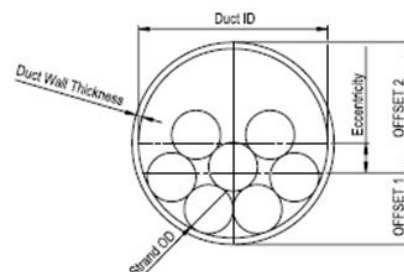
www.vsl.net • 888-489-2687



Type	Unit	Dimensions (Inches)							
		ØA	ØB	ØC	D	E	F	G	H
59mm	6-7	2.28	2.48	2.87	0.10	1.65	3.23	4.25	4.17
76mm	6-12	2.99	3.19	3.58	0.10	2.00	3.94	4.57	4.88
100mm	6-19 / 22	3.94	4.17	4.57	0.12	2.00	4.84	4.96	5.79
115mm	6-27	4.53	4.76	5.16	0.12	2.36	5.43	5.00	5.83
130mm	6-31 / 37	5.12	5.35	5.75	0.12	2.00	6.14	5.47	6.97
150mm	6-43 / 55	5.91	6.18	6.57	0.14	2.36	6.89	4.96	7.28

Eccentricity of the Center of Gravity of Strands

Duct	System	Eccentricity	Offset 1	Offset 2
59mm	6-7	0.36	0.88	1.60
76mm	6-12	0.48	1.11	2.08
100mm	6-19	0.72	1.37	2.81
100mm	6-22	0.57	1.51	2.66
115mm	6-27	0.75	1.63	3.13
130mm	6-31	0.99	1.73	3.71
130mm	6-37	0.77	1.95	3.48
150mm	6-43	1.11	1.99	4.20
150mm	6-55	0.72	2.37	3.82



VSL US Technical Data and Dimensions • Multistrand Duct • 0708 ©VSL Structures, LLC

Appendix D. Daily Reports for Fabrication

This appendix provides the research team's daily reports documenting the fabrication activities. The fabrication was performed at Valley Prestress Products (VPP) in Eagle Lake, Texas, between February 25 through March 11, 2020. During this period, the UT team was on-site daily to document the details of the test specimens, install the embedded vibrating wire gauges (VWGs) and setup the data acquisition (DAQ) system, and collect concrete and reinforcing steel samples for materials testing. Note that the figure and table numbers are not provided in this appendix due to the template, which is different to other appendices.

D1. Working Day 1 (Feb. 25, 2020)

Event

- Initiation of specimen fabrication for TxDOT Project No. 5-6652-01, Shear Behavior of Spliced Post-Tensioned Girders with UngROUTED Tendons.
- Start at 9:00 AM, end at 6:00 PM
- Location: Valley Prestress Products, Inc. (VPP)

Attendees from TxDOT

Justin Schneider, QA inspector

Attendees from UT

Sangyoung (Thomas) Han, Graduate Research Assistant

Hansol Jang, Graduate Research Assistant

Weather

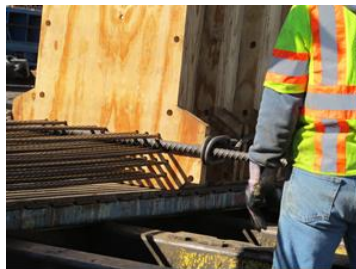
- Sunny; tomorrow, 2/26, is expected to be windy

Overall Working Progress

	0SU	0SG	P0U	P0G	PSU	PSG
Pretensioning	Completed	Completed	Completed	Completed	Completed	Completed
PT hardware placement	Ongoing					
Rebar placement	Ongoing					
Lifting hooks placement						
Sensor installation						
Concrete casting						
DAQ connection						

Work performed by VPP, 2/25

- Rescheduling of production (all dates 2020)
 - o Pretensioning (complete): start and end Feb. 25
 - o Rebar & PT hardware placement (incomplete): start Feb. 26; end Mar. 4
 - o Concrete casting (ongoing): start Mar. 2; end Mar. 7
 - o Prestress release (ongoing): start and end Mar. 13
- Strand pretensioning
 - o VPP construction team started the strands placement before 9:00 am. All wooden end forms are designed to extend one in. to each side—through-thickness direction—in accordance with the confirmed shop drawing. VPP made use of a single strand stressing method rather than gang stressing. First, they cut the end of the unnecessary strand and performed the first stressing of each strand up to 5,000 lbs. After all strands were uniformly elongated due to the initial stress of 5,000 lbs, the process of final stressing was conducted up to the designed prestress level of 43,900 lbs., as shown in the below figure.
 - o Quality-control professionals from VPP (Steven) and TxDOT (Justin) inspected the pretensioning process.



1) Strand & End
form placement 1



2) Strand & End
form placement 2



3) Fix strand



4) Cut redundant
strand



5) 1st single strand
stressing



6) Final single strand
stressing



7) Measure
elongation of strand
at the final strand
stressing



8) Strand end after
final stressing



9) Overall
prestressed strand

VPP's plan for tomorrow, 2/26

- Place rebar and post-tensioning hardware (first girder)
- Re-order “DS bar”

Work performed by UT Research Team, 2/25

- Attended the pretensioning process
- Moved DAQ equipment, including the supplement parts, to the secured storage area
- Checked the inventory of PT hardware
 - o All necessary PT hardware is in VPP including spiral bars before concrete casting
 - o A part of PVC Ball Valve, which is necessary during grouting, is missing. Thomas will follow up with this item until received by FSEL

UT Research Team's plan for tomorrow, 2/26

- Check rebar and PT hardware placement for as-built DWG
- Follow the concrete sample test plan at VPP

D2. Working Day 2 (Feb. 26, 2020)

Event

- Fabrication of specimens for TxDOT Project No. 5-6652-01, Shear Behavior of Spliced Post-Tensioned Girders with UngROUTED Tendons
- Start at 9:00 AM, end at 7:00 PM
- Location: Valley Prestress Products, Inc.

Attendees from TxDOT

Justin Schneider, QA inspector

Attendees from UT

Sangyoung (Thomas) Han, Graduate Research Assistant

Hansol Jang, Graduate Research Assistant

Weather

- Windy; tomorrow, 2/27, is expected to be sunny

Overall Working Progress

	0SU	0SG	P0U	P0G	PSU	PSG
Pretensioning	Completed	Completed	Completed	Completed	Completed	Completed
PT hardware placement	Completed	Ongoing				
Rebar placement	Ongoing					
Lifting hooks placement						
Sensor installation						
Concrete casting						
DAQ connection						

Work performed by VPP, 2/26 (Manpower: 10 people):

- Placed PT hardware
 - o VPP construction team started the first assembly of PT hardware for the Tx62-0SU girder with one straight tendon. As this was their first time connecting the coupler, the work process was slow, but the install time will decrease (9:00 am–1:00 pm).
- Placed rebar
 - o Overall, 60% of rebar for the Tx62-0SU girder has been placed, including the finished regions of one end-block and the R bar in the general section (2:00–7:00 pm). Placement of the remaining parts of the Tx62-0SU girder will continue tomorrow.

VPP's plan for tomorrow, 2/27:

- Place rebar (1st girder)
- Place rebar post-tensioning (PT) hardware (2nd girder)

Work performed by UT Research Team, 2/26:

- Checked rebar and PT hardware placement for as-built DWG
- Checked the inventory of PT hardware

		Coupler half	Coupler w/ vent	Clamp	Connection between duct & duct	Connection between duct & trumpet
Girder1	Tx62-0SG	8	0	8	2	2
Girder2	Tx62-0SU	8	0	8	2	2
Girder3	Tx62-P0G	9	1	10	3	2
Girder4	Tx62-P0U	9	1	10	3	2
Girder5	Tx62-PSG	17	1	18	5	4
Girder6	Tx62-PSU	17	1	18	5	4
Total Required (a)		68	4	72		
Used Today (b)		8	0	8		
Still Needed (c=a-b)		60	4	64		
In Inventory (d)		42	10	45		
Number to Be Ordered (e=c-d)		18	NA (-6)	19		

UT's plan for tomorrow, 2/27:

- Check rebar and PT hardware placement for as-built DWG
- Check side form modification
- Follow VPP's plan for the concrete sample test

D3. Working Day 3 (Feb. 27, 2020)

Event

- Fabrication of specimens for TxDOT Project No. 5-6652-01, Shear Behavior of Spliced Post-Tensioned Girders with UngROUTed Tendons
- Start at 6:30 AM, end at 5:00 PM(UT team continued working until 7:00 PM on the VWGs installation)
- Location: Valley Prestress Products, Inc.

Attendees from TxDOT

Justin Schneider, QA inspector

Attendees from UT

Dr. Jongkwon Choi, Postdoctoral Fellow

Sangyoung (Thomas) Han, Graduate Research Assistant

Hansol Jang, Graduate Research Assistant

Yousun Yi, Graduate Research Assistant

Weather

- Sunny; tomorrow, 2/28, is expected to be sunny

Overall Working Progress

	0SU	0SG	P0U	P0G	PSU	PSG
Pretensioning	Completed	Completed	Completed	Completed	Completed	Completed
PT hardware placement	Completed	Completed	Completed	Ongoing		
Rebar placement	Completed	Completed	Ongoing			
Lifting hooks placement	Ongoing	Ongoing	Ongoing			
Sensor installation	Completed	Ongoing	Ongoing			
Concrete casting						
DAQ connection						

- Placed PT hardware
 - The process of PT installation led to delays in yesterday's work. The UT team supports installing PT hardware in advance of rebar placement to keep to the original schedule as shown in the Overall Working Progress table. The UT team kept installing PT hardware in order to maintain the schedule.
- Planned concrete material test
 - Dr. Choi has a meeting with Ben from VPP pertaining to the concrete material test. The following will be discussed:
 - VPP will perform the Slump flow test in accordance with ASTM C1611/ C1611M (2021): Standard Test Method for Slump Flow of Self-Consolidating Concrete.
 - The production of concrete samples should follow the procedure for ASTM C1758 / C1758M (2011): Standard Practice for Fabricating Test Specimens with Self-Consolidating Concrete.
 - Four trucks will pour the concrete for one T_x62 girder. The UT team will use concrete from the first truck for 10 of the 20 concrete cylinder samples, and the remaining samples will come from the fourth truck's concrete.
- Requested strands for post-tensioning from VPP
 - The UT team needs more strands on top of one strand bundle, which is stored in FSEL for post-tensioning. The UT team (Thomas) will ask Ben from VPP to arrange for the one strand bundle to be brought to FSEL on Friday. The truck with one strand will stay inside FSEL over the weekend. On Monday morning, Thomas will ask the FSEL staff to unload the strand using the forklift, and then the truck will go back to VPP.
 - The total length of strands needed = 55 ft (length of a single strand with considering extra) x 19 (number of strands needed for one duct) x 8 (number of total ducts for 6 girders) = 8,360 ft
- Tracked the VSL shipment, which is expected on Friday.
- Due to the hectic schedule, the UT team could not take the photo. Tomorrow morning, 2/28, Thomas will take the photo as planned.

D4. Working Day 4 (Feb. 28, 2020)

Event

- Fabrication of specimens for TxDOT Project No. 5-6652-01, Shear Behavior of Spliced Post-Tensioned Girders with UngROUTed Tendons
- Start at 6:30 AM, end at 5:00 PM (UT team worked until 7:00 PM on the VWGs installation)
- Location: Valley Prestress Products, Inc.

Attendees from TxDOT

Alan Huggins, QA inspector

Attendees from UT

Sangyoung (Thomas) Han, Graduate Research Assistant

Yousun Yi, Graduate Research Assistant

Weather

- Sunny; Monday, 3/2, is expected to be cloudy

Overall Working Progress

	0SU	0SG	P0U	P0G	PSU	PSG
Pretensioning	Completed	Completed	Completed	Completed	Completed	Completed
PT hardware placement	Completed	Completed	Completed	Completed	Ongoing	Ongoing
Rebar placement	Completed	Completed	Completed	Ongoing	Ongoing	
Lifting hooks placement	Completed	Ongoing	Ongoing			
Sensor installation	Completed	Completed	Ongoing	Ongoing		
Concrete casting	Ongoing					
DAQ connection						

Note: There is no major job on Saturday except the side form close. The UT team will start work at 8:00 am on Monday.

- Main working role and responsibilities
 - o Wire connection to VWGs for Tx62-0SG, morning (Thomas)
 - o Duct connection for PSU and Tx62-PSG, morning (Hansol and Soonkwang)
 - o Coordinate slump flow and specimen fabrication, afternoon (Hansol)
 - o Coordinate concrete placement, afternoon (Thomas)
 - o Install lifting hook, afternoon (Soonkwang)
 - o Install VWGs, afternoon (Thomas, Hansol)
- Performed concrete material test:
 - o Steve (QC from VPP) is going to support the slump flow test and the production of test specimens in accordance with the following ASTM Standards:
 - ASTM C1611/ C1611M (2021): Standard Test Method for Slump Flow of Self-Consolidating Concrete
 - ASTM C1758 / C1758M (2011): Standard Practice for Fabricating Test Specimens with Self-Consolidating Concrete
 - o The UT team requested to conduct the slump flow test and fabricate specimens from the first and last batches of fresh concrete (Hansol will coordinate and record this process).
 - Four trucks pour the concrete for one Tx62 girder. The UT team will use fresh concrete from the first batch for 10 concrete cylinder samples out of 20 and the remaining 10 samples will come from the fourth (i.e., last) batch.
- Followed the donation of strands for post-tensioning from VPP:
 - o Thomas asked Ben from VPP to donate one roll of strand (8,000 ft). However, the rental truck does not have the capacity to load the weight of one roll of strand. Ben is checking the transportation method.
 - o $55 \text{ ft (a length of a single strand with additional allowance)} \times 19 \text{ (number of strands required for one duct)} \times 8 \text{ (number of total ducts for 6 girders)} = 8,360 \text{ ft (total length needed)}$
- VSL shipment of couplers and clamps arrived at VPP today. The PT inventory will now cover all girders' fabrication.

D5. Working Day 5 (Mar. 2, 2020)

Event

- Fabrication of specimens for TxDOT Project No. 5-6652-01, Shear Behavior of Spliced Post-Tensioned Girders with UngROUTED Tendons
- Start at 6:30 AM, end at 5:00 PM (UT team working by 5:00 PM due to the VWGs installation)
- Location: Valley Prestress Products, Inc.

Attendees from TxDOT

Justin Schneider, QA inspector

Attendees from UT

Dr. Jongkwon Choi, Postdoctoral Fellow

Zach Webb, Research Staff

Sangyoung (Thomas) Han, Graduate Research Assistant

Hansol Jang, Graduate Research Assistant

Soonkwang Jeong, Graduate Research Assistant

Weather

- sunny; tomorrow, 3/3, isolated thunderstorms are expected

Overall Working Progress

	0SU	0SG	P0U	P0G	PSU	PSG
Pretensioning	Completed	Completed	Completed	Completed	Completed	Completed
PT hardware placement	Completed	Completed	Completed	Completed	Completed	Ongoing
Rebar placement	Completed	Completed	Completed	Completed	Ongoing	Ongoing
Lifting hooks placement	Completed	Completed	Completed	Completed	Ongoing	Ongoing
Sensor installation	Completed	Completed	Ongoing	Ongoing		
Concrete casting	Completed	Ongoing				
DAQ connection						

- Main working role and responsibilities
 - o Connect duct for Tx62-PSG, morning (Thomas)
 - o Adjust the parabolic duct profile for all girders, morning (Thomas)
 - o Install VWGs, morning (Hansol and Soonkwang)
 - o Coordinate slump flow test and specimen fabrication, afternoon (Hansol)
 - o Coordinate concrete placement, afternoon (Thomas)
 - o Install lifting hook, afternoon (Soonkwang)
- PT hardware connection issue
 - o More supports are provided in order to prevent detachment between bearing plate and trumpet during concrete placement
 - o Thomas will adjust all parabolic ducts to match with the shop DWG.



Rebar, PT hardware, and VWGs installation



Concrete casting

D6. Working Day 6 (Mar. 3, 2020)

Event

- Fabrication of specimens starting for TxDOT Project No. 5-6652-01, Shear Behavior of Spliced Post-Tensioned Girders with Ugrouted Tendons
- Start at 6:30 AM, end at 5:00 PM (UT team at work by 6:00 PM due to the VWGs installation)
- Location: Valley Prestress Products, Inc.

Attendees from TxDOT

Alan Huggins, QA inspector

Justin Schneider, QA inspector

Attendees from UT

Sangyoung (Thomas) Han, Graduate Research Assistant

Hansol Jang, Graduate Research Assistant

Soonkwang Jeong, Graduate Research Assistant

Weather

- Cloudy and sunny; tomorrow, 3/4, rain and clouds are expected. The concrete placement of the third girder may be postponed due to rain. However, VWGs installation will continue regardless of weather conditions.

Overall Working Progress

	0SU	0SG	P0U	P0G	PSU	PSG
Pretensioning	Completed	Completed	Completed	Completed	Completed	Completed
PT hardware placement	Completed	Completed	Completed	Completed	Completed	Completed
Rebar placement	Completed	Completed	Completed	Completed	Completed	Completed
Lifting hooks placement	Completed	Completed	Completed	Completed	Completed	Ongoing
Sensor installation	Completed	Completed	Completed	Ongoing	Ongoing	Ongoing
Concrete casting	Completed	Completed	Ongoing			
DAQ connection						

- Main working role and responsibilities
 - o Adjust the parabolic duct profile for 6th girder, morning (Thomas)
 - o Install VWGs, morning (Hansol and Yousun)
 - o Coordinate slump flow and specimen fabrication, afternoon (Hansol)
 - o Coordinate concrete placement, afternoon (Thomas)
 - o Install lifting hook, afternoon (Thomas)
- Cast concrete
 - o 1st girder (OSU): Cast yesterday (Mar. 2, 3:00 pm), side form removed today (Mar. 3, 1:00 pm)
→ currently curing with wetted curing blanket after side form removal
 - o 2nd girder (OSG): Cast today (Mar. 3, 4:00 pm)
 - o 3th girder (P0U): Casting expected tomorrow (Mar. 4).
- Reinforced VWGs frame
 - o UT provided the epoxy on the connection between frame and rebar that increases the strong fixed condition.
- Placed end of PT hardware and rebar; adjustment of duct profile of the 6th girder will be done by tomorrow morning
- Sampled rebar and strand
 - o UT took the sample of unstressed rebar and strand as planned. When prestressing is released, UT will finally collect the stressed strand for sample test. The following table presents detailed information on the sample.

Type	Stressing History	Nominal Diameter (in.)	Sample Length (in.)	Minimum Quantity	Collection
#4 reinforcing bar	No	0.5	40	6	Done
#5 reinforcing bar	No	0.625	40	6	Done
0.6-in. seven-wire strand (low relaxation)	No	0.6	48	6	Done
0.6-in. seven-wire strand (low relaxation)	Yes	0.6	48	6	Yet

Note: Sample length is out to out.



Rebar work done today



Concrete curing after casting for Tx62-0PU



PT, rebar & VWG placement of Tx62-0SG



Form removal of Tx62-0SU & close of Tx-0SG



Concrete casting of Tx62-0SG



Tx62-0SG covered by curing blanket



Spraying water after concrete casting



QC teams of TxDOT & VPP during casting

- The working schedule and manpower so far are as follows:

	Work Item	Feb					March			Working days
		25	26	27	28	29	1	2	3	
		Tue	Wed	Thur	Fri	Sat	Sun	Mon	Tue	
Scope of Valley	1 Gang Prestressing	1								1
	2 Rebar placement		1	2	3			4	5	5
	3 Anchorage & duct Placement		1	2	3			4	5	5
	4 Concrete casting							1	2	2
	5 Side form removal								1	1
	6 Prestress release									0
Scope of UT	1 Material delivery	1								1
	2 Solar panel + battery (1)									0
	3 Solar panel + battery (2)									0
	4 Lifting hooks placement				1			2	3	3
	5 VWGs + Wire installation			1	2			3	4	4
	6 Concrete sample							1	2	2
	7 Start monitoring (DAQ)									0
	8 ID printing on each girder									0
	9 Material test (f'ci)									0
Manpower	1 Dr. Choi, Jongkwon			1				2		2
	2 Webb, Zach							1		1
	3 Han, Sangyoung	1	2	3	4			5	6	6
	4 Jang, Hansol	1	2	3				4	5	5
	5 Yi, Yousun			1	2					2
	6 Jeong, Soonkwang							1	2	2

D7. Working Day 7 (Mar. 4, 2020)

Event

- Fabrication of specimens starting for TxDOT Project No. 5-6652-01, Shear Behavior of Spliced Post-Tensioned Girders with Ungrouted Tendons
- Start at 7:30 AM, end at 3:00 PM (UT team working by 7:00 PM due to the VGWs installation)
- Location: Valley Prestress Products, Inc.

Attendees from UT

Sangyoung (Thomas) Han, Graduate Research Assistant

Hansol Jang, Graduate Research Assistant

Yousun, Yi, Graduate Research Assistant

Weather

- Rain and clouds; tomorrow, 3/5, is expected to be mostly sunny

Overall Working Progress

	0SU	0SG	P0U	P0G	PSU	PSG
Pretensioning	Completed	Completed	Completed	Completed	Completed	Completed
PT hardware placement	Completed	Completed	Completed	Completed	Completed	Completed
Rebar placement	Completed	Completed	Completed	Completed	Completed	Completed
Lifting hooks placement	Completed	Completed	Completed	Completed	Completed	Completed
Sensor installation	Completed	Completed	Completed	Completed	Ongoing	Ongoing
Concrete casting	Completed	Completed	Completed	Ongoing		
DAQ connection	Ongoing	Ongoing	Ongoing			

- Main working role and responsibilities
 - o VWGs installation, morning (Hansol and Thomas)
 - o Coordinate slump flow and specimen fabrication, afternoon (Hansol)
 - o Coordinate concrete placement, afternoon (Thomas)
 - o DAQ system connection, afternoon (Hansol and Thomas)

- Concrete casting
 - o 1st girder (0SU): Cast (Mar. 2, 3:00 pm), side form removed (Mar. 3, 1:00 pm)
→ currently curing with a wetted curing blanket after removal of side form
 - o 2nd girder (0SG): Cast (Mar. 3, 4:00 pm), side form removed (Mar. 4, 1:00 pm)
→ currently curing with a wetted curing blanket after removal of side form
 - o 3rd girder (P0U): Cast (Mar. 4, 2:00 pm)
- Schedule after the end of concrete placement
 - o UT discussed the schedule after the end of concrete placement with Ben and Allen from VPP. Concrete casting is ongoing, as planned, and all girders are expected to be finished by Saturday, Mar. 7. VPP plans to remove the side form of Tx62-PSG (i.e., 6th girder) on Monday (Mar. 9). After removing the side form from the prestressing bed, UT will start monitoring and check the system by Tuesday (Mar. 10). After the UT team successfully starts monitoring, the prestress release will be performed on Wednesday (Mar. 11). On the same day, VPP will move all 6 girders to the UT storage yard.
- Trumpet and bearing plate connected during concrete casting
 - o VPP provided the extra D & DS bars under the trumpet region and adjacent duct for strong support. Today, the first casting of the parabolic tendon was performed, and the UT team checked that the connection between trumpet and bearing plate was solid, as this is a feeble region.








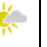
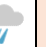


Tx62-P0U girder before concrete placement



Tx62-0SG girder after side form removal

- Working schedule and manpower so far:

	Work Item		Feb					March				Working days
			25	26	27	28	29	1	2	3	4	
			Tue	Wed	Thur	Fri	Sat	Sun	Mon	Tue	Wed	
												
Scope of Valley	1	Gang Prestressing	1									1
	2	Rebar placement		1	2	3			4	5		5
	3	Anchorage & duct Placement		1	2	3			4	5		5
	4	Concrete casting							1	2	3	3
	5	Side form removal								1	2	2
	6	Prestress release										0
Scope of UT	1	Material delivery	1									1
	2	Solar panel + battery (1)									1	1
	3	Solar panel + battery (2)										0
	4	Lifting hooks placement				1			2	3	4	4
	5	VWGs + Wire installation			1	2			3	4	5	5
	6	Concrete sample							1	2	3	3
	7	Start monitoring (DAQ)										0
	8	ID printing on each girder										0
	9	Material test (f'ci)										0
Manpower	1	Dr.Choi, Jongkwon			1				2			2
	2	Webb, Zach							1			1
	3	Han, Sangyoung	1	2	3	4			5	6	7	7
	4	Jang, Hansol	1	2	3				4	5	6	6
	5	Yi, Yousun			1	2					3	3
	6	Jeong, Soonkwang							1	2		2

D8. Working Day 8 (Mar. 5, 2020)

Event

- Fabrication of specimens for TxDOT Project No. 5-6652-01, Shear Behavior of Spliced Post-Tensioned Girders with UngROUTed Tendons
- Start at 7:30 AM, end at 12:00 PM (UT team working by 5:00 PM)
- Location: Valley Prestress Products, Inc.

Attendees from UT

Sangyoung (Thomas) Han, Graduate Research Assistant

Hansol Jang, Graduate Research Assistant

Weather

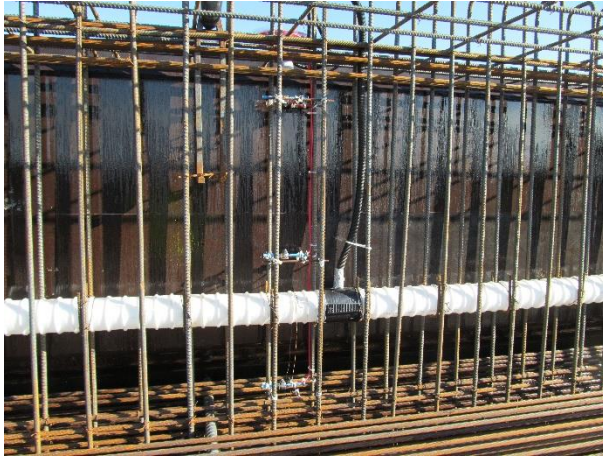
- Mostly sunny; tomorrow, 3/6, is expected to be mostly sunny

Overall Working Progress

	0SU	0SG	P0U	P0G	PSU	PSG
Pretensioning	Completed	Completed	Completed	Completed	Completed	Completed
PT hardware placement	Completed	Completed	Completed	Completed	Completed	Completed
Rebar placement	Completed	Completed	Completed	Completed	Completed	Completed
Lifting hooks placement	Completed	Completed	Completed	Completed	Completed	Completed
Sensor installation	Completed	Completed	Completed	Completed	Completed	Ongoing
Concrete casting	Completed	Completed	Completed	Completed	Ongoing	
DAQ connection	Ongoing	Ongoing	Ongoing			

- Main working role and responsibilities
 - o Coordinate slump flow and fabricating specimen, morning (Hansol)
 - o Coordinate concrete placement, morning (Thomas)
 - o VWGs installation, afternoon (Hansol and Thomas)
 - o DAQ system connection, afternoon (Hansol and Thomas)

- Concrete casting
 - o 1st girder (OSU): Cast (Mar. 2, 3:00 pm), side form removed (Mar. 3, 1:00 pm)
→ currently curing with a wetted curing blanket since removal of side form
 - o 2nd girder (OSG): Cast (Mar. 3, 4:00 pm), side form removed (Mar. 4, 1:00 pm)
→ currently curing with a wetted curing blanket since removal of side form
 - o 3rd girder (POU): Cast (Mar. 4, 2:00 pm), side form removed (Mar. 5, 8:00 am)
→ currently curing with a wetted curing blanket since removal of side form
 - o 4th girder (POG): Cast (Mar. 5, 11:00 pm)
- Confirmed schedule after the end of concrete placement.
 - o Mar. 9th (Mon): Side form removal of PSG (6th girder) and removal of all curing blankets. Start monitoring all girders to calculate stress loss.
 - o Mar. 10th (Tue): Check DAQ. Take aerial photo of the prestressing bed with the cast specimens.
 - o Mar. 11th (Wed): Prestress release and store all specimens in VPP.
- Aerial Photo
 - o VPP will provide a manlift with a height of 30 ft accompanied by a specialized technician. UT will take bird's-eye-view photos of the 6 girders on top of the stressing bed. A drone ended up being used instead.
- Honeycomb on the top surface of the bottom flange and end-block region.
 - o VPP will conduct more vibrating time to provide sufficient opportunity for enclosed air to escape. However, when compared with the other cast Tx-62 girders excluding UT specimens, the level of honeycomb is acceptable.
- Concrete sample delivery
 - o Connection samples were weighed: $(4")^2 / 4 \times \pi \times 8" \times 150 \text{ pcf} \times 120 \text{ ea} / 1000 / 123 = 1 \text{ kip}$. A payload of truck (Currently used rental car): 1.6 kip
 - o Thomas will deliver the whole samples in a wooden box to FSEL next week.



P0G girder before concrete placement



Observed honeycomb in POU girder

- Work and manpower schedule so far:

	Work Item	Feb					March					Working days
		25	26	27	28	29	1	2	3	4	5	
		Tue	Wed	Thur	Fri	Sat	Sun	Mon	Tue	Wed	Thur	
Scope of Valley	1 Gang Prestressing	1										1
	2 Rebar placement		1	2	3			4	5			5
	3 Anchorage & duct Placement		1	2	3			4	5			5
	4 Concrete casting							1	2	3	4	4
	5 Side form removal								1	2	3	3
	6 Prestress release											0
Scope of UT	1 Material delivery	1										1
	2 Solar panel + battery (1)									1		1
	3 Solar panel + battery (2)											0
	4 Lifting hooks placement				1			2	3	4		4
	5 VWGs + Wire installation			1	2			3	4	5	6	6
	6 Concrete sample							1	2	3	4	4
	7 Start monitoring (DAQ)											0
	8 ID printing on each girder											0
	9 Material test (f'ci)											0
Manpower	1 Dr.Choi, Jongkwon			1				2				2
	2 Webb, Zach							1				1
	3 Han, Sangyoung	1	2	3	4			5	6	7	8	8
	4 Jang, Hansol	1	2	3				4	5	6	7	7
	5 Yi, Yousun			1	2					3		3
	6 Jeong, Soonkwang							1	2			2

D9. Working Day 9 (Mar. 6, 2020)

Event

- Fabrication of specimens for TxDOT Project No. 5-6652-01, Shear Behavior of Spliced Post-Tensioned Girders with UngROUTED Tendons
- Start at 7:30 AM, end at 12:00 PM (UT team working by 5:00 PM)
- Location: Valley Prestress Products, Inc.

Attendees from UT

Sangyoung (Thomas) Han, Graduate Research Assistant

Hansol Jang, Graduate Research Assistant

Weather

- Mostly sunny; tomorrow, 3/7, is expected to be cloudy

Overall Working Progress

	0SU	0SG	P0U	P0G	PSU	PSG
Pretensioning	Completed	Completed	Completed	Completed	Completed	Completed
PT hardware placement	Completed	Completed	Completed	Completed	Completed	Completed
Rebar placement	Completed	Completed	Completed	Completed	Completed	Completed
Lifting hooks placement	Completed	Completed	Completed	Completed	Completed	Completed
Sensor installation	Completed	Completed	Completed	Completed	Completed	Completed
Concrete casting	Completed	Completed	Completed	Completed	Completed	Ongoing
DAQ connection	Ongoing	Ongoing	Ongoing			

- Main working role and responsibilities
 - o Coordinate slump flow and specimen fabrication, morning (Hansol)
 - o Coordinate concrete placement, morning (Thomas)
 - o DAQ system connection, afternoon (Hansol and Thomas)

- Concrete casting schedule:

	Casting	Form removal	Curing sheet removal
OSU (1 st girder)	Mar. 2, 3:00 am	Mar. 3, 1:00 pm	Mar. 10, 12 pm
OSG (2 nd girder)	Mar. 3, 4:00 pm	Mar. 4, 1:00 pm	Mar. 10, 12 pm
POU (3 rd girder)	Mar. 4, 2:00 pm	Mar. 5, 8:00 am	Mar. 10, 12 pm
POG (4 th girder)	Mar. 5, 11:00 am	Mar. 6, 8:00 am	Mar. 10, 12 pm
PSU (5 th girder)	Mar. 6, 9:30 am		Mar. 10, 12 pm
PSG (6 th girder)			Mar. 10, 12 pm

- Work and manpower schedule so far:

	Work Item	Feb					March						Working days
		25	26	27	28	29	1	2	3	4	5	6	
		Tue	Wed	Thur	Fri	Sat	Sun	Mon	Tue	Wed	Thur	Fri	
Scope of Valley	1 Gang Prestressing	1											1
	2 Rebar placement		1	2	3			4	5				5
	3 Anchorage & duct Placement		1	2	3			4	5				5
	4 Concrete casting							1	2	3	4	5	5
	5 Side form removal								1	2	3	4	4
	6 Prestress release												0
Scope of UT	1 Material delivery	1											1
	2 Solar panel + battery (1)									1			1
	3 Solar panel + battery (2)												0
	4 Lifting hooks placement				1			2	3	4			4
	5 VWGs + Wire installation			1	2			3	4	5	6		6
	6 Concrete sample							1	2	3	4	5	5
	7 Start monitoring (DAQ)												0
	8 ID printing on each girder												0
	9 Material test (f'ci)												0
Manpower	1 Dr.Choi, Jongkwon			1				2					2
	2 Webb, Zach							1					1
	3 Han, Sangyoung	1	2	3	4			5	6	7	8	9	9
	4 Jang, Hansol	1	2	3				4	5	6	7	8	8
	5 Yi, Yousun			1	2					3			3
	6 Jeong, Soonkwang							1	2				2

D10. Working Day 10 (Mar. 7, 2020)

Event

- Fabrication of specimens for TxDOT Project No. 5-6652-01, Shear Behavior of Spliced Post-Tensioned Girders with UngROUTED Tendons
- Start at 7:30 AM ~ End at 10:00 PM (UT team working by 5:30 PM)
- Location: Valley Prestress Products, Inc.

Attendees from UT

Sangyoung (Thomas) Han, Graduate Research Assistant

Hansol Jang, Graduate Research Assistant

Weather

- Cloudy; Monday, 3/10, is expected to be cloudy

Overall Working Progress

	0SU	0SG	P0U	P0G	PSU	PSG
Pretensioning	Completed	Completed	Completed	Completed	Completed	Completed
PT hardware placement	Completed	Completed	Completed	Completed	Completed	Completed
Rebar placement	Completed	Completed	Completed	Completed	Completed	Completed
Lifting hooks placement	Completed	Completed	Completed	Completed	Completed	Completed
Sensor installation	Completed	Completed	Completed	Completed	Completed	Completed
Concrete casting	Completed	Completed	Completed	Completed	Completed	Completed
DAQ connection	Ongoing	Ongoing	Ongoing			

- Main working role and responsibilities
 - o Side form removal, morning (Thomas)
 - o 2nd DAQ system connection, afternoon (Thomas)
 - o Start monitoring (Thomas)

- Concrete casting

- o The concrete casting was done today without any issues. Honeycomb on the surface of web and bubble on the top surface of top flange are observed. UT will measure the size of honeycomb on Tuesday after complete curing sheet removal to determine the patch on the surface.

	Casting	Form removal	Curing sheet removal
0SU (1 st girder)	Mar. 2, 3:00 am	Mar. 3, 1:00 pm	Mar. 10, 12 pm
0SG (2 nd girder)	Mar. 3, 4:00 pm	Mar. 4, 1:00 pm	Mar. 10, 12 pm
P0U (3 rd girder)	Mar. 4, 2:00 pm	Mar. 5, 8:00 am	Mar. 10, 12 pm
P0G (4 th girder)	Mar. 5, 11:00 am	Mar. 6, 8:00 am	Mar. 10, 12 pm
PSU (5 th girder)	Mar. 6, 9:30 am	Mar. 7, 8:00 am	Mar. 10, 12 pm
PSG (6 th girder)	Mar. 7, 9:00 am		Mar. 10, 12 pm

- Change batch plant (Missing item from the previous daily report)

- o Because the first batch plant, which provided the fresh concrete for the first three girders (i.e., 0SU, 0SG, P0U), has been stopped since last Thursday, the second batch plant started to provide the concrete for the second three girders (i.e., P0G, PSU, PSG).



First batch plant covers 0SU, 0SG, and P0U



Second batch plant covers P0G, PSU, and PSG



- Connection of the 1st DAQ
 - o Three girders, 0SU, 0SG, and P0U, are successfully connected with the first DAQ. This time the solar panel was not used since these girders will be relocated immediately after prestressing release. When girders are in the stockyard, the installed solar panels will provide the power source for a couple of months.
- Major work next week
 - o Side form removal (Monday)
 - o 2nd DAQ connection (Monday)
 - o Start monitoring (Monday) and checking again (Tuesday)
 - o Curing blanket and plastic sheet removal (Tuesday)
 - o Aerial photo for six girders (Tuesday)
 - o Compressive strength test, f'_{ci} (Wednesday)
 - o Prestress release (Wednesday)
 - o Move girders to stockyard (Wednesday)
 - In order to follow up these activities, UT (Thomas) will plan another business trip from Monday through Wednesday.
- Compressive strength test
 - o VPP is going to measure the compressive strength, f'_{ci} , before prestressing release. After finishing measuring f'_{ci} , UT will bring remaining samples to FSEL for future test when necessary.
- Remaining agenda with VPP
 - o Donation of strands and strand cage
 - o Schedule girder delivery
 - o Patch for honeycomb



1st DAQ connection for 0SU, 0SG, P0U



Honeycomb on the web

- Schedule of work and manpower so far:

	Work Item	Feb					March							Working days
		25	26	27	28	29	1	2	3	4	5	6	7	
		Tue	Wed	Thur	Fri	Sat	Sun	Mon	Tue	Wed	Thur	Fri	Sat	
Scope of Valley	1 Gang Prestressing	1												1
	2 Rebar placement		1	2	3			4	5					5
	3 Anchorage & duct Placement		1	2	3			4	5					5
	4 Concrete casting							1	2	3	4	5	6	6
	5 Side form removal								1	2	3	4	5	5
	6 Prestress release													0
Scope of UT	1 Material delivery	1												1
	2 Solar panel + battery (1)									1			2	2
	3 Solar panel + battery (2)													1
	4 Lifting hooks placement				1			2	3	4				4
	5 VWGs + Wire installation			1	2			3	4	5	6			6
	6 Concrete sample							1	2	3	4	5	6	6
	7 Start monitoring (DAQ)													0
	8 ID printing on each girder													0
	9 Material test (f'ci)													0
Manpower	1 Dr.Choi, Jongkwon			1				2						2
	2 Webb, Zach							1						1
	3 Han, Sangyoung	1	2	3	4			5	6	7	8	9	10	10
	4 Jang, Hansol	1	2	3				4	5	6	7	8	9	9
	5 Yi, Yousun			1	2					3				3
	6 Jeong, Soonkwang							1	2					2

D11. Working Day 11 (Mar. 9, 2020)

Event

- Fabrication of specimens for TxDOT Project No. 5-6652-01, Shear Behavior of Spliced Post-Tensioned Girders with UngROUTed Tendons
- Start at 7:00 AM, end at 13:00 PM (UT team working by 7:00 PM)
- Location: Valley Prestress Products, Inc.

Attendees from UT

Sangyoung (Thomas) Han, Graduate Research Assistant

Weather

- Rain; tomorrow, 3/9, is expected to be cloudy and rainy

Overall Working Progress

	0SU	0SG	P0U	P0G	PSU	PSG
Pretensioning	Completed	Completed	Completed	Completed	Completed	Completed
PT hardware placement	Completed	Completed	Completed	Completed	Completed	Completed
Rebar placement	Completed	Completed	Completed	Completed	Completed	Completed
Lifting hooks placement	Completed	Completed	Completed	Completed	Completed	Completed
Sensor installation	Completed	Completed	Completed	Completed	Completed	Completed
Concrete casting	Completed	Completed	Completed	Completed	Completed	Completed
DAQ connection	Completed	Completed	Completed	Completed	Completed	Completed

- Main working role and responsibilities
 - o Check DAQs, morning (Thomas)
 - o Follow compressive strength test (f'_{ci}), morning (Thomas)
 - o Prestressing release, afternoon (Thomas)
 - o Disconnect DAQ for move to yard, afternoon (Thomas)

- Concrete casting completed:

	Casting	Form removal	Curing sheet removal
OSU (1 st girder)	Mar. 2, 3:00 am	Mar. 3, 1:00 pm	Mar. 9, 1 pm
OSG (2 nd girder)	Mar. 3, 4:00 pm	Mar. 4, 1:00 pm	Mar. 9, 1 pm
POU (3 rd girder)	Mar. 4, 2:00 pm	Mar. 5, 8:00 am	Mar. 9, 1 pm
POG (4 th girder)	Mar. 5, 11:00 am	Mar. 6, 8:00 am	Mar. 9, 1 pm
PSU (5 th girder)	Mar. 6, 9:30 am	Mar. 7, 8:00 am	Mar. 9, 1 pm
PSG (6 th girder)	Mar. 7, 9:00 am	Mar. 9, 8:00 am	Mar. 9, 1 pm

- Prestressing release
 - VPP is going to conduct the prestressing release tomorrow afternoon. Before this procedure, at about 9 am, VPP will measure the compressive strength (f'_{ci}) with Thomas. After finishing measuring f'_{ci} , Thomas is going to report the compressive strength result to the UT team.
 - Thomas will check the DAQ system one more time. All DAQs are now installed and currently working perfectly with a sampling rate of 30 min.
- Schedule of work and manpower so far:

	Work Item	Feb					March									Working days
		25	26	27	28	29	1	2	3	4	5	6	7	8	9	
		Tue	Wed	Thur	Fri	Sat	Sun	Mon	Tue	Wed	Thur	Fri	Sat	Sun	Mon	
Scope of Valley	1 Gang Prestressing	1														1
	2 Rebar placement		1	2	3			4	5							5
	3 Anchorage & duct Placement		1	2	3			4	5							5
	4 Concrete casting							1	2	3	4	5	6			6
	5 Side form removal								1	2	3	4	5		6	6
	6 Prestress release															0
Scope of UT	1 Material delivery	1														1
	2 Solar panel + battery (1)									1			2			2
	3 Solar panel + battery (2)														1	1
	4 Lifting hooks placement				1			2	3	4						4
	5 VWGs + Wire installation			1	2			3	4	5	6					6
	6 Concrete sample							1	2	3	4	5	6			6
	7 Start monitoring (DAQ)														1	1
	8 ID printing on each girder															0
	9 Material test (f'_{ci})															0
Manpower	1 Dr.Choi, Jongkwon			1				2								2
	2 Webb, Zach							1								1
	3 Han, Sangyoung	1	2	3	4			5	6	7	8	9	10		11	11
	4 Jang, Hansol	1	2	3				4	5	6	7	8	9			9
	5 Yi, Yousun			1	2					3						3
	6 Jeong, Soonkwang							1	2							2

D12. Working Day 12 (Mar. 10, 2020)

Event

- Fabrication of specimens for TxDOT Project No. 5-6652-01, Shear Behavior of Spliced Post-Tensioned Girders with UngROUTED Tendons
- Start at 2:00 PM, end at 5:00 PM (UT team worked until 6:00 PM)
- Location: Valley Prestress Products, Inc.

Attendees from UT

Sangyoung (Thomas) Han, Graduate Research Assistant

Weather

- Cloudy and sunny; tomorrow, 3/11, clouds and rain are expected

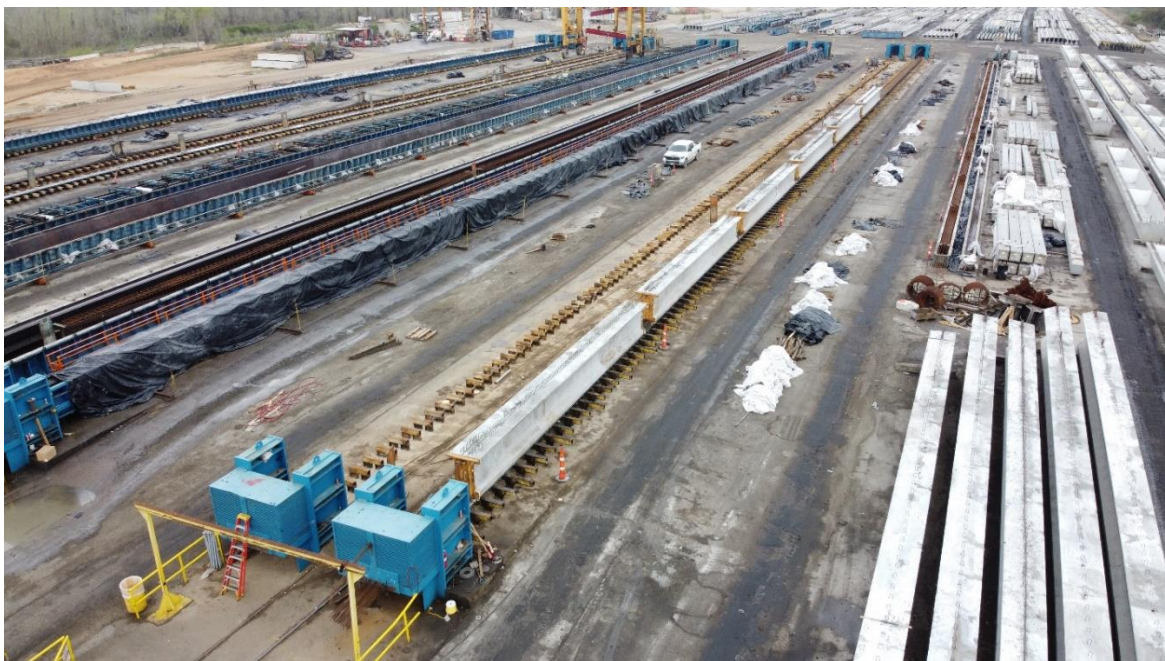
Overall Working Progress

- Main working role and responsibilities
 - o Relocation of DAQs, morning and afternoon (Thomas, Hansol, Sunkwang)
 - o Move girders to storage yard by VPP, morning (Hansol, Sunkwang)
 - o Install solar panel, afternoon (Thomas, Hansol, Sunkwang)
 - o Pack concrete cylinder samples, afternoon (Hansol, Sunkwang)
 - o Pack materials and equipment, afternoon (Thomas)
 - o Clean area (Thomas, Hansol, Sunkwang)

- Single prestressing release
 - The compressive strength (f'_{ci}) of the Tx62-PSG sample (the last girder cast) satisfactorily reaches 8.5 ksi in the morning; the expected designed strength is 7.5 ksi.
 - Single prestressing release runs from 2:25 to 4:15 pm. The strains of all girders are monitored during prestressing release and the data are successfully extracted from DAQs.
- Sample of rebar and strand
 - All samples are collected as planned.

Type	Stressing History	Nominal Diameter (in.)	Sample Length (in.)	Minimum Quantity	Collection
#4 reinforcing bar	No	0.5	40	6	Done
#5 reinforcing bar	No	0.625	40	6	Done
0.6-in. seven-wire strand (low relaxation)	No	0.6	48	6	Done
0.6-in. seven-wire strand (low relaxation)	Yes	0.6	48	6	Done

Note: Sample length is out to out.



Aerial photo from after the fabrication of prestressed girders on prestressing bed

- Schedule of work and manpower so far:

	Work Item	Feb					March										Working days
		25	26	27	28	29	1	2	3	4	5	6	7	8	9	10	
		Tue	Wed	Thur	Fri	Sat	Sun	Mon	Tue	Wed	Thur	Fri	Sat	Sun	Mon	Tue	
Scope of Valley	1 Gang Prestressing	1															1
	2 Rebar placement		1	2	3			4	5								5
	3 Anchorage & duct Placement		1	2	3			4	5								5
	4 Concrete casting							1	2	3	4	5	6				6
	5 Side form removal								1	2	3	4	5		6		6
	6 Prestress release															1	1
Scope of UT	1 Material delivery	1															1
	2 Solar panel + battery (1)									1			2				2
	3 Solar panel + battery (2)														1		1
	4 Lifting hooks placement				1			2	3	4							4
	5 VWGs + Wire installation			1	2			3	4	5	6						6
	6 Concrete sample							1	2	3	4	5	6				6
	7 Start monitoring (DAQ)														1	2	2
	8 ID printing on each girder																0
	9 Material test (f'ci)															1	1
Manpower	1 Dr.Choi, Jongkwon			1				2									2
	2 Webb, Zach							1									1
	3 Han, Sangyoung	1	2	3	4			5	6	7	8	9	10		11	12	12
	4 Jang, Hansol	1	2	3				4	5	6	7	8	9				9
	5 Yi, Yousun			1	2					3							3
	6 Jeong, Soonkwang							1	2								2

D13. Working Day 13 (Mar. 11, 2020)

Event

- Fabrication of specimens for TxDOT Project No. 5-6652-01, Shear Behavior of Spliced Post-Tensioned Girders with UngROUTED Tendons
- Start at 10:00 PM, end at 11:30 PM on Mar 11, 2020 (UT team working by 9:30 PM)
- Location: Valley Prestress Products, Inc.

Attendees from UT

Sangyoung (Thomas) Han, Graduate Research Assistant

Hansol Jang, Graduate Research Assistant

Sunkwang Jeong, Graduate Research Assistant

Weather

- cloudy and sunny

Overall Working Progress

- Main working role and responsibilities
 - o Relocating DAQs, morning and afternoon (Thomas, Hansol, Sunkwang)
 - o Moving girders to storage yard by VPP, morning (Hansol, Sunkwang)
 - o Installing solar panel, afternoon (Thomas, Hansol, Sunkwang)
 - o Packing concrete cylinder samples, afternoon (Hansol, Sunkwang)
 - o Packing materials and equipment, afternoon (Thomas)
 - o Cleaning area, afternoon (Thomas, Hansol, Sunkwang)

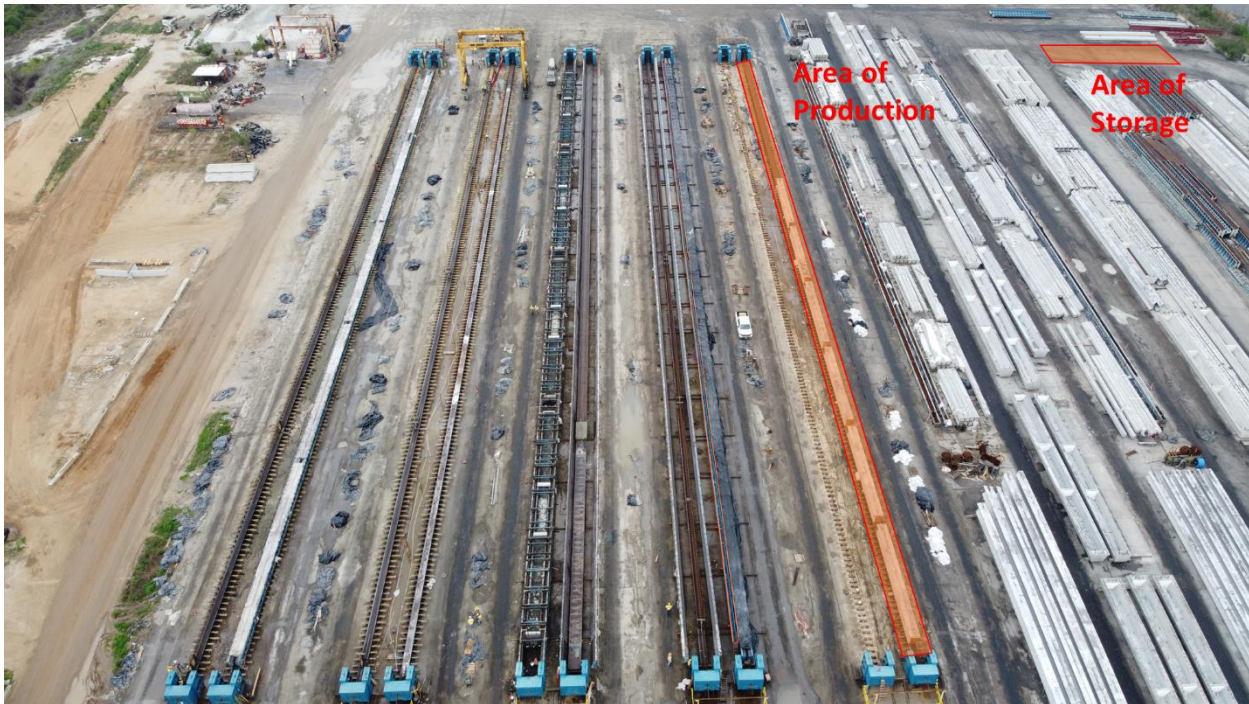
- Moving girder to storage yard and relocating of DAQs
 - o The girders will be kept in the storage area. The wooden end form will remain attached to the end of the girder until it arrives at FSEL to protect the embedded ducts from dust and water.



Taking off girders from prestressing bed



Girders stored in 2 divided rows, ungrouted and grouted



Prestressed girder production and storage locations

- Configuring DAQ system
 - o In order to make delivery efficient, the girders were divided into two groups in the storage area. Due to this arrangement, it was necessary to redesign the configuration of connections, as shown in the table below.

















Period	DAQ1			DAQ2		
From casting to taking off	0SU	0SG	P0U	P0G	PSU	PSG
From storage (VPP) to the storage yard	0SU	P0U	PSU	0SG	P0G	PSG

- Delivering concrete samples
 - o The UT team moved the concrete cylinder samples to FSEL for future test.
- Extracting VWGs data
 - o Before prestressing release, embedded VWGs started to record the internal strain behavior at three identical locations on each girder (top, middle, and bottom). The monitored data were successfully extracted from the DAQs. The differences in strain behavior exhibited after the prestressing release were as expected. The strain data for Tx62-0SU are presented in the table below.

	Time	Top ($\mu\epsilon$)	Middle ($\mu\epsilon$)	Bottom ($\mu\epsilon$)
Start of single prestressing release	2:25 pm	2,948	2,897	2,956
End of single prestressing release	4:25 pm	2,842	2,542	2,393

- End of prestressed girder production
 - o The prestressed girders were fabricated and then stored from Feb. 25 to Mar. 11 at VPP without incident. The UT team will now focus on post-tensioning and structural test. Before transferring the specimens to FSEL, the UT team will go to VPP again to check the DAQ system.

- The final working schedule, including manpower:

	Work Item	Feb					March											Working days
		25	26	27	28	29	1	2	3	4	5	6	7	8	9	10	11	
		Tue	Wed	Thur	Fri	Sat	Sun	Mon	Tue	Wed	Thur	Fri	Sat	Sun	Mon	Tue	Wed	
																		
Scope of Valley	1 Gang Prestressing	1																1
	2 Rebar placement		1	2	3			4	5									5
	3 Anchorage & duct Placement		1	2	3			4	5									5
	4 Concrete casting							1	2	3	4	5	6					6
	5 Side form removal								1	2	3	4	5		6			6
	6 Prestress release															1		1
Scope of UT	1 Material delivery	1																1
	2 Solar panel + battery (1)									1			2					2
	3 Solar panel + battery (2)														1			1
	4 Lifting hooks placement				1			2	3	4								4
	5 VWGs + Wire installation			1	2			3	4	5	6							6
	6 Concrete sample							1	2	3	4	5	6					6
	7 Start monitoring (DAQ)														1	2	3	3
	8 ID printing on each girder																1	1
	9 Material test (f'ci)															1		1
Manpower	1 Dr.Choi, Jongkwon			1				2										2
	2 Webb, Zach							1										1
	3 Han, Sangyoung	1	2	3	4			5	6	7	8	9	10		11	12	13	13
	4 Jang, Hansol	1	2	3				4	5	6	7	8	9				10	10
	5 Yi, Yousun			1	2					3								3
	6 Jeong, Soonkwang							1	2								3	3

Appendix E. Embedded Location of VWGs

E1. Required Number of VWGs

Table E.1 Proposed number of VWGs for each test specimen

	Tx62-0SG	Tx62-P0G	Tx62-PSG	Tx62-0SU	Tx62-P0U	Tx62-PSU
Longitudinal Direction	8	4	4	4	4	4
Out-of-Plane Direction	8	12	8	4	4	6
Total	16	16	12	8	8	10

E2. 1st Delivery to FSEL

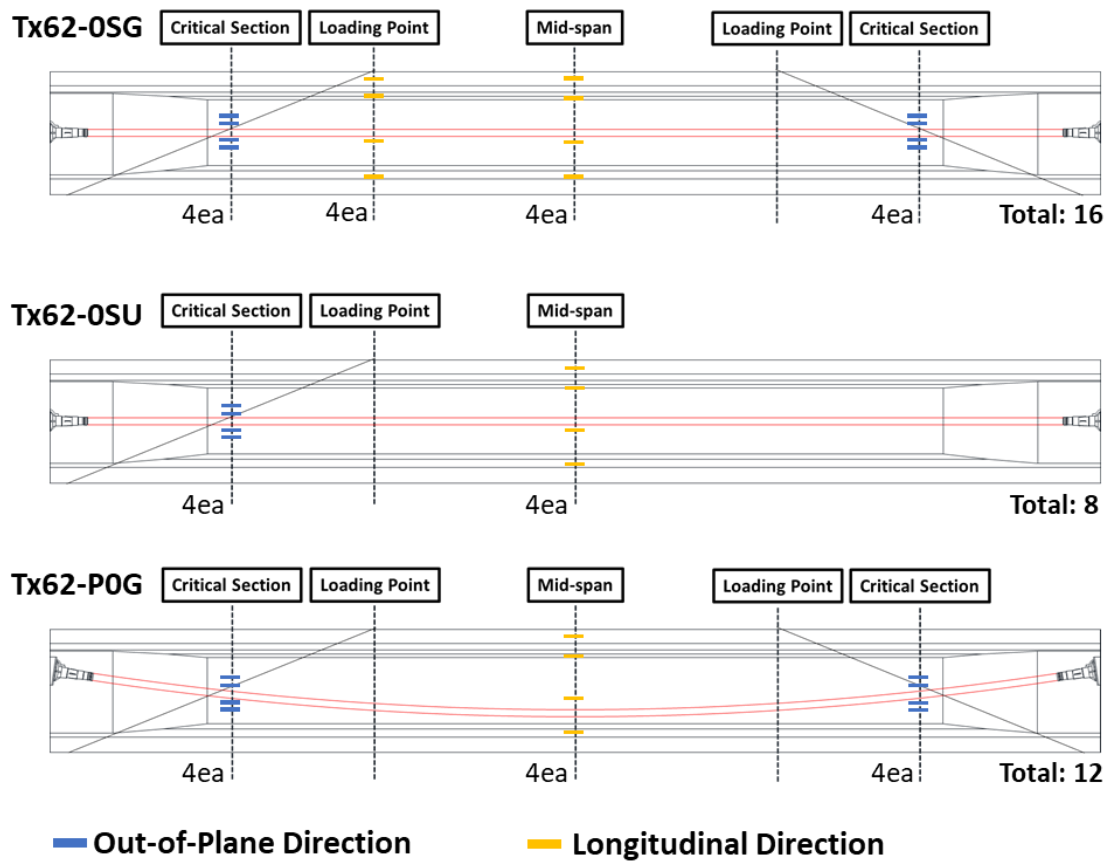


Figure E.1 Proposed Location of VWGs for the Test Specimens Containing the Grouted Tendon

E3. 2nd Delivery to FSEL

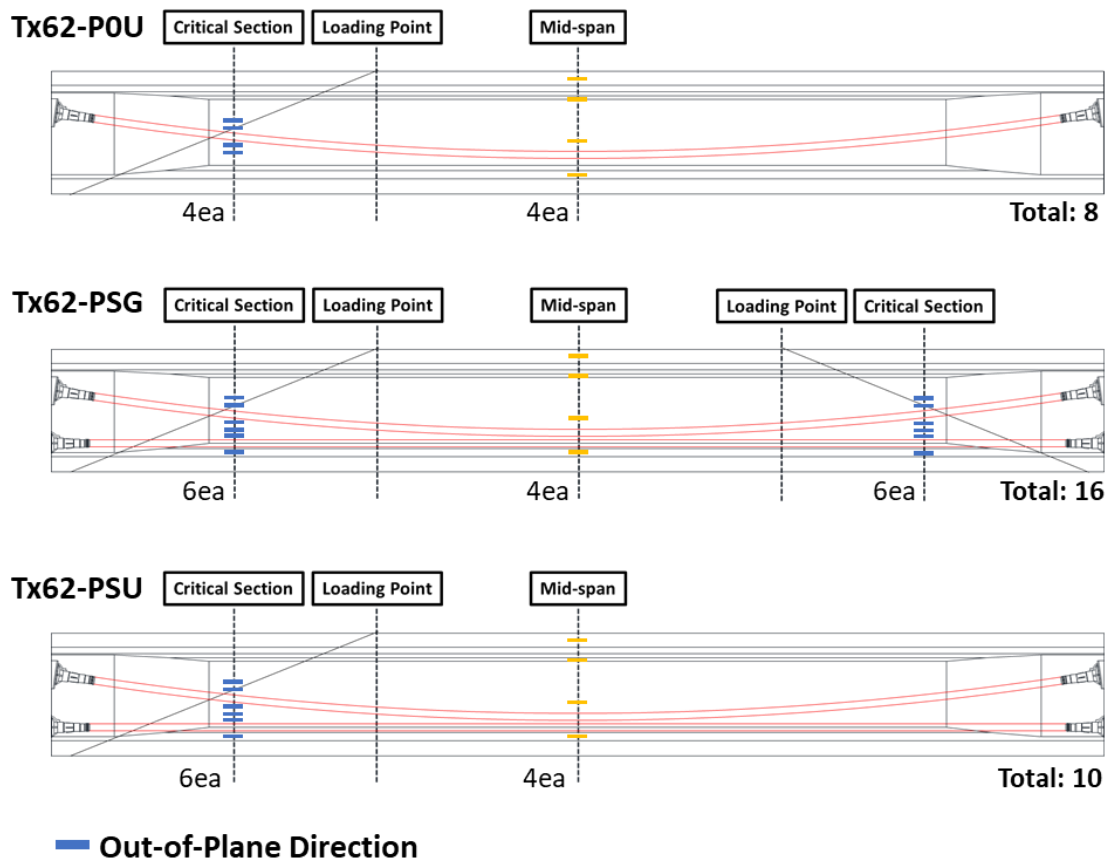


Figure E.2 Proposed Location of VWGs for the Test Specimens Containing the Ungrouted Tendon

Appendix F. Prestress Loss Calculation

Between fabrication and structural test, significant events such as prestressing transfer, post-tensioning, and deck casting result in prestress loss. The research team has monitored the longitudinal strain behaviors at the middle section to capture the aforementioned events. The collected strain data estimate the prestress loss for each test specimen by using the Garber model. In order to validate the prestress loss from strain data, the former is calculated from AASHTO LRFD (2020) for (i) before deck placement and (ii) after deck placement. Since the total prestress loss from AASHTO LRFD aggregates the effects of elastic shortening, shrinkage, creep, and stress relaxation, it is possible to compare the prestress loss from AASHTO LRFD to the prestress loss measured by the Garber model directly. Here, the prestress loss calculation procedure is summarized and the prestress loss estimations are compared to the actual prestress losses using the Garber model.

- The design equation from AASHTO LRFD (2020) Article 5.9.3 is used to calculate total loss of prestress.
- The final time was chosen for the first test day.
- The modulus of elasticity at time of transfer, deck placement, and final time were all estimated using AASHTO LRFD (2020) Equation 5.4.2.4-1.
- Average relative humidity (H) for Texas was assumed to be 60%.

F1. Before Deck Placement

Since total prestress loss results from the various effects of elastic shortening, shrinkage, creep, and stress relaxation on each strand, each effect is calculated separately. The losses due to the elastic shortening from the pretensioning procedure and post-tensioning are calculated using the following equation:

$$\Delta f_{pES} = \frac{A_{ps} f_{psi} (I_g + e_m^2 A_g) - e_m M_g A_g}{A_{ps} (I_g + e_m^2 A_g) + \frac{A_g I_g E_{ci}}{E_p}} \quad \text{Equation F.1}$$

While the elastic shortening is considered a short-term behavior, aspects of shrinkage, creep, and stress relaxation are the long-term effects. Prestress loss because of shrinkage of the test specimen results from average relative humidity. For this calculation, average relative humidity in Texas was estimated at 60% based on the average annual ambient relative humidity map (AASHTO LRFD [2020] Figure 5.4.2.3.3.-1). The shrinkage strain of the girder, strand MOE, and transformed section coefficient of non-composite girder are used to estimate the effect of shrinkage.

$$\Delta f_{pSR} = \varepsilon_{bid} E_p K_{id} \quad \text{Equation F.2}$$

$$\varepsilon_{bid} = 1.2 k_s k_{hs} k_f k_{td} (t_d, t_c) (0.48 \cdot 10^{-3}) \quad \text{Equation F.3}$$

As shown in Equation F.3, the shrinkage of strain in the girder accounts for aspects of material coefficients, such as volume-to-surface area ratio (k_s), relative humidity (k_{hs}), concrete strength at the time of release (k_f), and the time development factor (k_{td}).

Creep also contributes to an increase in the prestress loss with respect to time-dependent behavior. Time-dependent creep coefficient $\psi_b(t_d, t_i)$ in particular is used for the prestress loss, as shown in Equation F.4.

$$\Delta f_{pCR} = \frac{E_p}{E_{ci}} f_{cgp} \Psi_b(t_d, t_i) K_{id} \quad \text{Equation F.4}$$

Equation F.5 calculates the strand relaxation in a pretensioned strand that develops between the time of prestressing transfer and deck placement:

$$\Delta f_{pR1} = \frac{f_{pt}}{K_L} \left(\frac{f_{pt}}{f_{py}} - 0.55 \right) \quad \text{Equation F.5}$$

where, for this project, $K_L = 30$ for low relaxation strands.

Finally, as shown in Equation F.6, the total prestress loss before deck placement is the sum of each estimated prestress loss due to aspects of elastic shortening, shrinkage, creep, and relaxation in the strand.

$$\Delta f_{pt} = \Delta f_{pES} + (\Delta f_{pSR} + \Delta f_{pCR} + \Delta f_{pR1})_{id} \quad \text{Equation F.6}$$

F2. After Deck Placement

Deck placement results in prestress development, including shrinkage in girder, creep in girder, shrinkage in deck, and strand relaxation. Before deck placement, the placement transformed section coefficient before deck casting K_{id} is used. However, it is recalculated to the transformed section coefficient after deck casting K_{df} . Thus, the prestress loss due to the effect of shrinkage in the girder can be calculated as:

$$\Delta f_{pSD} = \varepsilon_{bdf} E_p K_{df} \quad \text{Equation F.7}$$

The shrinkage in the deck should be also considered due to the prestress gains from this shrinkage, which can be determined by the following:

$$\Delta f_{pSS} = \frac{E_p}{E_c} \Delta f_{cdf} K_{df} \left[1 + 0.7 \Psi_b(t_f, t_d) \right] \quad \text{Equation F.8}$$

in which:

$$\Delta f_{cdf} = \frac{\varepsilon_{ddf} A_d E_{cd}}{\left[1 + 0.7 \Psi_d(t_f, t_d) \right]} \left(\frac{1}{A_c} - \frac{e_{pc} e_d}{I_c} \right) \quad \text{Equation F.9}$$

The prestress loss by creep effect takes into account the concrete stress at the centroid of the pretensioning strands due to both the prestressing force f_{cgp} and the long-term losses between transfer and deck placement Δf_{cd} , which can be expressed as:

$$\Delta f_{pCD} = \frac{E_p}{E_{ci}} f_{cgp} \left[\Psi_b(t_f, t_i) - \Psi_b(t_d, t_i) \right] K_{df} + \frac{E_p}{E_c} \Delta f_{cd} \Psi_b(t_f, t_d) K_{df} \quad \text{Equation F.10}$$

The prestress loss by strand relaxation after deck casting is assumed to be the same as the prestress loss before deck casting.

$$\Delta f_{pR1} = \frac{f_{pt}}{K_L} \left(\frac{f_{pt}}{f_{py}} - 0.55 \right) \quad \text{Equation F.11}$$

F3. Total Prestress Loss

In conclusion, the total prestress loss is the sum of each prestress loss before and after deck placement.

$$\Delta f_{pt} = \Delta f_{pES} + \Delta f_{pLT_BeforeDeck} + \Delta f_{pLT_AfterDeck} \quad \text{Equation F.12}$$

in which:

$$\Delta f_{pLT_BeforeDeck} = (\Delta f_{pSR} + \Delta f_{pCR} + \Delta f_{pR1})_{id} \quad \text{Equation F.13}$$

$$\Delta f_{pLT_AfterDeck} = (\Delta f_{pSD} + \Delta f_{pCD} + \Delta f_{pR2} - \Delta f_{pSS})_{df} \quad \text{Equation F.14}$$

With the aforementioned procedure, total prestress losses from each test specimen were respectively estimated to compare the monitored prestress loss using the Garber model. Table F.2 and Table F.3 present the comparison of estimated prestress loss from AASHTO LRFD and the loss calculated from the data using the Garber model. Notably, VWG reads the strain development of concrete directly to estimate the strand behavior indirectly using the strain compatibility condition. VWGs did not capture the stress relaxation in tensioned strands. For comparison, the prestress loss from VWG adds the effect of stress relaxation calculated from AASHTO LRFD so that the two results can be compared directly.

Table F.2 Comparison of prestress loss between AASHTO LRFD estimation and actual prestress loss using the monitored strain data in test specimens with grouted tendon

	Tx62-0SG			Tx62-P0G			Tx62-PSG		
	AASHTO (2020)	Strain data	Diff.	AASHTO (2020)	Strain data	Diff.	AASHTO (2020)	Strain data	Diff.
Before strand release	0.0	0.0	0.0	0.0	0.0	0.0	0.0	0.0	0.0
Prestress transfer	20.9	23.6	-2.7	20.2	20.9	-0.8	21.5	21.9	-0.3
Before post-tensioning	39.4	37.4	2.0	36.8	34.2	2.6	42.9	36.6	6.4
After post-tensioning	43.3	39.4	4.0	40.2	37.4	2.8	50.2	44.4	5.8
Before first test	43.5	43.5	0.0	40.3	40.9	-0.6	50.4	50.4	0.0

*note: all values are in *ksi*.

Table F.3 Comparison of prestress loss between AASHTO LRFD estimation and actual prestress loss using the monitored strain data in test specimens with ungrouted tendon

	Tx62-0SU			Tx62-P0U			Tx62-PSU		
	AASHTO (2020)	Strain data	Diff.	AASHTO (2020)	Strain data	Diff.	AASHTO (2020)	Strain data	Diff.
Before strand release	0.0	0.0	0.0	0.0	0.0	0.0	0.0	0.0	0.0
Prestress transfer	24.4	21.3	3.1	19.9	24.2	-4.3	20.8	21.5	-0.7
Before post-tensioning	42.6	37.2	5.4	37.2	35.8	1.3	41.0	39.7	1.3
After post-tensioning	42.6	39.1	3.5	40.7	39.4	1.3	48.6	47.6	0.9
Before first test	42.8	39.5	3.3	40.7	40.8	-0.1	48.7	48.4	0.3

*note: all values are in *ksi*.

Appendix G. Internal Cracking Survey

UT research team conducted to dissect the critical section for the analysis of web expansion behavior. The analysis and the internal cracking survey of the test specimens at the 1st test were provided in Section 4.3.2. In addition, the internal cracking survey from the 2nd test is provided herein for the more reference. Note that the cross-sectional view at the critical section is not available for the test specimens of Tx62-0SU and PSU at the 2nd test due to the repair concrete, resulting in the necessary of adjustment for the cutting section owing to the logistic plan in FSEL.

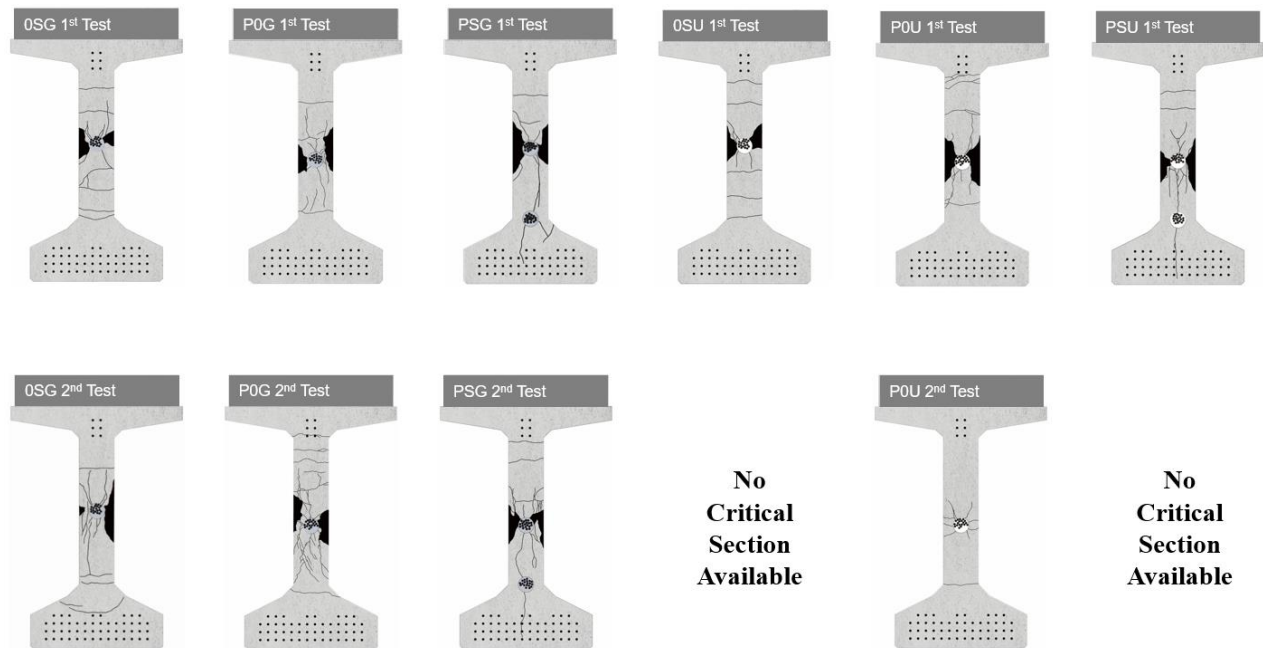


Figure G.3 Internal Cracking Survey at Critical Section from all 12 tests

Appendix H. Strength Capacity Calculation

The moment capacity calculation procedure is summarized in this section.

- The rectangular stress block approach is used primarily.
- The ultimate compressive concrete strain is assumed to be 0.003 in./in.
- The Ramberg-Osgood Function is used to calculate the stresses for pretensioning strands and bonded post-tensioning strands.
- The design equation from AASHTO LRFD (2020) Article 5.6.3.1.2 is used to calculate stresses for unbonded post-tensioning strands.

Shear and moment demands (V_u and M_u) are used to evaluate the primary controlling failure mechanism of test specimens as well as to estimate their shear capacities using the MCFT-based sectional design method in AASHTO LRFD (2020).

H1. Moment Capacity

Moment capacities of the test specimens were calculated using the rectangular stress block approach. Concrete strain at failure is assumed to be 0.003 in./in., and the rupture strain of strands uses the minimum value of 0.035 in./in. per ASTM 416 (2018). A bi-linear function was used for the stress-strain response of conventional reinforcement, and the Ramberg-Osgood function was used for both pretensioning and bonded post-tensioning strands. In the case of unbonded post-tensioning strands, the stress in prestressing strands was calculated based on the design equation of Article 5.6.3.1.2 in AASHTO LRFD (2020). The moment capacities of each specimen, summarized in Table H.1, are evaluated at the critical section and at the loading point.

Table H.1 Moment capacity of each specimen at critical section and loading point

Specimen ID	M_n (k-in.)	
	at critical section	at loading point
Tx62-0SG	196,699	196,699
Tx62-0SU	195,889	195,889
Tx62-P0G	197,736	206,244
Tx62-P0U	196,198	205,217
Tx62-PSG	241,549	250,137
Tx62-PSU	238,452	247,754

The bending-dominant failure of the test girders is an undesired failure mechanism. To ensure a shear-dominant failure of test specimens, the anticipated applied moment at the loading point was increased by 20% and compared to the moment capacity. Based on the criteria proposed above, all of the elevated maximum moments $1.2 M_u$ are less than the moment capacity M_n . As such, the controlling failure mechanism for all girders is expected to be the shear failure.

H2. Shear Capacity

For the purpose of estimating the shear capacity of test girders, the general shear design procedure in AASHTO LRFD (2020) was used. Using shear and moment demands (V_u and M_u) expressed as a function of an applied load, P , in Section 4.2.1, the shear capacity is iteratively obtained until shear demand V_u and shear capacity V_n are equal. Since the primary purpose of this procedure is to evaluate the shear capacity of test girders, load and resistance factors are assumed as 1.0.

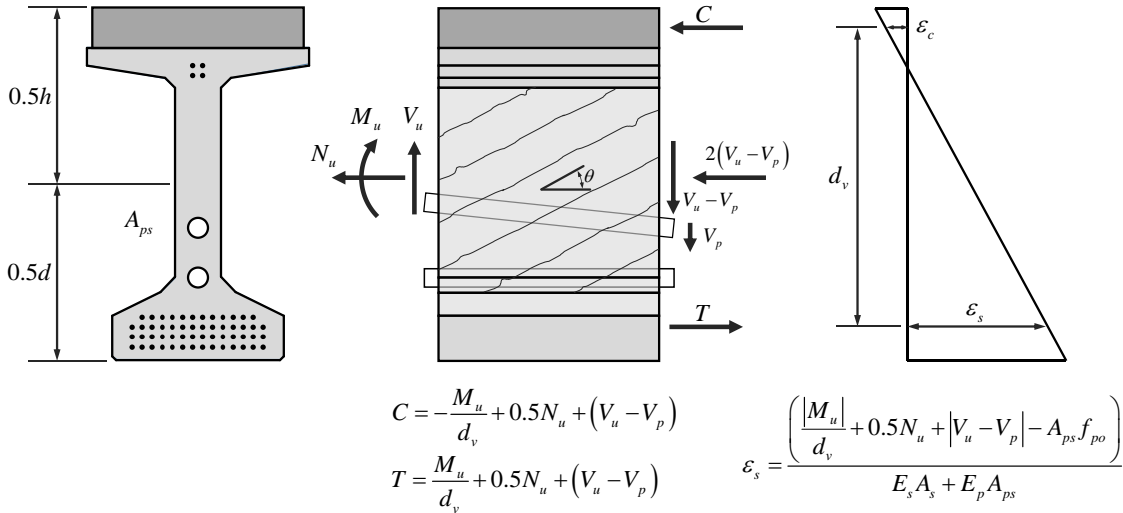


Figure H.1 Shear Parameters for Shear Capacity Estimations

Shear capacity calculation procedures for both grouted and ungrouted tendons are summarized in this section.

- General shear design procedure in accordance with AASHTO LRFD (2020) Article 5.7.3 is used to iteratively calculate the shear capacity.
- The effective web width is calculated in accordance with AASHTO LRFD (2020) Article 5.7.2.1 and Article 5.7.2.8.

$$b_v = b_w - k \cdot \phi_{duct} \quad \text{Equation H.1}$$

where $k = 0$ for grouted tendon and $k = 1$ for ungrouted tendon.

The effective shear depth, d_v , is the maximum value of the following equations:

$$d_v = \frac{M_n}{A_s f_y + A_{ps} f_{ps}} \quad \text{or} \quad \text{Equation H.2}$$

$$d_v = 0.9d_e \quad \text{where} \quad d_e = \frac{A_{ps} f_{ps} d_p + A_s f_y d_s}{A_{ps} f_{ps} + A_s f_y} \quad \text{or}$$

$$d_v = 0.72h$$

The shear force and moment at the critical section are expressed using applied load P_u :

$$V_u = 0.613P_u \quad \text{Equation H.3}$$

$$M_u = 49.17P_u \quad \text{Equation H.4}$$

The maximum moment at the loading point is also expressed using applied load P_u :

$$M_u = 103.8P_u \quad \text{Equation H.5}$$

The shear contribution of post-tensioning should be calculated considering the tendon angle ϕ with respect to the longitudinal direction of the girder. The tendon angle at the critical section is 7.0 degrees.

$$V_p = A_{ps, \text{parabolic}} f_{ps} \sin \phi \quad \text{Equation H.6}$$

The strain at the centroid of the steel in the tension side should be calculated using the following equation:

$$\epsilon_s = \frac{\left(\frac{|M_u|}{d_v} + 0.5N_u + |V_u - V_p| - A_{ps} f_{po} \right)}{E_s A_s + E_p A_{ps}} \quad \text{Equation H.7}$$

However, the value of ϵ_s is negative, so the denominator of the above equation is replaced.

$$\epsilon_s = \frac{\left(\frac{|M_u|}{d_v} + 0.5N_u + |V_u - V_p| - A_{ps} f_{po} \right)}{E_s A_s + E_p A_{ps} + E_c A_{ct}} \quad \text{Equation H.8}$$

Using the value of ϵ_s , β and θ are calculated using the following equations, assuming at least the minimum amount of transverse reinforcement:

$$\beta = \frac{4.8}{(1 + 750\varepsilon_s)} \quad \text{Equation H.9}$$

$$\theta = 29 + 3500\varepsilon_s \quad \text{Equation H.10}$$

Using the values of β and θ , V_c and V_s are calculated using the following equations:

$$V_c = 0.0316\beta\lambda\sqrt{f'_c}b_vd_v \quad \text{Equation H.11}$$

$$V_s = \frac{A_vf_yd_v(\cot\theta + \cot\alpha)\sin\alpha}{s} \cdot \lambda_{duct} \quad \text{Equation H.12}$$

Then, the shear capacity, V_n , is obtained as follows:

$$V_n = V_c + V_s + V_p < 0.25f'_cb_vd_v + V_p \quad \text{Equation H.13}$$

If the shear capacity and shear demand are not the same, repeat this process using the updated load P_u . Repeat this process until the shear capacity, V_n , is equal to the shear demand, V_u .

Appendix I. Proposed Modification of AASHTO LRFD

This project aimed to evaluate the penalty-based shear design factors accounting for the actual failure mechanism of post-tensioned member, which thoroughly discussed in this study. For reader's references, the proposed in-line revisions to the current edition of AASHTO LRFD (2020) are herein provided. Note that the removal contents are shown with the strikethrough line and the addition contents are shown with the underline in red color.

5.7.2.1—General

Torsion effects shall be investigated where:

$$T_u > 0.25\phi T_{cr} \quad (5.7.2.1-3)$$

- For solid shapes:

$$T_{cr} = 0.126K\lambda\sqrt{f'_c} \frac{A_{cp}^2}{p_c} \quad (5.7.2.1-4)$$

- For hollow shapes:

$$T_{cr} = 0.126K\lambda\sqrt{f'_c} 2A_o b_e \quad (5.7.2.1-5)$$

in which

$$K = \sqrt{1 + \frac{f_{pc}}{0.126\lambda\sqrt{f'_c}}} \leq 2.0 \quad (5.7.2.1-6)$$

where:

- T_u = applied factored torsional moment (kip-in.)
- ϕ = resistance factor specified in Article 5.5.4.2
- T_{cr} = torsional cracking moment (kip-in.)
- λ = concrete density modification factor as specified in Article 5.4.2.8
- f'_c = compressive strength of concrete for use in design (ksi)
- A_{cp} = area enclosed by outside perimeter of concrete cross section (in²)
- p_c = length of outside perimeter of the concrete section (in.)
- A_o = area enclosed by the shear flow path, including any area of holes therein (in.²)
- b_e = effective width of the shear flow path taken as the minimum thickness of the exterior webs or flanges comprising the closed box section (in.). b_e shall be adjusted to account for the presence of ducts.

f_{pc} = unfactored compressive stress in concrete after prestress losses have occurred either at the centroid of the cross section resisting transient loads or at the junction of the web and flange where the centroid lies in the flange (ksi)

b_e defined above shall not exceed A_{cp}/p_c , unless a more refined analysis is utilized to determine a larger value.

The effects of any openings or ducts in members shall be considered. K shall not be taken greater than 1.0 for any section where the stress in the extreme tension fiber, calculated on the basis of gross section properties due to factored load and effective prestress force after losses exceed $0.19 \lambda \sqrt{f'_c}$ in tension.

When calculating K for a section subject to factored axial force, N_u , f_{pc} shall be replaced with $f_{pc} - N_u/A_g$. N_u shall be taken as a positive value when the axial force is tensile and as a negative value when it is compressive.

An example of a more refined analysis would be a plate model of the cross section subjected to a torsional load.

The current recommendation for determining the effective web or flange thickness, b_e , is that the diameters of corrugated metal or plastic ungrouted ducts or one half the diameters of grouted ducts be subtracted from the web or flange thickness at the location of these ducts (AASHTO, 1999). ~~For determining the shear capacity of girders containing grout ducts in the web, no reduction in effective web or flange thickness is required provided the λ_{duct} factor of Article 5.7.3.3 is employed in calculating V_s . This approach is consistent with the fundamentals of MCFT, which is rooted in the ability of cracked concrete to transfer shear.~~

5.7.3.3—Nominal Shear Resistance

The nominal shear resistance, V_n , shall be determined as the lesser of both of the following:

$$V_n = V_c + V_s + V_p \quad (5.7.3.3-1)$$

$$V_n = 0.25f'_c b_v d_v + V_p \quad (5.7.3.3-2)$$

in which:

~~$$V_c = 0.0316\beta\lambda\sqrt{f'_c} b_v d_v \quad (5.7.3.3-3)$$~~

$$V_c = 0.0316\beta\lambda\sqrt{f'_c} b_w d_v \quad (5.7.3.3-3)$$

$$V_s = \frac{A_v f_y d_v (\cot \theta + \cot \alpha) \sin \alpha}{s} \lambda_{duct} \quad (5.7.3.3-4)$$

$$\lambda_{duct} = 1 - \delta \left(\frac{\phi_{duct}}{b_w} \right)^2 \quad (5.7.3.3-5)$$

where:

- V_p = component of prestressing force in the direction of the shear force; positive if resisting the applied shear
- b_v = effective web width taken as the minimum web width within the depth d_v as determined in Article 5.7.2.8 (in.); for girders containing a post-tensioning duct, reduce b_v by the diameter of the duct (in.)
- d_v = effective shear depth as determined in Article 5.7.2.8 (in.)
- β = factor indicating ability of diagonally cracked concrete to transmit tension and shear as specified in Article 5.7.3.4
- λ = concrete density modification factor as specified in Article 5.4.2.8
- A_v = area of transverse reinforcement within a distance, s (in.²)
- θ = angle of inclination of diagonal compressive stresses as determined in Article 5.7.3.4 (degrees)

C5.7.3.3

As noted in Article 5.7.2.3 for members subjected to flexural shear without torsion, transverse reinforcement with specified minimum yield strengths up to 100 ksi is permitted for elements and connections specified in Article 5.4.3.3.

The limit in Article 5.7.3.3 was derived from the Modified Compression Field Theory (Vecchio and Collins, 1986) and has been validated by numerous experiments on prestressed and nonprestressed concrete members (Saleh and Tadros, 1997; Lee et al., 2010).

The upper limit of V_n , given by Eq. 5.7.3.3-2, is intended to ensure that the concrete in the web of the beam will not crush prior to yield of the transverse reinforcement.

Where $\alpha = 90$ degrees, Eq. 5.7.3.3-4 reduces to:

$$V_s = \frac{A_v f_y d_v \cot \theta}{s} \lambda_{duct} \quad (C5.7.3.3-1)$$

For girders designed as individual girders, or as individual webs lines, A_v is taken as the reinforcing in the single web of the girder being considered. For box girders designed as a single unified section, A_v is taken as the total reinforcing in all the webs in the cross section.

The angle θ is also taken as the angle between a strut and the longitudinal axis of a member.

The traditional approach to proportioning transverse reinforcement involves the determination of the required stirrup spacing at discrete sections along the member. The stirrups are then detailed such that this spacing is not exceeded over a length of the beam extending from the design section to the next design section out into the span. In such an approach, the shear demand and resistance provided is as shown in Figure C5.7.3.3-1.

In situations where a significant amount of the load is applied below the mid-depth of the member, such as inverted T-beam pier caps, and the section model is used to design for shear, it is more appropriate to use the traditional approach to the design of transverse reinforcement shown in Figure C5.7.3.3-1.

- α = angle of inclination of transverse reinforcement to longitudinal axis (degrees)
- s = spacing of transverse reinforcement measured in a direction parallel to the longitudinal reinforcement (in.)
- λ_{duct} = shear strength reduction factor accounting for the reduction in the shear resistance provided by transverse reinforcement due to the presence of a post-tensioning duct. ~~Taken as 1.0 for ungrouted post-tensioning ducts and with a reduced web or flange width to account for the presence of ungrouted duct.~~
- δ = duct diameter correction factor, taken as 2.0 for grouted ducts grouted or ungrouted post-tensioning ducts
- ϕ_{duct} = diameter of post-tensioning duct present in the girder web within depth d_v (in.)
- b_w = gross width of web, not reduced for the presence of post-tensioning ducts (in.)

Where transverse reinforcement consists of a single longitudinal bar or a single group of parallel longitudinal bars bent up at the same distance from the support, the shear resistance V_s provided by these bars shall be determined as:

$$V_s = A_v f_y (\sin \alpha) \lambda_{duct} \leq 0.095 \lambda \sqrt{f'_c} b_v d_v \quad (5.7.3.3-6)$$

Where bent longitudinal reinforcement is used, only the center three fourths of the inclined portion of the bent bar shall be considered effective for transverse reinforcement.

Where more than one type of transverse reinforcement is used to provide shear resistance in the same portion of a member, the shear resistance V_s shall be determined as the sum of V_s values computed from each type.

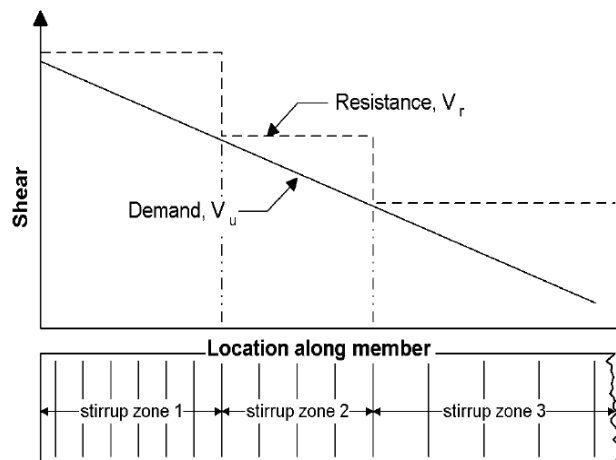


Figure C5.7.3.3-1—Traditional Shear Design

For typical cases where the applied load acts at or above the mid-depth of the member, it is practical to take the traditional approach as shown in Figure C5.7.3.3-1 or a more liberal yet conservative approach as shown in Figure C5.7.3.3-2 which has the effect of extending the required stirrup spacing for a distance of $0.5d_v \cot \theta$ toward the bearing.

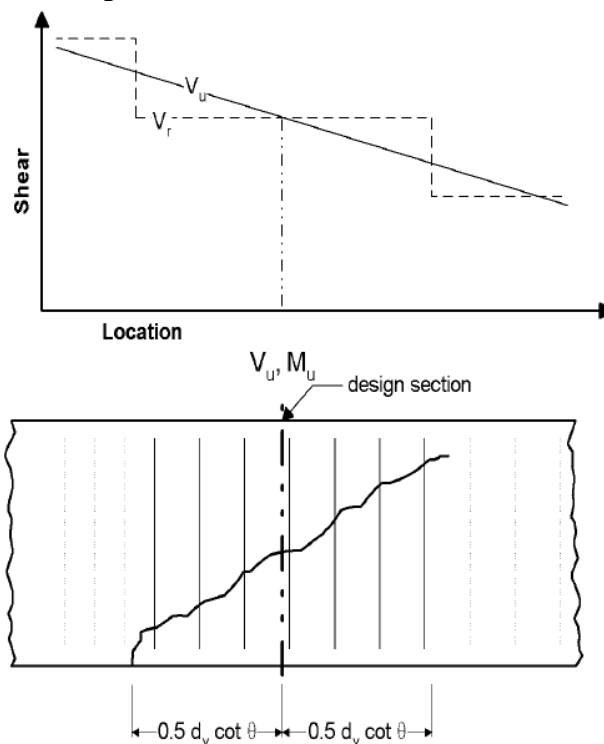


Figure C5.7.3.3-2—Simplified Design Section for Loads Applied at or above the Mid-Depth of the Member

Requirements for bent bars were added to make the provisions consistent with those in AASHTO (2002).

The shear strength reduction factor λ_{duct} is based on research that conducted and examined full-scale tests of post-tensioned concrete girders (Moore et al. 2015 and Han et al. 2022). girder bridges. Research by Moore et al. (2015) examined both plastic and metal grouted ducts used in spliced girders used in spliced girders. If the λ_{duct} factor is used in determining the shear capacity of post tensioned girders containing ducts in the web, no reduction in effective web thickness is required (i.e., $b_e = b_w$). For elements with ungrouted ducts, λ_{duct} factor must be taken as 1.0 and b_v must be reduced to account for the duct diameter. This is consistent with methods used in past editions of the LRFD Bridge Design Specifications (Moore et al., 2015).

In the calculation of the shear nominal resistance given in Eq. 5.7.3.3-2, the effective web width, b_v , is taken as the minimum web width within the depth d_v , reduced by the diameter of the duct to account for the observed ultimate failure of localized web crushing in the vicinity of a post-tensioning duct (Han et al. 2022).

While Moore et al. (2015), ~~and~~ Williams et al. (2015) ~~and Han et al. (2022)~~ did not conduct tests to study torsional behavior, it is reasonable to apply λ_{duct} to the capacity calculation by Eq. 5.7.3.6.2-1 to be consistent with the fundamentals of the Modified Compression Field Theory. In this way, shear resulting from torsion and that resulting from direct shear can be combined consistently in webs or flanges of members that contain post-tensioning ducts embedded in concrete.